Investigation of the Band Alignment of Long-Wavelength InGa(N)As(Sb) Quantum Wells on GaAs and InP Substrates

M.Sc. Thesis
in
Engineering Physics
University of Gaziantep

Supervisor
Prof. Dr. Beşire GÖNÜL

by

Ebru BAKIR

ABSTRACT

INVESTIGATION of THE BAND ALIGNMENT of LONG WAVELENGTH InGa(N)As(Sb) QUANTUM WELLS ON GaAs and InP SUBSTRATES

BAKIR Ebru

M.Sc. in Engineering Physics

Supervisor: Prof. Dr. Beşire GÖNÜL

January 2007, 94 pages

The aim of this thesis work is to investigate the band alignment configuration of InGa(N)As(Sb) and its related alloys on common substrates of GaAs and InP. We employed the Model Solid theory to obtain the band offsets. This work also aims to compare our calculated results with those of the conventional laser structures. By means of using different barriers we try to find the ideal band alignment configuration for InGa(N)As(Sb) quantum well lasers and offer the best material system suitable for long wavelength emission.

Key Words: Long wavelength, GaInNAs, GaInNAsSb, dilute nitrides, band anti-crossing model, band offsets, band alignment, dilute antimonides.

ÖZET

GaAs ve InP ALT TABAKALAR ÜZERINDEKİ UZUN DALGA BOYLU InGa(N)As(Sb) KUANTUM KUYUSUNUN BANT DİZİLİMİNİN ARAŞTIRILMASI

BAKIR Ebru
Yüksek Lisans Tezi, Fizik Mühendisliği Bölümü
Tez Yöneticisi: Prof. Dr. Beşire GÖNÜL
Ocak 2007, 94 sayfa

Bu tez çalışmasının amacı InGa(N)As(Sb) ve ilgili alaşımlarının yaygın GaAs ve InP alt tabakalar üzerindeki bant dizilim biçimini araştırmaktır. Bant derinliklerini elde etmek için "Model Solid" teorisini kullandık. Bu çalışma ayrıca hesaplanan sonuçların geleneksel lazer yapılarıyla karşılaştırılmasını amaçlar. InGa(N)As(Sb) kuantum kuyu lazerleri için farklı bariyerler kullanarak ideal bant dizilim biçimi bulmaya ve uzun dalga boyu yayımı için uygun materyal sistemleri önermeye çalıştık.

Anahtar Kelimeler: Uzun dalgaboyu, GaInNAs, GaInNAsSb, hafif nitratlar, band anti-crossing modeli, bant derinliği, band hizalanması, hafif antimon

ACKNOWLEDGEMENT

First and foremost, I must acknowledge my supervisor, Professor Beşire GÖNÜL who conscientiously supported me throughout this work. Without her invaluable support and guidance, I would not have managed to reach this far. However, my supervisor is more than a fountain of semiconductor wisdom; she is a great mentor on life. Second, I wish to express my sincere gratitude to my teacher Professor Bülent GÖNÜL who is always ready to listen and give help whenever I need.

I am particularly grateful to Koray KÖKSAL, benefiting from his knowledge and our discussions about theoretical and computer subjects. Koray has not only been a great colleague, but also a reliable friend. I also would like to thank you Murat ODUNCUOĞLU, Hüseyin TOKTAMIŞ, Mehmet KOÇAK, Vural KAFADAR for their support and friendship. And finally I would like to thank all the Engineering Physics staff.

On a personal level, I would like to deeply thank my parents Servet and Sıtkı, my one and only sister Arzu and her cheerful husband Ömer and my love Erdem for their encouragement, support and prayers throughout my education. Finally I would like to thank to my little lovely niece Öykü and nephew Onur for giving hapiness and cheerfullness to our family.

CONTENTS

LIST of FIGURES

LIST of TABLES

CHAPTER 1

INTRODUCTION

The invention of the semiconductor laser in the early 1960s [1] can be considered as a major breakthrough in photonic technology. Nowadays, such devices are widely used in areas like optical data storage and retrieval, laser-printing, or optical pumping of solid-state lasers. Apart from these areas, semiconductor lasers rapidly evolved as the ultimate light source for optical communication systems. The simultaneous development of semiconductor lasers, optical amplifiers, detectors and high-speed electronics, along with the invention of the optical fiber, revolutionized the information technology, allowing transmitting huge amounts of data at an unprecedented speed across the world.

For long wavelength quantum well (QW) semiconductor lasers, operating at around 1550 nm, InP based latticed matched III-V semiconductors draw considerable interest because of their usage in low-loss optical fiber communications [2]. In this wavelength region, much of the research and development effort has been concentrated on InGaAsP based laser technology. However, this material system has relatively poor high-temperature characteristics and the power output is limited due to the poor electron confinement in the QWs. Therefore, there has been an intense effort to realize both low cost, long wavelength vertical cavity surface emitting lasers VCSELs and high power pump lasers between 1.3 and 1.6 μm over the past decade [3]. Semiconductor lasers operating in the 1.3–1.6 μm region require materials with bandgaps between 0.95 and 0.78 eV. One of the requirements for alloy semiconductor is that they must be reasonably closely lattice-matched to readily available binary substrates (GaAs or InP). For many years, it was believed that there was no suitable alloy adequately lattice matched to GaAs that would emit at > 1.1 μm, so InGaAsP on InP was the only material system that met the perceived criteria, and %100 of the long-wavelength communications lasers today are fabricated from this system [4].

In 1996 Kondow *et al* [5] proposed a novel quaternary material GaInNAs, which could be grown lattice matched on GaAs and used to fabricate long-wavelength lasers with better temperature characteristics compared to InP-based lasers. This discovery was clearly far from obvious from the known properties of all other III-V ternary and quaternary alloys, where the general rule was that alloys with a smaller lattice constant had an increased bandgap. By combining GaInNAs with GaAs or any other wide-gap materials that can be grown on GaAs substrate, it is possible to achieve a Type I band lineup. In order to apply a material to the quantum-well active layer of a laser diyode, a Type I band lineup is essential so that both electrons and holes are confined to the quantum-well layer. The addition of small amounts of nitrogen into InGaAs has allowed the growth of dilute-nitride materials which have much longer emission wavelengths than previously attainable on GaAs. GaInNAs has enabled the development of lasers at the important fiber communication wavelength of 1.3 μm with some advantages of [6];

i. Conduction band well is deeper providing better confinement for electrons.
ii. Electron effective mass is larger resulting better match of the valance- and conduction-band densities of states.
iii. GaInNAs/GaAs lasers have excellent high-temperature performance, higher T_o, higher efficiency and output power.
iv. The stability of the lasing wavelength is excellent despite the changes in temperature.
v. The operation speed is high.
vi. GaInNAs/GaAs lasers can be grown on a highly reflective GaAs/AlAs DBR mirror over a GaAs substrate in a single stage of epitaxial growth.

Because of the above advantages, “dilute nitride” or “low-band-gap nitride” GaInNAs alloys have quickly become an excellent candidate for low cost, high performance 1.3–1.55 μm vertical cavity surface emitting lasers (VCSELs) and high power edge emitting lasers in the past few years. In summary GaInNAs and other III-N-

V alloys are very promising and their future looks bright. Since GaInNAs system has been proposed as a material for 1.3 μm emitting lasers on GaAs substrate, it has been realized that the optical quality of the material deteriorates due to a restriction in the optimal growth parameters when the nitrogen concentration is above 2.5%. The degradation results in a higher threshold current density for lasers. InGaNAs is not without its own set of difficulties. The incorporation of nitrogen into (In)GaAs degrades the optical properties of the material due to the non-radiative traps, phase segration and/or relaxation. These materials issues are even more apparent when adding more indium and nitrogen to InGaNAs to reach the technologically important wavelengths near 1.55 μm. Extensive theoretical and experimental studies have been performed on the nature of the defects in dilute nitride materials, but the original causes of these defects are uncertain [7, 8, 9]. It is difficult to grow good material with very reactive species such as atomic nitrogen. Adding Sb to the GaInNAs remove of the major types of defects in GaInNAs(Sb), such as plasma damage early in the growth, as well as ion damage, which occurs during the growth of actual GaInNAs(Sb) layers. In an effort to further enhance crystal quality, Sb present during GaInNAs growth is thought to act as a surfactant to maintain surface planarity, and phase coherence, resulting in increased photoluminescence PL efficiency. To introduce Sb atoms to the GaInNAs compound is an approach in order to shift the laser emission of GaInNAs/GaAs system to 1.55 μm. This makes it possible to obtain low band gap energy at relatively low nitrogen content. Therefore, with the development of GaInNAsSb alloys and strain compensated barriers, even longer wavelengths are possible on GaAs, greatly strengthening the dilute nitride system as the technology of the future for long wavelength optoelectronic devices.

In order to achieve optimal laser performance and temperature stability, electrons should be confined in as deep of a quantum well as possible due to their smaller effective mass. In almost all material systems, sacrificing valence band well depth for conduction band well depth is quite desirable. The added degree of freedom of the quinary InGaNAsSb alloy compared to a quaternary alloy, e.g. InGaNAs of InGaAsP,

enables additional material engineering since the bandgap and lattice constant, i.e. strain, can be held constant while the offset ratio is independently tuned. However, in the dilute nitrides, it was not known if antimony would only affect the valence band (as in most other III-V) semiconductors) or if there would be a more complex interaction of the valence and conduction bands due to effects such as band-anticrossing.

The aim of this thesis is to investigate long-wavelength GaInNAs and GaInNAsSb quantum well laser on GaAs and InP substrate. The main subject of the study is the investigation and modelling of band alignment of quaternary GaInNAs and new quinary GaInNAsSb material system with different barrier and substrates.

In chapter 2, revolution of telecommunication and the theoretical fundamentals of semiconductor lasers are reviewed covering the basic concepts required in the remainder of the thesis. In chapter 3, we present the theoretical models of band structure, band lineup and material parameter calculations which are used throughout the thesis for III-N-V QW laser systems. We aim to analyse the band alignment of higly strained indium rich (In>0.535%) GaInNAs QWs on InP substrates, in chapter 4. First of all we present required parameters for calculations. Then we examine the band alignment configuration of InGaAs on InP substrate. We investigate the effect of the introduction of nitrogen N into InGaAs QW with InP barrier and show that long wavelength emission of 2.3 μm and more can be achieved by means of InGaNAs QW with InP barrier on InP substrates with a suitable band alignment. In addition, we present the effect of the usage of the different barriers on band configuration of InGaNAs/InP QWs. We offer the ideal material system which provides the best band alignment. Finally we compare the substrate dependence of strain as a function of nitrogen and indium concentration of $Ga_{1-x}In_xN_yAs_{1-y}$ QW.

The band alignment of compressively- and tensile-strained and strained compensated GaInNAs QWs on GaAs and InP substrates is studied in chapter 5. In the first part of this chapter we first provide the benefits of adding N to InGaAs QW with GaAs barrier on GaAs substrate. Then we try to find the suitable barrier material to compensate the compressive strain in the well material. In the second part of the chapter we firstly illustrate the introduction of nitrogen into InGaAs QW with InP barrier on InP substrate to provide a comparison with strain compensated system. We continue our calculations dividing this material system into low- and high-indium regions, since the behaviour is different in these two regions. We also provide the comparison of band alignment of compensated system with that of uncompensated system.

It has been stated that GaInNAsSb has been found to be a potentially superior material to GaInNAs for long wavelength laser applications. It has been explored that the addition of antimonite Sb to the GaInNAs system improves the crystal quality. Antimony acts as a surfactant and constituent when introduced during dilute-nitride growth, forming InGaNAsSb and GaNAsSb. The improvement in material quality and reduction of band gap, by adding antimony, has enabled the development of GaAs-based laser out to 1.5 μm. Therefore, in chapter 6, we provide an understanding of the heterojunction band offsets for the new quinary material system of dilute-nitride-antimoninides of GaInNAsSb. We try to determine what effect the addition of antimony would have on the band alignment of InGaNAsSb on GaAs and InP substrates.

Finally, we provide a summary of the thesis work in chapter 7.

CHAPTER 2

THEORETICAL BACKGROUND

2.1. Revolution of Telecommunication: The Fiber Optic and Semiconductor Lasers

Light has an information-carrying capacity 10,000 times greater than the highest radio frequencies. Additional advantages of fiber over copper include the ability to carry signals over long distances, low error rates, immunity to electrical interference, security, and light weight. Aware of these characteristics, researchers in the mid-1960s proposed that optical fiber might be a suitable transmission medium. There was an obstacle, however, and that was the loss of signal strength, or attenuation, seen in the glass they were working with. Further developments in fiber optics are closely tied to the use of the specific regions on the optical spectrum where optical attenuation is low. These regions, called windows, lie between areas of high absorption. The primary factors affecting attenuation in optical fibers are the length of the fiber and the wavelength of the light [10]. Fig. 2.1 shows three curves. The top, dashed, curve corresponds to early 1980's fiber, the middle, dotted, curve corresponds to late 1980's fiber, and the bottom, solid, curve corresponds to modern optical fiber. The earliest fiber optic systems were developed at an operating wavelength of about 850 nm. This wavelength corresponds to the so-called "first window" in a silica-based optical fiber. This window refers to a wavelength region that offers low optical loss. It sits between several large absorption peaks caused primarily by moisture in the fiber and Rayleigh scattering.

The 0.85 μm region was initially attractive because the technology for light emitters at this wavelength had already been perfected in visible indicator LEDs. Low-cost silicon detectors could also be used at the 0.85 μm wavelength. As technology progressed, the first window became less attractive because of its relatively high 3 dB/km loss limit. Most companies jumped to the "second window" at 1.31 μm with lower attenuation of about 0.5 dB/km. In late 1977, Nippon Telegraph and Telephone

(NTT) developed the "third window" at 1.55 μm. It offered the theoretical minimum optical loss for silica-based fibers, about 0.2 dB/km.

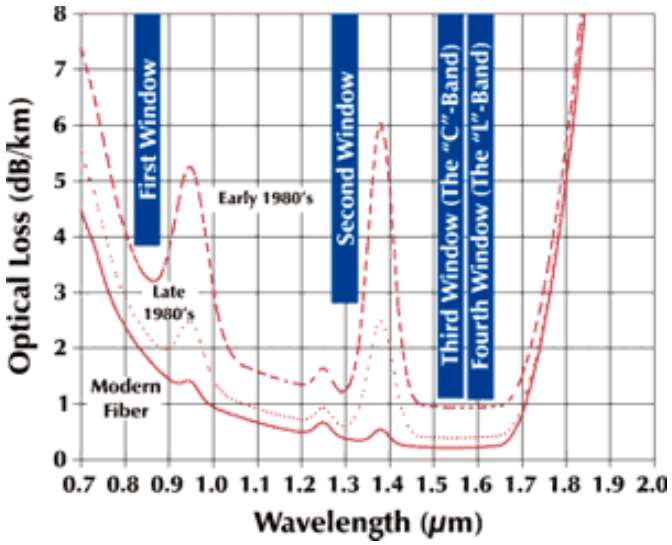

Figure 2.1: Four Wavelength Regions of Optical Fiber [11]

Today, 850 nm, 1310 nm, and 1550 nm systems are all manufactured and deployed along with very low-end, short distance, systems using visible wavelengths near 660 nm. Each wavelength has its advantage. Longer wavelengths offer higher performance, but always come with higher cost. The shortest link lengths can be handled with wavelengths of 660 nm or 850 nm. The longest link lengths require 1550 nm wavelength systems. A "fourth window," near 1625 nm, is being developed. While it is not lower loss than the 1550 nm, the loss is comparable, and it might simplify some of the complexities of long-length, multiple-wavelength communications systems [11] . The transmission distance decreases rapidly as a function of the data bandwidth of the optical network. At low data rates, the transmission distance in fiber is limited by optical attenuation. At high data rates, the distance is limited by group velocity dispersion.

During the past two decades, fiber-optic communication systems have grown spectacularly. The field of optics has been used to develop the field of high-speed data communications in wide-ranging technology areas including, among a variety of others, laser printers, optical image storage, submarine optical cable systems, home systems and optical telecommunications.

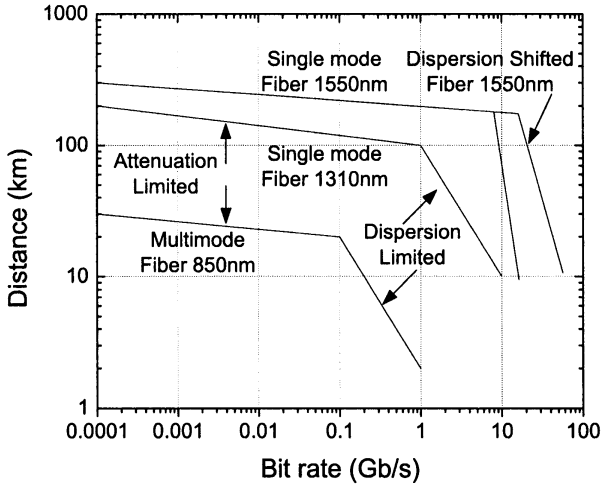

Figure 2.2: Signal transmission distance versus data bandwidth for various fiber systems and operation wavelength [12]

Tremendous increase in communication bandwidth, mainly as a result of the fast development of the Internet. Vast fiber optical networks with high demands on capacity and reliability connect cities and countries around the world. To support this development large efforts have been made towards improving the performance of optical fibers and semiconductor lasers. The light source used in the design of a system is an important consideration because it can be one of the most costly elements. Its characteristics are often a strong limiting factor in the final performance of the optical link. Conventionally optical networks use semiconductor laser especially vertical-cavity surface-emitting lasers (VCSELs) [11].

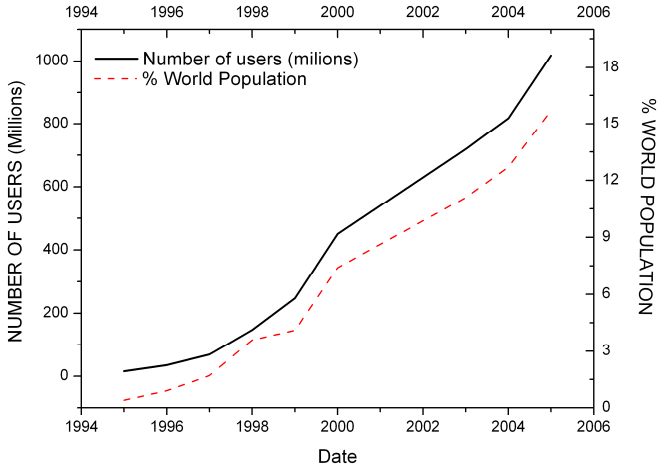

Figure 2.3: Growth of the Internet (internet usage trends in recent years) Datas are taken from [13]

2.2 Overview of Semiconductor Lasers

The laser is one of the most remarkable scientific and technological advances of the 20th century. After significant contributions from Albert Einstein, Charles Townes, Gordon Gould, and several others, Theodore Maiman created the first working laser using a solid-state flash lamp-pumped synthetic ruby crystal in 1960 at Hughes Research Laboratories. Since then, the field of lasers has diversified extensively, using many different methods and materials to create lasing action. The semiconductor laser was first proposed by Basov and Javan and the first laser diode was demonstrated by Robert Hall at General Electric Laboratories in 1962. This GaAs-based device emitted light at 850 nm, but required liquid nitrogen cooling and could only operate under pulsed conditions. The first semiconductor heterojunction laser was independently developed by Zhores Alferov in the former Soviet Union and Mort Panish and Izuo Hayashi at Bell Laboratories in 1970, leading to continuous wave, room temperature operation of the laser diode. When Maiman created the first laser 45 years ago, no one could have imagined the wide range of applications or the ubiquity of lasers found in today's technology [14].

2.3 Lasing Material

The lasing material may be elemental, but more generally is a compound semiconductor. Fig. 2.4 shows the elements that have been used as constituents to achieve laser action in elemental and compound semiconductor materials.

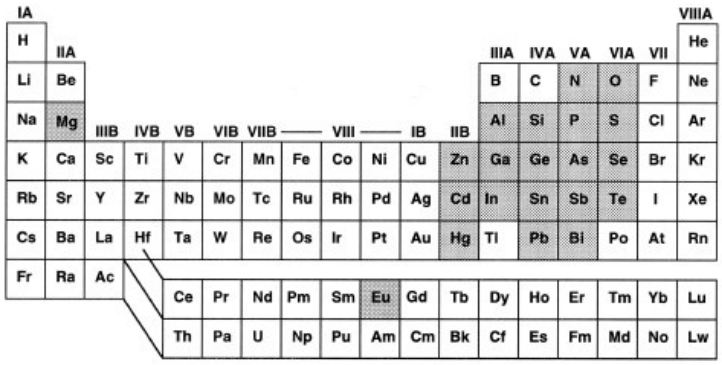

Figure 2.4: Elemental semiconductors [15]

The wavelength ranges of various types of semiconductor lasers are shown in Fig. 2.5 III-V compound lasers, including antimonide-based III-V compounds, emit in the visible and the near- and mid-infrared regions. II-VI compound lasers generally emit at shorter wavelengths; mercury-based II-VI compounds extend the coverage over the range 1.9–5.4 μm. Longer wavelength diode lasers are based on IV-VI compounds (lead salts) and can be tuned by changing the temperature or current.

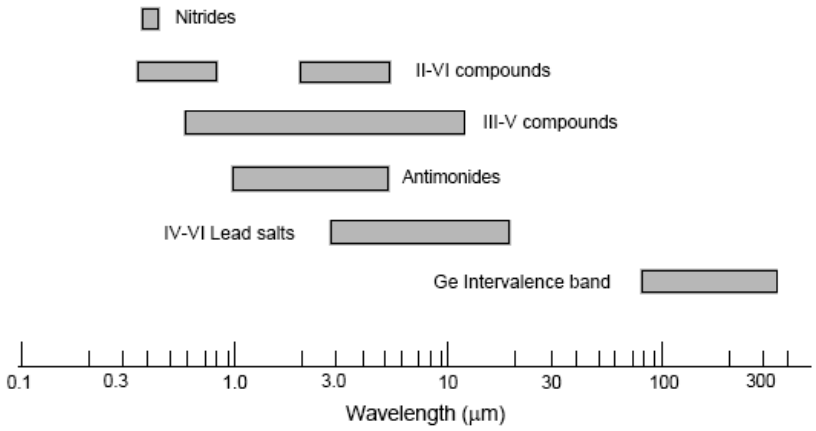

Figure 2.5: Reported ranges of output wavelengths of various types of semiconductor lasers [15]

The wavelength of quantum cascade lasers, unlike that of diode lasers, is determined by the active layer thickness rather than the band gap of the material. Multiple quantum well lasers have been tailored to operate in the range ~3–13 μm, thereby extending the range of III-V compound lasers. Germanium intervalence band lasers have thus far been operated in the range 75–360 μm. In edge-emitting lasers the light output is in the plane of the gain medium; in surface-emitting lasers the light output is normal to the axis of the gain medium. The lasing wavelength is determined by the equivalent laser cavity thickness which can be varied by changing the thickness of either the wavelength spacer or the distributed Bragg reflector layers. Vertical-cavity surface-emitting lasers (VCSELs) can be prepared in two dimensional arrays of independently modulated lasers.

Table 2.1: Semiconductor lasers; operational wavelengths, and applications [16]

Laser gain medium and type	**Operation wavelength(s)**	**Pump source**	**Applications and notes**
Semiconductor laser diode	0.4-20 µm, depending on active region material.	Electrical current	Telecommunications, holography, printing, weapons, machining, welding, pump sources for other lasers.
GaN	0.4 µm		Optical discs.
AlGaAs	0.63-0.9 µm		Optical discs, laser pointers, data communications. 780 nm Compact Disc player laser is the most common laser type in the world. Solid-state laser pumping, machining, medical.
InGaAsP	1.0-2.1 µm		Telecommunications, solid-state laser pumping, machining, medical..
Vertical cavity surface emitting laser (VCSEL)	850 - 1500 nm, depending on material		Telecommunications
Quantum cascade laser	Mid-infrared to far-infrared.		Research, Future applications may include collision-avoidance radar, industrial-process control and medical diagnostics such as breath analyzers.
Hybrid silicon laser	Mid-infrared		Research

Optical Networks conventionally use Vertical-cavity surface-emitting lasers (VCSELs). Vertical Cavity Surface Emitting Laser diodes (VCSELs) are semiconductor devices. They have come a long way from the research curiosity they were in the late seventies. The basic concept of the “vertical-cavity laser” arose from the simple interest in having a semiconductor laser with the lasing direction perpendicular rather than parallel to the wafer surface. Laser resonator consists of two distributed Bragg reflector (DBR) mirrors parallel to the wafer surface with an active region in between. If the middle layer (active layer) is made thin enough, it acts as a quantum well. This means that the vertical variation of the electron's wavefunction, and thus a component of its energy, is quantized.

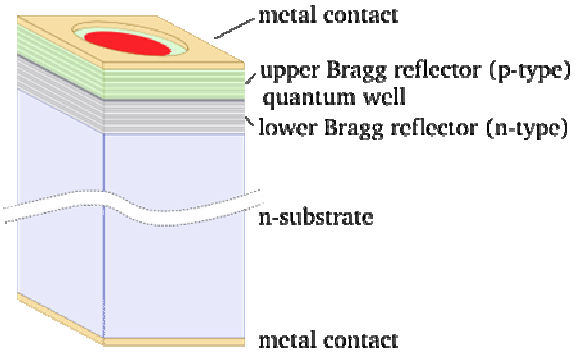

Figure.2.6: Diagram of a simple VCSEL structure [16]

2.4. Heterostructures

In a semiconductor heterostructure, two different semiconductors are brought into physical contact. In practice, different semiconductors are "brought into contact" by epitaxially growing one semiconductor on top of another semiconductor. When a heterojunction is formed, the conduction and valance band alignment is dependent upon the properties of the constituent materials such as their bandgap, the doping and the electron affinity.

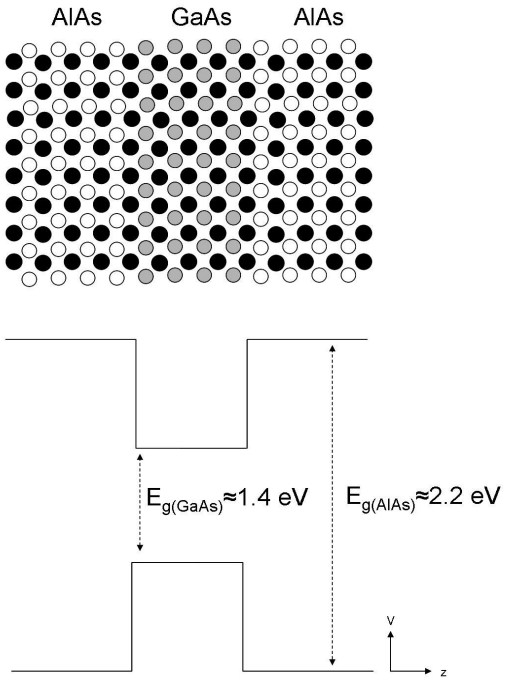

Figure 2.7: Band diagram of AlAs/GaAs heterostructure

Heterostructures can be classified depending on the band alignment formation between the two semiconductor materials. The possible band alignment combinations include “type I”, “type II staggered” and “type III broken gap” . When the valance and conduction band of one material “straddles” the bands of the narrow gap material, the heterojunction band alignment is termed type I. (An example of type I band alignment is shown in Fig. 2.8 (a)) Semiconductor heterojunctions may also form where the conduction and valance bands in one material are both slightly below the corresponding band energies in the adjacent semiconductor. This band alignment is termed type II staggered, and is shown in Fig.2.8 (b). Type III broken gap alignment occurs when the conduction of one material is at a lower energy than the valance band of the adjacent semiconductor. An example of broken gap band alignment is shown Fig.2.8 (c)

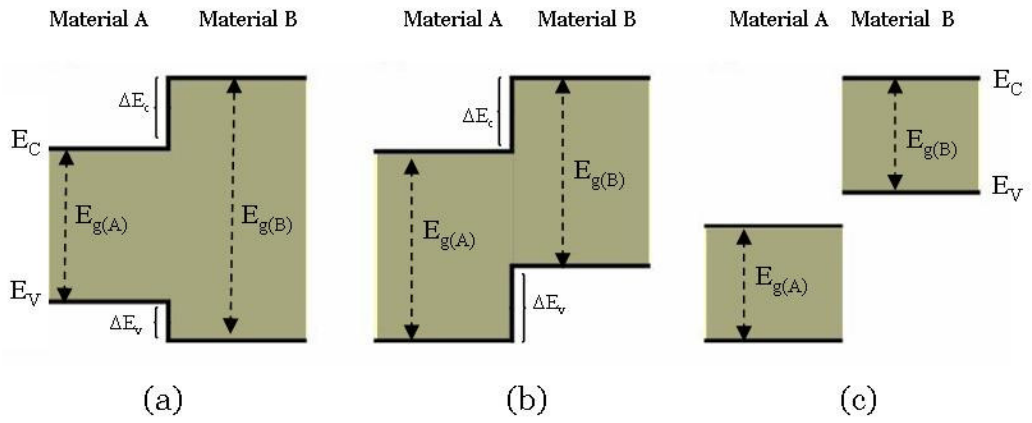

Figure 2.8: Types of energy band lineups [17]

(a) Straddled or “Type I” lineup: the most widely studied heterostructure, that is the GaAs/AlGaAs heterostructure, exhibits this straddled band alignment. ΔE_c and ΔE_v represent band offset, in Type I lineup both of them are positive

(b) Staggered or “Type II” lineup: the steps in the valance and conduction band go in the same direction. While ΔE_c is positive, ΔE_v becomes negative in this Type II lineup

(c) Broken or “Type III” lineup: the most extreme band alignment, occurs in the InAs/GaSb material system

In band alignment analysis, band offset is the one of the most important parameters that's why there have been numerous attempts and models to predict and calculate the energy band offsets in semiconductor heterostructures;

- Anderson, 1962;
- Harrison, 1977, 1980,1985;
- Frensley and Kroemer, 1977;
- Kroemer, 1985;
- Ruan and Ching, 1987;
- Van de Walle, 1989;
- Van de Walle and Martin, 1986;
- Harrison and Tersoff, 1986).

The different models have been reviewed by Kroemer (1985) and by Ruan and Ching (1987). However, none of the theoretical approaches can reliably predict the band offsets of all semiconductor heterostructure combinations.

2.5 Quantum Well Laser

If one makes a heterostructure with sufficiently thin layers (50 A˚ - 0.1μm), quantum interference effects begin to appear prominently in the motion of the electrons. The simplest structure in which these may be observed is a quantum well, which simply consists of a thin layer of a narrower-gap semiconductor between thicker layers of a wider-gap material. Reducing dimensionality of the active region of heterostructure improves significantly the performance of semiconductor lasers [18]. In the early 1970s by C. Henry [18] predicted the advantages of using quantum wells as the active layer in such lasers: the carrier confinement and nature of the electronic density of states should result in more efficient devices operating at lower threshold currents than lasers with "bulk" active layers. In addition, the use of a quantum well, with discrete transition energy levels dependent on the quantum well dimensions (thickness), provides a means of "tuning" the resulting wavelength of the material. The critical feature size-in this case, the thickness of the quantum well-depends on the desired spacing between energy levels.

For energy levels of greater than a few tens of milielectron volts (meV, to be compared with room temperature thermal energy of 25 meV), the critical dimension is approximately a few hundred angstroms. Although the first quantum well laser, demonstrated in 1975, was many times less efficient than a conventional laser (van der Ziel et al. 1975), the situation was reversed by 1981 through the use of new materials growth capabilities (molecular beam epitaxy), and optimization of the heterostructure laser design (Tsang 1982). Quantum wells are formed in semiconductors by having a material, like gallium arsenide sandwiched between two layers of a material with a wider bandgap, like aluminium arsenide which can be seen in Fig.2.9. These structures can be grown by molecular beam epitaxy or chemical vapor deposition with control of the layer thickness down to monolayers. The efficiency of a quantum well laser is greater than that of a bulk laser because the density of states function of electrons in the quantum well system has an abrupt edge that concentrates electrons in energy states that contribute to laser action. Simple quantum well diode described above is that the thin layer is simply too small to effectively confine the light. To compensate, another two layers are added on, outside the first three, in below Fig.2.9 we only showed center layer and cladding layer. These layers have a lower refractive index than the centre layers, and hence confine the light effectively.

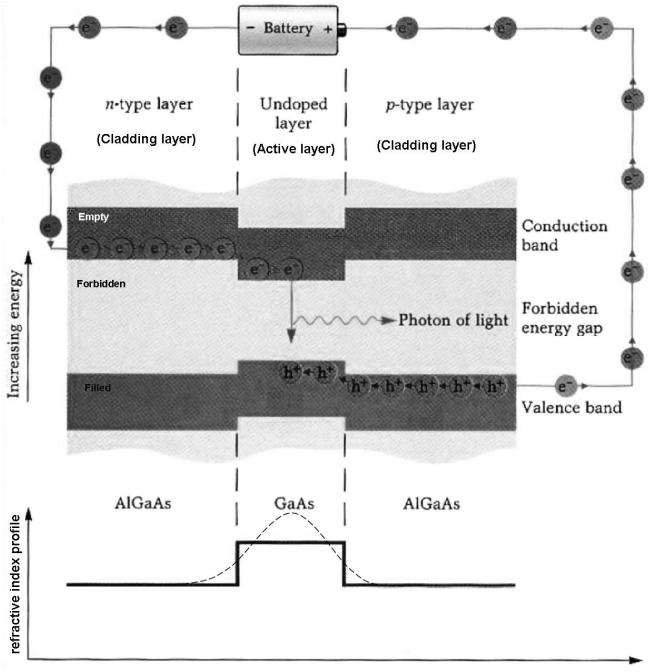

Figure 2.9: Simple quantum well diode

The motion of electrons and holes in a quantum-well are confined in one direction, usually it is growth direction - z axis, and therefore only have two degrees of freedom. This means that they effectively behave as two-dimensional (2-D) materials and electrons and holes are free to move in x and y axis. If the thickness of the quantum-well layer is thin enough quantum confinement effect starts. According to the Heisenberg uncertainty principle if we confine a particle to a region of the z axis (growth direction) of length Δz that represents the quantum well thickness, then we introduce an uncertainty in its momentum can be calculated as,

$$\Delta P_z \sim \frac{\hbar}{\Delta z}. \tag{2.1}$$

In quantum well structure particles (electrons and holes) is otherwise free, and if we assume particle has a mass m, the confinement in the z direction gives it an additional kinetic energy of magnitude

$$E_{confinement} = \frac{(\Delta P_z)^2}{2m} \sim \frac{\hbar^2}{2m(\Delta z)^2}. \tag{2.2}$$

This confinement energy will be significant if it is comparable to or greater than the kinetic energy of the particle due to its thermal motion in the z direction. This condition may be written:

$$E_{confinement} \sim \frac{\hbar^2}{2m(\Delta z)^2} > \frac{1}{2}k_B T. \tag{2.3}$$

and tells us that quantum size effects will be important if

$$\Delta z \sim \sqrt{\frac{\hbar^2}{mk_B T}}. \tag{2.4}$$

This is equivalent to saying that quantum well thickness Δz must be of the order of magnitude as the de Broglie wavelength $\lambda_{deB} \equiv h / P_z$ for the thermal motion.

Various design such as single-quantum-well (SQW), multiple-quantum-well (MQW) and graded-index separate-confinement heterostructures (GRINSCH) have been used for semiconductor lasers, see Fig.2.10.

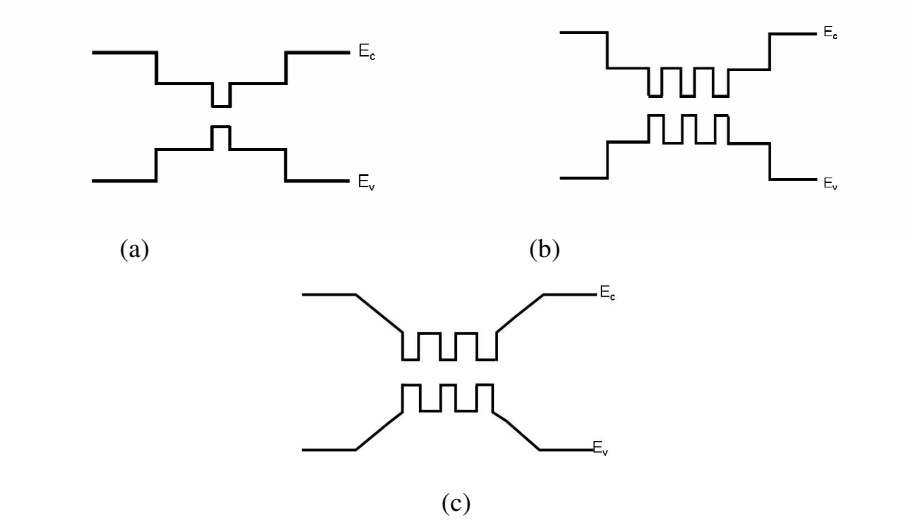

Figure 2.10: Band-gap profiles for (a) single-quantum-well, (b) multiple-quantum-well, and (c) graded-index separate-confinement heterostructure (GRINSCH) semiconductor lasers [19]

Quantum well structures show quantized subbands and steplike densities of states as shown in Fig. 2.11. The density of states for a quasi-two dimensional structure has been used to reduce threshold current density and improve temperature stability.

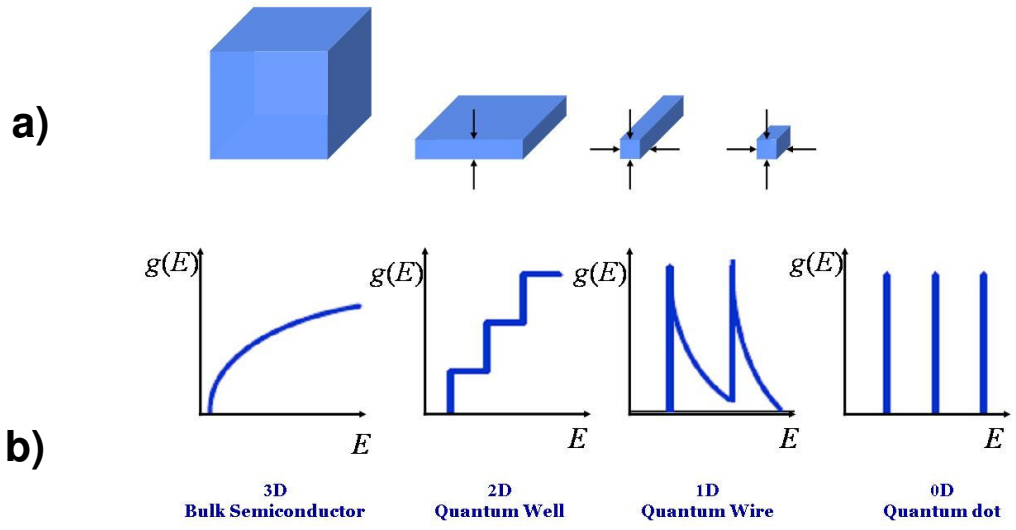

Figure 2.11: (a) Different configurations and (b) corresponding forms of the density of states for bulk, quantum well, quantum wire, and quantum dot semiconductors.

Energy quantization provides another degree of freedom to tune the lasing wavelength by varying the well width and the barrier height. Scaling laws for quantum well lasers and quantum wire lasers show significant reduction of threshold current in reduced dimensions [19].

2.6 Long Wavelength Active Regions

To obtain VCSELs with desired fiber wavelengths at 1.31 and 1.55 μm, the semiconductor must have a band gap such that radiative carrier recombination results in emission near those two wavelengths. Fig. 2.12 shows several III-V and IV semiconductors which have band gaps that can emit light at the desired fiber wavelengths. However, many choices are not feasible, for efficient VCSELs we need direct bandgap semiconductor. Also we need high quality growth of the semiconductor to ensure efficient device performance. This eliminates some mixed group-V alloys (such as phosphide-antimonides) due to miscibility issues. In addition, the limited availability of substrates dictates the materials which may be grown coherently. Large differences in lattice constants lead to the introduction of deleterious mechanical defects. Finally, although not directly related to the active region itself, the material system chosen for long-wavelength emission must also have a compatible DBR material system.

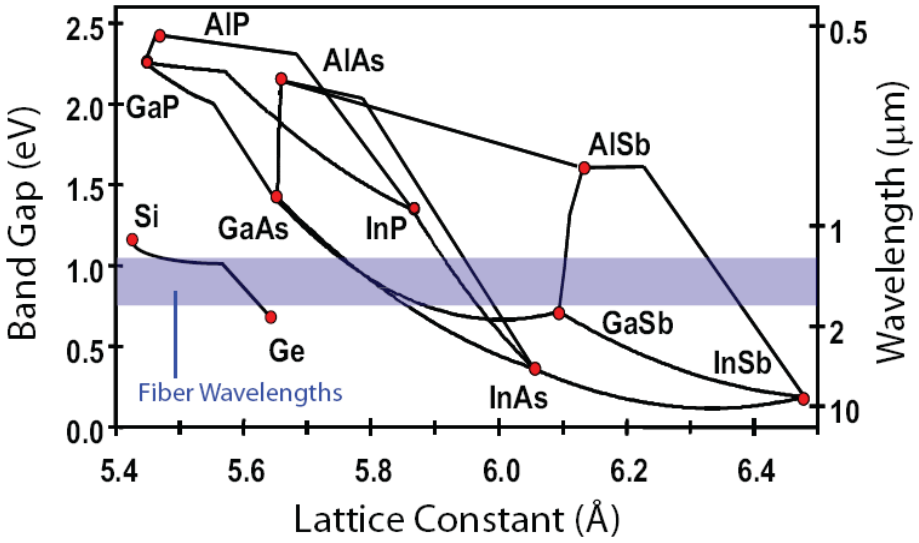

Figure 2.12: Band gap versus lattice constant for a variety of zincblende III-V and IV semiconductors. Ternary alloys are shown as lines between their respective binary consituents. [14]

Current long-wavelength technology employs the InGaAsP alloy grown on InP substrates. InGaAsP has been able to reach 1.55 μm and 1.31 μm, with slightly more difficulty. InGaAsP does have some disadvantages including cost, performance issues, and VCSEL integration difficulties. The properties of InGaAsP lasers have strong temperature dependences [20] due to the heterojunction band alignment to InP. InGaAsP has a relatively small conduction band offset to InP of $\Delta E_c = 0.4 \Delta E_g$ [21, 22]. Electrons have low mass and are more susceptible to escape the confinement of the QW with sufficient thermal energy. As the temperature increases, as it does during operation, electrons will leak out of the QW decreasing efficiency and power by reducing the available gain. To compensate for the decreased gain, additional current is required, further increasing the temperature of the active region. To prevent a thermal run-away process and ensure stable operation, InGaAsP lasers require external cooling packages. This unfortunately increases the cost and makes monolithic integration with other devices more difficult. In addition, as a mixed group-V system, InGaAsP growth is extremely dependent upon many growth parameters, this high sensitivity decreases yield, further increasing the production cost. InP substrates cannot be made in large diameters reliably and are expensive compared to GaAs. Thus, the largest problem with widespread distribution of InGaAsP lasers is cost. These lasers cost several hundreds to thousands of dollars and will never enter the home-user market.

CHAPTER 3

THEORETICAL MODELS

The purpose of this chapter is to describe the theoretical models and relevant to the study of quantum well laser systems which are used throughout the thesis.

3.1. Vegard's Law (Interpolation Method): Semiconductor Alloys Parameter Calculations

Optoelectronic devices often employ alloys of binary materials. Because of the random distribution of elements from the same group within the alloy lattice, exact calculations of material parameters are hardly possible. The most important parameters of a semiconductor are the bandgap and the lattice constant. To calculate the lattice constant of semiconductor alloys, Vegard's law is usually employed [23]. It states that the lattice constant of a semiconductor alloy is calculated by a linear interpolation between the lattice constant of the constituent semiconductor. If one uses linear interpolation, the ternary material parameter (T) can be derived from binary parameters (B's) by

$$T_{ABC}(x) = xB_{AC} + (1-x)B_{BC} \tag{3.1}$$

for alloy of the form given by $A_xB_{1-x}C$. Some material parameters, however, deviate largely from the linear relation of Eqn.(3.1), ternary parameter, in such case, can be very efficiently approximated by the relationship of

$$T_{ABC}(x) = xB_{AC} + (1-x)B_{BC} + Cx(1-x) \tag{3.2}$$

The parameter C is usually called a "bowing" or "non linear" parameter. For most III-V alloy bandgap is typically smaller than the linear interpolation result and so C is positive.

The quaternary material $A_{1-x}B_xC_yD_{1-y}$ is thought to be constructed of four binaries: AC, AD, BC, and BD. If one uses a linear interpolation scheme, the quaternary parameter (Q) can be derived from the binary parameters by

$$Q(x,y) = (1-x)yB_{AC} + (1-x)(1-y)B_{AD} + xyB_{BC} + x(1-y)B_{BD} \tag{3.3}$$

If one of the four binary parameters is lacking (e.g., B_{AD}), the quaternary parameter can be estimated from

$$Q(x,y) = (1-x)B_{AC} + (x+y-1)B_{BC} + (1-y)B_{BD} \tag{3.4}$$

The quaternary material $A_{1-x}B_xC_yD_{1-y}$ is thought to be constructed of three binaries: AD, BD, and CD. The corresponding linear interpolation can be given by

$$Q(x,y) = xB_{AD} + yB_{BD} + (1-x-y)B_{CD} \tag{3.5}$$

If relationships for the ternary parameters (T's) are available, the quaternary parameter can be expressed either as ($A_{1-x}B_xC_yD_{1-y}$)

$$Q(x,y)\frac{x(1-x)\left[yT_{ABC}(x)+(1-y)T_{ABD}(x)\right]+y(1-y)\left[xT_{ACD}(y)+(1-x)T_{BCD}(y)\right]}{x(1-x)+y(1-y)} \tag{3.6}$$

or ($A_{1-x}B_xC_yD_{1-y}$)

$$Q(x,y)\frac{xyT_{ABD}(u)+y(1-x-y)T_{BCD}(v)+(1-x-y)xT_{ACD}(w)}{xy+y(1-x-y)+(1-x-y)x} \tag{3.7}$$

with

$$\begin{aligned} u &= (1-x-y)/2 \\ v &= (2-x-2y)/2 \\ w &= (2-2x-y)/2 \end{aligned} \tag{3.8}$$

For the quinary $A_{1-x}B_xC_yD_{1-y-z}E_z$, the average can be expressed in terms of the nine ternary alloys (ABC, ABD, BCD, ACD, ACE, BCE, ADE, ABE and BDE):

$$P_{ABCDE} = \frac{\sum c_{ijk}P_{ijk}}{\sum c_{ijk}} \tag{3.9}$$

where c_{ijk} are the fractional composition components, e.g. $c_{ijk} = xy(1-y-z)$ for BCD.

3.2. Temperature Effects

Both direct and indirect energy gaps in semiconductor materials are temperature-dependent quantities. The origin of the temperature-dependent bandgap is due to thermal expansion of the lattice and the changes in the electron-phonon interaction. The band edge energy shifts to lower energy as the temperature is increased. The band gap energy of the material decreases due to the temperature relationship of the band gap.

Traditionally, temperature variation of the band-gap energy Eg is expressed in terms of the Varshni formula [24] ;

$$E_g(T) = E_g(0) - \frac{\alpha T^2}{T + \beta} \tag{3.10}$$

where $E_g(0)$ is the band-gap energy at T=0 K, α is in the electron volts per Kelvin and β is closely related to the Debye temperature of the material (in Kelvin).

3.3. Strain Effects (Zinc Blende)

The lattice parameters of the semiconductor materials constituting the well and the barrier are different in the relaxed materials. If one grows a thin layer of the well semiconductor on a thick layer of the barrier semiconductor, the barrier semiconductor imposes its lattice parameter in the well plane. It is thus possible to grow elastically strained quantum wells in compression or tension. The epilayer is under a biaxial stress such that its in-plane lattice constant $a_{\parallel}$ equals the substrate lattice constant a_s. For the purposes of this thesis growth along the (001) direction is only considered. The net strain in the layer plane $\varepsilon_{\parallel}$ is given by

$$\varepsilon_{II} = \varepsilon_{xx} = \varepsilon_{yy} = \frac{a_s - a_e}{a_e} \tag{3.11}$$

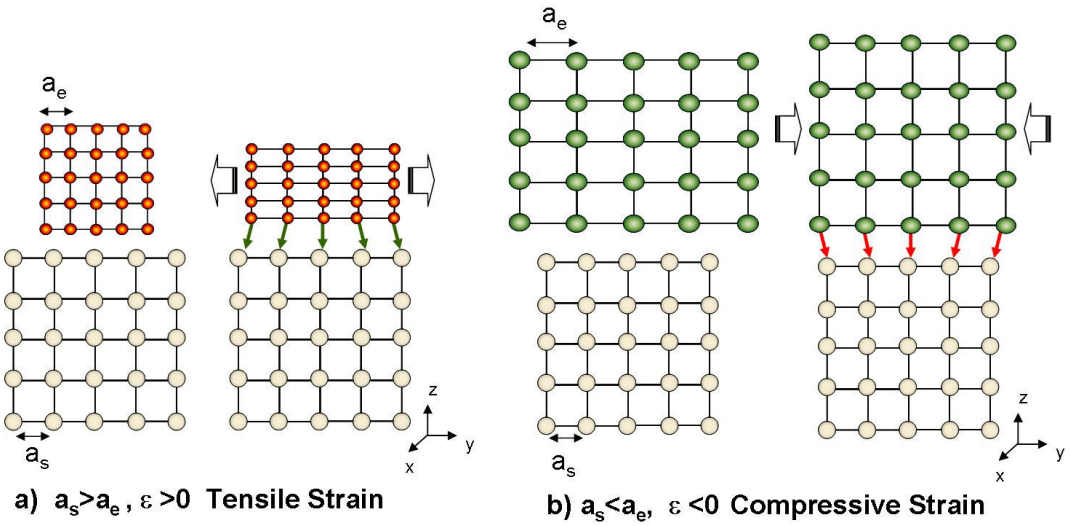

Figure 3.1: Schematic diagram (a) tensile-strained and (b) compressively-strained layers grown on thick substrates

In response to the biaxial stress, the layer relaxes along the growth direction, the strain $\varepsilon_{\perp}$ (= ε_{zz}) being of opposite sign to $\varepsilon_{\parallel}$ and given by

$$\varepsilon_{\perp} = -2\frac{\sigma}{1-\sigma} = -\frac{2C_{12}}{C_{11}}\varepsilon_{\mathrm{II}} \tag{3.12}$$

where σ is the Poisson's ratio and C_{11} and C_{12} is elastic stiffness constants. For compressive strain, $a_e < a_s$, $\varepsilon_{xx} = \varepsilon_{yy} < 0$, and $\varepsilon_{zz} > 0$. The total strain can be resolved into a purely axial component, ϵ_{ax}, given by:

$$\varepsilon_{ax} = \varepsilon_{\perp} - \varepsilon_{\parallel} \approx -2\varepsilon_{\parallel} \tag{3.13}$$

and a hydrostatic component ϵ_{vol} (=ΔV/V), given by:

$$\varepsilon_{vol} = \varepsilon_{xx} + \varepsilon_{yy} + \varepsilon_{zz} \approx \varepsilon_{\parallel} \tag{3.14}$$

the resolution of the strain into components is important when modelling the effects of strain on the band structure of semiconductors. The strain is then a new degree of freedom available to optimize the semiconductor laser, characteristics: the structural modifications with respect to a bulk, relaxed semiconductor, added to the size

quantization effects, lead to drastic changes of the electronic properties. Fig. 3.2 shows that in a compressively strained structure, the heavy hole, light-hole splitting at k=0 increases and the heavy-hole effective mass decreases. This leads to the reduction of the hole density of states, DOS, and thus to a reduction of the threshold current density. Moreover, the light-hole states, which do not participate in the lasing transition, are further in energy from the heavy-hole states compressively strained structures compared to the unstrained one. These states are thus less populated, which leads to an increase of the semiconductor laser efficiency. One can also demonstrate that the differential gain is higher in a strained structure than in a lattice matched one.

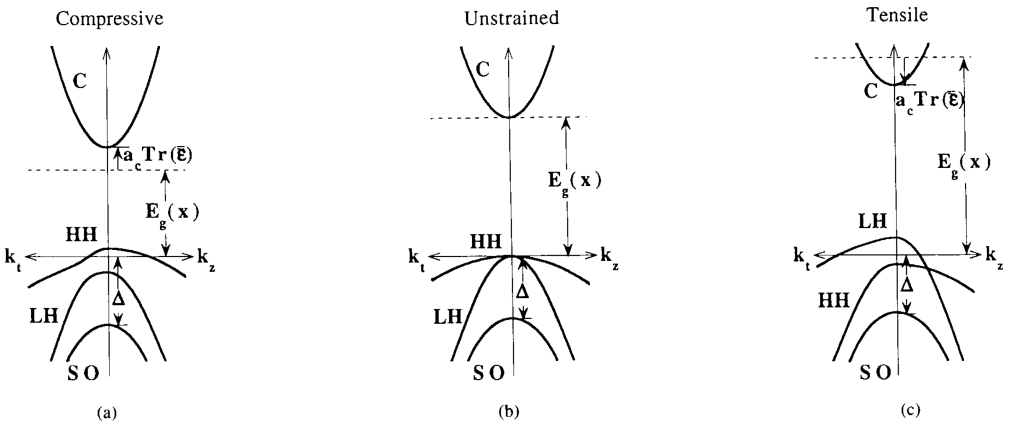

Figure 3.2: Schematic diagram showing the bulk band structure of three $In_{1-x}Ga_xAs$ ternary strained layers grown on InP substrate [25]

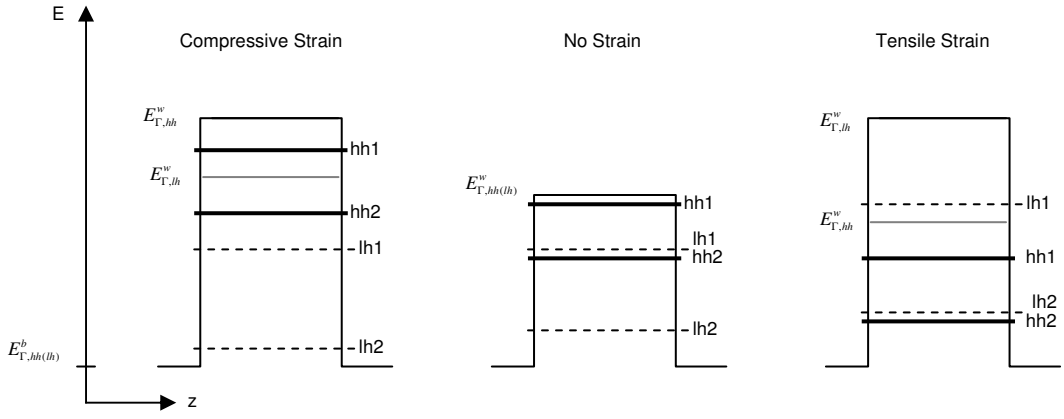

Figure 3.3: Illustration of the positions of confined states in strained and unstrained QW structures. Note that the left and right figures, only the well material is assumed to be strained, which can be seen by considering the bulk band edge labels to the left of each figure. $E^{w}_{\Gamma,hh}$ is the bulk band edge of the well material [26]

The band structure is illustrated in Fig. 3.2 in the k_z direction, the bulk bands are still parabolic with effective masses identical to the unstrained case of

$$m_{hh}^{z} = \frac{m_0}{\gamma_1 - 2\gamma_2} \tag{3.15}$$

$$m_{lh}^{z} = \frac{m_0}{\gamma_1 + 2\gamma_2} \tag{3.16}$$

However, within the k_x-k_y plane, the bands become nonparabolic and the effective masses depend on the wave number. Near the Γ point, the transversal effective masses are [27]

$$m_{hh}^{t} = \frac{m_0}{\gamma_1 + \gamma_2} \tag{3.17}$$

$$m_{lh}^{t} = \frac{m_0}{\gamma_1 - \gamma_2}. \tag{3.18}$$

Strained quantum-well lasers have some advantages like low-threshold current operation, high-power pump lasers. Although most of the early theoretical and experimental work on strained quantum wells focused on compressively strained structures, both compressively and tensile strained quantum-well lasers have been shown to have superior operational characteristics compared with those for the unstrained quantum-well lasers. The major reasons are that the compressively strained quantum wells have a reduced effective mass for the top heavy-hole subband in the plane of the quantum well. This reduced effective mass reduces the density of states and, therefore, lowers the threshold carrier density. It will lead to a reduced Auger recombination rate and a lower threshold current density. While low threshold current densities have been achieved in compressively strained quantum-well lasers, improvements in tensile strained quantum-well lasers have only recently been demonstrated.

3.3.1 Strain Compensated Systems

The magnitude of the strain in the well can be compensated by applying an opposite strain to the barrier. By this way the well width can be increased since the increase in strain cause a critical thickness of the well layer of which the misfit dislocations can occur.

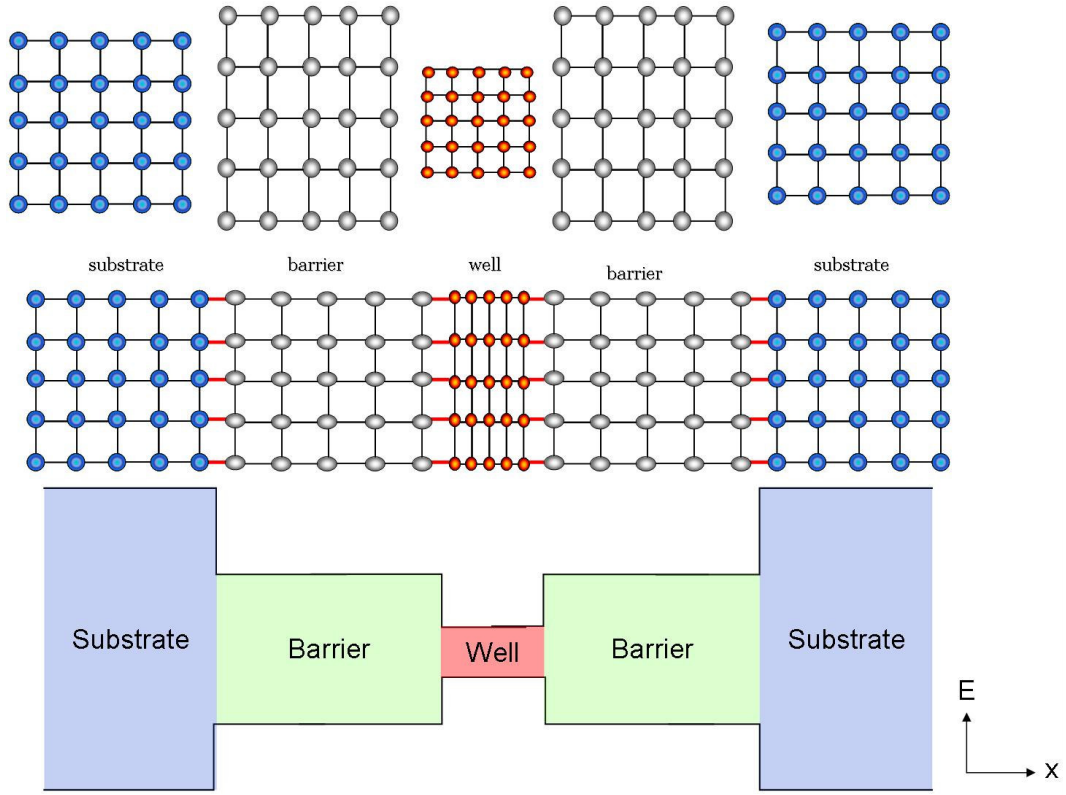

Figure 3.4: Illustration of strain compensated system. Tension in well, compressive strain in barrier

As the number of strained QWs is increased, the total strain in the structure accumulates and the total strained-layer thickness approaches a critical thickness at which lattice misfit dislocations start to form [28].

$$N_w t_w \varepsilon_w + N_b t_b \varepsilon_b \cong 0 \tag{3.19}$$

where N_w, N_b are the number of wells and barriers, t_w, t_b are the thickness of well and barrier and finally ε_w, ε_b are strain in well and barrier.

Experimental results [29,30] showed that the strain compensated QW lasers are desirable for optical applications with low threshold current and high quantum efficiency [28].

3.4. Model Solid Theory

The model-solid theory was first proposed by van de Walle and Martin [31-33], followed by others [34-36], to calculate strain effects on the band lineups. The relative band alignment of the band edges between quantum well and barrier is the total band discontinuity distributed over the conduction and valence bands, ΔE_c and ΔE_v, respectively. The band discontinuity depends on the semiconductors and the amount of mismatch strain at the interface. According to Van de Walle's model solid theory [31], the band offset ratio for conduction and valence band, $Q_{c,v}$, is determined by discontinuity fractions of $\Delta E_{c,v}/\Delta E_g$. The energy of the potential barrier, ΔE_g is determined from the difference between the bulk bandgap energy of the barrier layers and the strained bandgap energy of the active layer.

3.4.1 Model solid theory for unstrained semiconductors

If material A and B have the same lattice constants, we may have an ideal heterojunction and there is no strain in the semiconductors. For this case, the heavy hole and light-hole band edges (E_{HH} and E_{LH}) are degenerate at the zone center, and their energy position is denoted as E_v:

$$E_v = E_{v,av} + \frac{\Delta}{3} \tag{3.20}$$

where Δ is the spin-orbit splitting energy, and the spin-orbit split-off band edge energy E_{so} is

$$E_{so} = E_v - \Delta = E_{v,av} - \frac{2\Delta}{3}. \tag{3.21}$$

The conduction band edge is obtained by adding the band-gap energy E_g to E_v :

$$E_c = E_v + E_g. \tag{3.22}$$

Note that in the model-solid theory, the spin-orbit splitting energy Δ and the band gap energy E_g are taken from experimental results. The band lineups between materials A and B are shown in Fig.3.5.

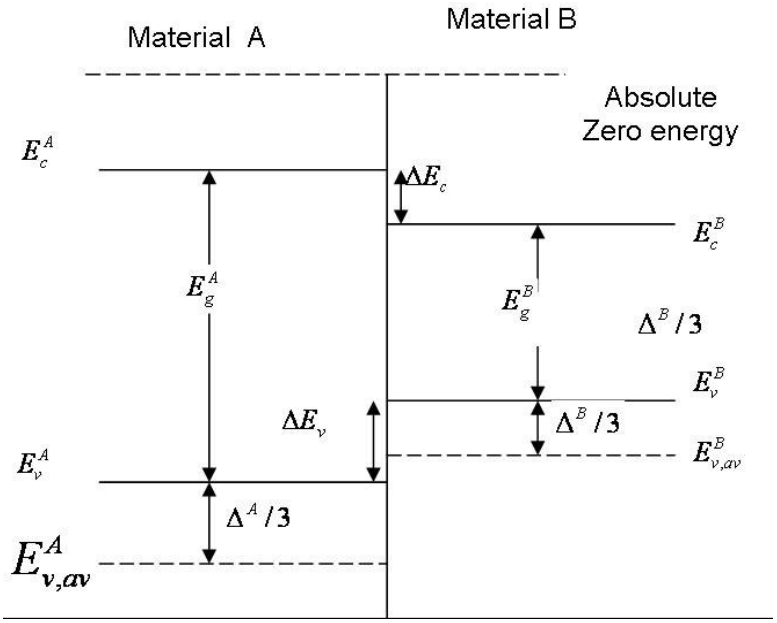

Figure 3.5: Band lineups in the model-solid theory

The bangap difference is

$$\Delta E_g = E_g^A - E_g^B \tag{3.23}$$

and the band-edge discontinuities are

$$\Delta E_c = E_c^A - E_c^B \text{ ,} \tag{3.24}$$

$$\Delta E_v = E_v^B - E_v^A \text{ , and} \tag{3.25}$$

$$\Delta E_g = \Delta E_c + \Delta E_v \tag{3.26}$$

The band offsets ratios of the band-edge discontinuities for conduction and valance bands, respectively,

$$Q_c = \Delta E_c / \Delta E_g \text{ , and} \tag{3.27}$$

$$Q_v = \Delta E_v / \Delta E_g \tag{3.28}$$

are obtained from this theory can also be compared with experimental data.

3.4.2. Model solid theory for strained semiconductors

The band discontinuity depends on the semiconductors and the amount of mismatch strain at the interface. According to Van de Walle's model solid theory [31] the energy of the potential barrier, ΔE_g is determined from the difference between the bulk bandgap energy of the barrier layers and the strained bandgap energy of the active layer.

The conduction band position can be calculated by simply adding the strained bandgap energy to the valence band position. The unstrained valence band-edge of the active region material is set as the reference energy of zero. The valence band position is given by

$$E_v(x,y) = \begin{cases} E_{v,av}(x,y) + \dfrac{\Delta_0(x,y)}{3} + \delta E_{hh}(x,y), & for\ hh\ (compressive\ strain) \quad (3.29) \\ E_{v,av}(x,y) + \dfrac{\Delta_0(x,y)}{3} + \delta E_{lh}(x,y), & for\ lh\ (tensile\ strain). \quad (3.30) \end{cases}$$

where $E_{v,av}(x, y)$ is the average valence subband energy and Δ_0 is the spin-orbit split-off band energy. The conduction band is shifted by the energy $\delta Ec(x, y)$

$$\delta E_c(x,y) = 2a_c\left(1 - \frac{C_{12}}{C_{11}}\right)\varepsilon, \quad (3.31)$$

and the valence bands are shifted by energy, $\delta E_{hh}(x, y)$ and $\delta E_{lh}(x, y)$

$$\delta E_{hh}(x,y) = -P_\varepsilon - Q_\varepsilon \quad (3.32)$$

$$\delta E_{lh}(x,y) = -P_\varepsilon + Q_\varepsilon \quad (3.33)$$

where

$$P_\varepsilon = -2\left|a_v\right|\left(1 - \frac{C_{12}}{C_{11}}\right)\varepsilon \quad (3.34)$$

$$Q_\varepsilon = -b\left(1 + \frac{2C_{12}}{C_{11}}\right)\varepsilon \quad (3.35)$$

where a_c and a_v are the conduction- and valence-band hydrostatic deformation potentials, b is the valence band shear deformation potential and C_{11} and C_{12} are elastic stiffness constants. The absolute value of hydrostatic deformation potential for valance band, a_v, is used to reconcile differing sign conventions found in literature [37,38]. The strained band gaps can then be expressed as

$$E_{c-hh}(x,y) = E_g(x,y) + \delta E_c(x,y) - \delta E_{hh}(x,y) \tag{3.36}$$

$$E_{c-lh}(x,y) = E_g(x,y) + \delta E_c(x,y) - \delta E_{lh}(x,y) \tag{3.37}$$

The conduction band position is

$$E_c(x,y) = \begin{cases} E_v(x,y) + E_{c-hh}(x,y), & for\ hh\ (compressive\ strain); \\ E_v(x,y) + E_{c-lh}(x,y), & for\ lh\ (tensile\ strain). \end{cases} \tag{3.38}$$

(3.39)

The conduction band offset is given by

$$\frac{\Delta E_c}{\Delta E_g} = 1 - \frac{E_v^w - E_v^b}{E_g^b - E_g^w} \tag{3.40}$$

where E_v^w and E_v^b are the valence band positions in the well and barrier materials, respectively, and E_g^w and E_g^b are the strain adjusted bandgaps ($E_{c\text{-}hh}$, for compressive strain and $E_{c\text{-}lh}$, for tensile strain) for the well and barrier materials.

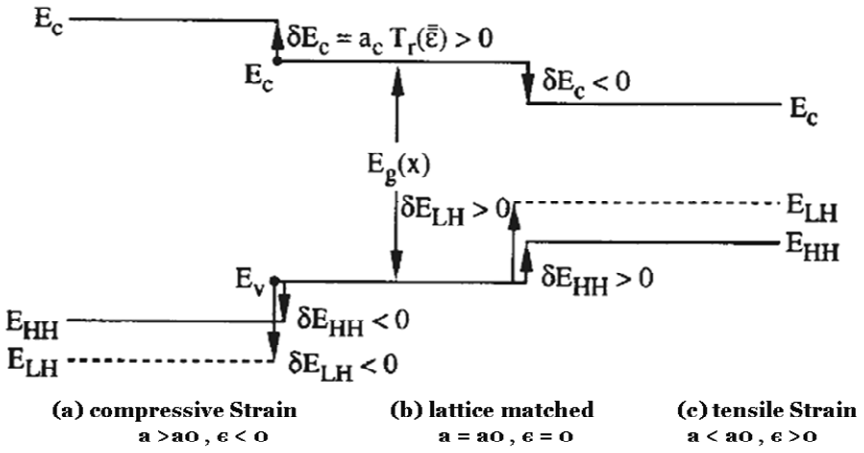

Figure 3.6: Band lineup of (a) compressively strained, (b) lattice matched, and (c) tensiley strained layer [39]

3.5. Band Anti-Crossing Model

While conventional semiconductors have the tendency of increasing bandgap energy with decreasing lattice constant, in the III-N-V system there is a dramatic reduction in fundamental bandgap energy and a huge increase in electron effective mass. Shan *et al* [40] have shown that these unusual behaviours can be quite well understood within a simple band anticrossing (BAC) model.

The proposed model has particular importance since, despite its simplicity, it manages to explain the basic properties of the material and to provide analytical expressions, such as conduction band edge dispersion relations and electron effective mass. The BAC has been successfully used to describe the dependences of the upper and lower subband energies on nitrogen concentration. The model is based on the interaction of the lowest conduction band with the highly localized N-induced energy level E_N.

It has been shown that an anti-crossing interaction of the localized N states with the extended state of GaAs, see Fig. 3.7, or GaInAs leads to a characteristic splitting of the conduction band into two non-parabolic subbands [40]

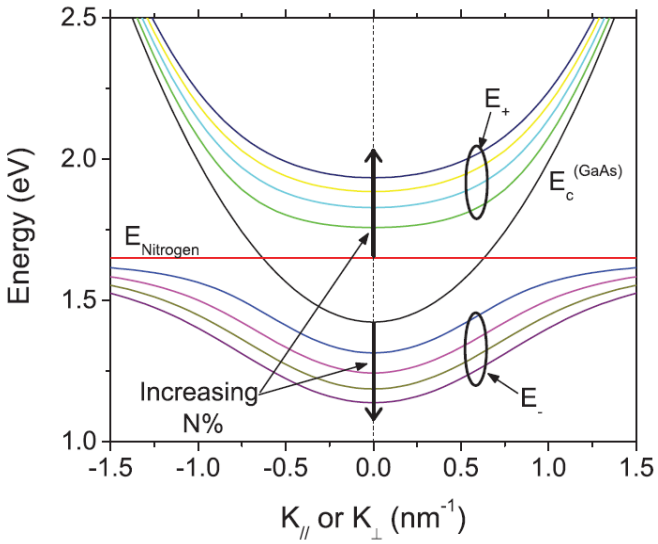

Figure 3.7: Illustration in *k*-space of the band anticrossing effects on the nitrogen level and GaAs conduction band [14]

The interaction between the extended conduction states of the matrix semiconductor (ie. GaAs is matrix semiconductor for GaN_xAs_{1-x} alloy) and the localized N states is treated as a perturbation which leads to the following eigenvalue problem

$$\begin{vmatrix} E - E_M & -V_{MN} \\ -V_{MN} & E - E_N \end{vmatrix} = 0 \tag{3.41}$$

where E_M is the conduction states of the matrix semiconductor, E_N is the localized nitrogen state energy (relative to the top of the valence band) and V_{MN} is the matrix element describing the interaction between these two states. Incorporation of the interaction represented by the matrix element V_{MN} leads to a mixing and anti-crossing of these states [41] equal to;

$$V_{MN} = C_{MN}\sqrt{y} \quad (eV) \tag{3.42}$$

where C_{MN} is the coupling constant and y is the N composition. The solution to this eigenvalue problem gives us the dispersion relation

$$E_{\pm} = \frac{E_N + E_M \pm \sqrt{(E_N - E_M)^2 + 4V_{MN}^2}}{2} \tag{3.43}$$

The predicted splitting of the conduction band into subbands has been confirmed experimentally as can be seen from the Fig. 3.8 [42]. The BAC model provides simple analytic expressions for the conduction band dispersion as a function of N concentration y and allows to calculate, for example, the strength of the optical transitions [43] in bulk materials and the transition energies between electronic states in quantum wells or the gain in laser structures [44].

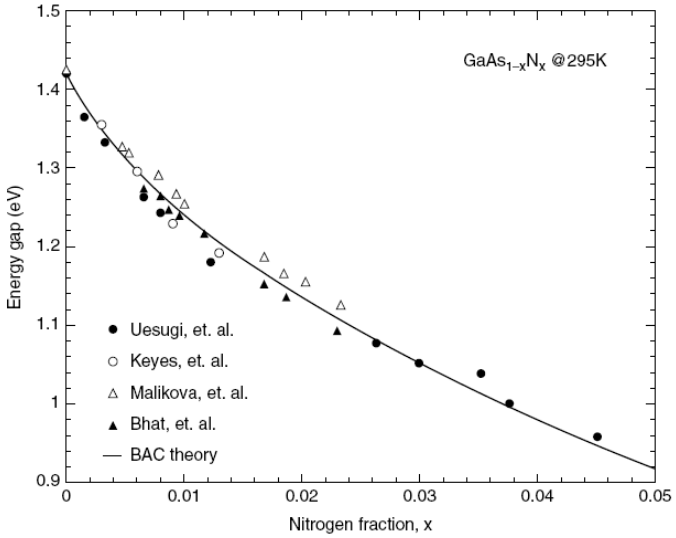

Figure 3.8: Comparison between the experimentally observed and calculated band-gap reduction of GaN_xAs_{1-x} as a function of N concentration. [42]

3.5.1 Electron effective mass

A knowledge of the carrier mass is necessary for analysis of important semiconductor properties. As is well known, the carrier mobility is strongly dependent upon the effective mass. In addition, the knowledge of the effect of the effective mass on gain parameters is of special importance for a full exploration and optimization of III-N-V material system in device applications. Unlike other conventional alloy semiconductors, the electron effective mass increases when the energy bandgap is reduced by adding nitrogen [45]. This has a profound influence on the strength of electron-photon and electron-electron interactions, and consequently on every aspect of the performance (threshold current, etc.) of semiconductor lasers. The change in electron effective mass due to the nitrogen modified conduction band can be found by Skierbiszewski *et al* [46] as

$$m^* = m_M \left[1 + \left(\frac{V_{MN}}{(E_N - E_-)} \right)^2 \right] \tag{3.43}$$

where m_M is the electron effective mass in the parabolic conduction of the semiconductor matrix. m_M is calculated by interpolation of constituent binaries.

CHAPTER 4

ANALYSIS OF THE BAND ALIGNMENT OF HIGHLY STRAINED INDIUM RICH GaInNAs QWs on InP SUBSTRATES

4.1 Introduction

Enormous progress has been achieved in GaInNAs semiconductor alloy on GaAs substrate for both its fundamental properties [40, 47] and its potential applications for 1.3 and 1.55 μm lasers [48,49]. In contrast to this large amount of work reported on dilute $Ga_{1-x}In_xN_yAs_{1-y}$ on GaAs, only a few studies have been published so far on high indium concentration (beyond 53%) $Ga_{1-x}In_xN_yAs_{1-y}$ on InP [50-54]. Gokhale *et al* [52] demonstrated that strained and lattice-matched GaInNAs alloys on InP can extend the wavelength of photonic device operation beyond that accessible to the GaInAsP/InP system.

GaInNAs alloy can be grown without any strain on two common substrates of GaAs and InP, due to the lattice parameters of the four parent compounds of GaN, InN, GaAs and InAs. Anomalous optical properties have been observed in both GaInNAs/GaAs and GaInNAs/InP. For example, the addition of nitrogen to lattice-matched or compressively strained GaInAs on InP results in a sizeable reduction of the band gap energy of the resulting InP based GaInNAs layer, accompanied by a reduction in the lattice constant as it is similar to dilute GaInNAs on GaAs. Increasing the indium concentration in GaInAs on InP beyond 53% results in a decrease of band gap energy. Adding nitrogen to GaInAs reduces the band gap energy even further. Moreover, the incorporation of nitrogen N compensates the compressive strain in the case of $x > 0.53$ and introduces or increases tensile strain in the case of $x < 0.53$, resulting in an additional reduction in band gap for both cases [50].

The relative band alignment of the band edges between the quantum well (QW) and the barrier is very important during modeling semiconductor quantum well structures. This is rather complicated for the strained case. The widely used long wavelength lasers of GaInAsP/InP have poor temperature characteristics at high temperature (25-85 C) due to the small conduction band discontinuity resulting in poor electron confinement in quantum wells. The hole confinement is less of a problem due to the heavier effective hole masses. It has been shown that the band alignment of GaInNAs/GaAs is suitable for high temperature operation due to the large conduction band discontinuity which results in good electron confinement [55]. It has been shown previously [56,57] that the band alignment of GaInNAs/GaAs laser systems can be analyzed by means of Van de Walle's model solid theory ignoring the presence of nitrogen in the average valence band energy values and taking into account the presence of nitrogen in all other laser parameters. The calculated results were in agreement with experimental data [57]. We have recently used [58] model solid theory to investigate the band alignment of GaInNAs for indium concentrations < 0.53. On the other hand, relatively little is known about the band alignment of the growth of GaInNAs containing more than 53% indium on InP substrates so far. Therefore, in this chapter we concentrate on the band alignment of indium rich highly compressively strained GaInNAs quantum wells on InP substrates which allows an emission wavelength of $2.3\,\mu m$ by means of using the model solid theory. Our chosen structures will be those of the structures proposed by Köhler *et al* [51] who demonstrated that long wavelength emission beyond $2\,\mu m$ can be achieved by means of $Ga_{0.22}In_{0.78}N_{0.01}As_{0.99}$ well with lattice-matched $In_{0.52}Al_{0.48}As$ barriers and $Ga_{0.22}In_{0.78}N_{0.01}As_{0.99}$ well with lattice-matched $Al_{0.15}Ga_{0.32}In_{0.53}As$ barrier quantum well laser structures.

4.2 Modelling GaInNAs QWs

The material parameters except for the band gap energies of $Ga_{1-x}In_xN_yAs_{1-y}$ laser systems are linearly interpolated from those of the binary materials [59] and these are tabulated in Table 4.1. For example, lattice constant interpolation scheme of the quaternary material $Ga_{1-x}In_xN_yAs_{1-y}$,

$$a_{GaInNAs} = (1-x)\,y\; a_{GaN} + (1-x)(1-y)a_{GaAs} + xya_{InN} + x(1-y)a_{InAs} \qquad (4.1)$$

where x is the fractional composition of indium, In, and y is the fractional composition of nitrogen, N, in GaInNAs.

Table 4.1: The material parameters of the binaries. The parameters are taken from Vurgaftman et al [59,60] except $E_{v,av}$ values [61]

Material	**GaAs**	**GaN**	**InAs**	**InP**	**InN**	**AlAs**
Lattice Constant a_0 (A)	5.6533	4.5	6.0584	5.8697	4.98	5.6611
Energy gap E_g (eV)	1.424	3.299	0.417	1.4236	0.78	3.099
Spin-orbit Splitting Δ_0 (eV)	0.34	0.017	0.39	0.108	0.005	0.28
Hydrostatic deformation potentia for CB a_c (eV)	-7.17	-6.71	-5.08	-6.0	-2.65	-5.64
Hydrostatic deformation potentia for VB a_v (eV)	-1.16	-0.69	-1.0	-0.6	-0.7	-2.47
Elastic Stiffness Constant C_{11} (G	1221.0	293.0	832.9	1011.0	187.0	1250.0
Elastic Stiffness Constant C_{12} (G	566.0	159.0	452.6	561.0	125.0	534.0
Deformation Potential b (eV)	-2.0	-2.0	-1.8	-2.0	-1.2	-2.3
$E_{v,av}$	-6.92	-	-6.67	-7.04	-	-7.49

The bulk band gap energy of $Ga_{1-x}In_xN_yAs_{1-y}$ is calculated by means of Eqn.3.3. and that of $In_{1-x-y}Al_xGa_yAs$ is calculated according to [62]

$$E_{g_{In_{1-x-y}Al_xGa_yAs}}(x,y)=0.36+2.093x+0.629y+0.577x^2+0.436y^2+1.013xy-2.0xy(1-x-y) \quad (eV)\ . \qquad (4.2)$$

To calculate the band offset, we use Model Solid Theory, needed average valence subband energy $E_{v,av}(x, y)$ are taken from ref [61].

4.3 Important Parameters Within the BAC Model for GaInNAs: V_{MN}, E_N and Electron Effective Mass

GaInNAs material can be modelled by using GaN, InN, InAs and GaAs binaries. The bandgap energy for GaN is 3.3eV for zinc-blende , which is much larger than the bandgap of GaAs 1.4eV. Thus, the rapid bandgap reduction of GaN_yAs_{1-y} [63] or $Ga_{1-x}In_xN_yAs_{1-y}$ [64] cannot be accurately modelled using interpolation, even if a bowing parameter is included in 1999. Semi-empirical Band Anticrossing model can explain the observed conduction band splitting and unusual bandgap reduction of InGaAs with the addition of dilute amounts of nitrogen [65].

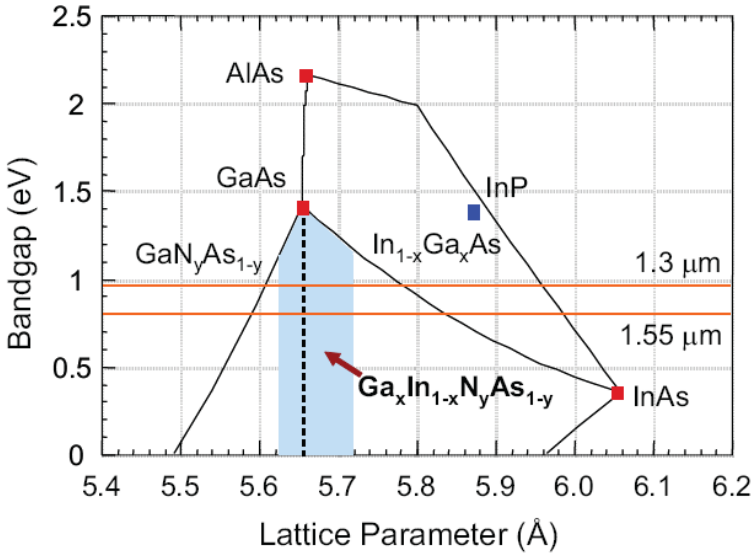

Figure 4.1: Band gap versus lattice parameter showing the effects of adding small amounts of nitrogen to GaAs and InGaAs [14]

Electronegativity of the elements is an important property of which Pauling has described in qualitative terms as "the power of an atom in a molecule to attract electrons to itself". [66]. Nitrogen has a large electronegativity. The electronegativities of Ga, In, N, As, and Sb are 1.81, 1.78, 3.04, 2.18, and 2.05, respectively [67,68]. The values of the electronegativity are plotted in Fig.4.2 for most of the group II, III, VI, V and VI elements [69]. The large electronegativity of N leads to stronger electron localization around the N atom in III-N bonds compared to the column III atoms or even the As or Sb atoms in III-As or IlI-Sb bonds. Since these electronic states are localized in real

space, they are spread out in momentum space and so flat energy-wavevector dispersion is assumed [12].

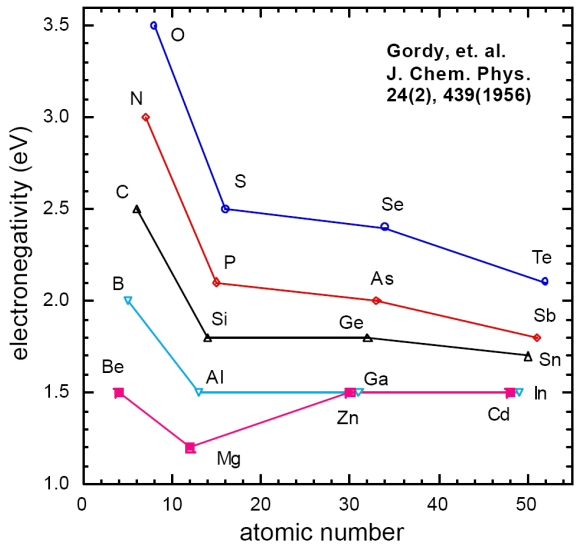

Figure 4.2: Electronegativity of the elements as a function of atomic number [69]

In order for the dispersion relation predicted by the model to reproduce the band structure of the real semiconductor as accurately as possible, the interaction matrix element V_{MN} and the nitrogen level E_N must be determined along with their dependence on composition. In addition, an accurate form for the electron effective mass is required for the calculation of various laser parameters [45] . The E_M is the energy of the InGaAs matrix conduction band and is given as [44],

$$E_M = xE_{InAs} + (1-x)E_{GaAs} - 1,55y \tag{4.3}$$

where y denotes the nitrogen concentration and E denotes the energygap. The energy of the nitrogen level is taken as

$$E_N = 1.52 - \gamma y \tag{4.4}$$

where $\gamma = 2.52$ for GaNAs and $\gamma = 3.9$ for GaInNAs. The strength of the $\Gamma - E_N$ interaction is described by the interband matrix element V_{MN} [45]. The square of the matrix element V_{MN}^2 is proportional to concentration of nitrogen atom as

$$V_{MN} = C_{MN}\sqrt{y}\,. \tag{4.5}$$

V_{MN} is the interaction matrix element between the two bands and y is the nitrogen concentration. E_N and V_{MN} are temperature independent empirical parameters. The value of V_{MN} is not constant and may be composition dependent [40,43,44,46,65,70]. V_{MN} is assumed to be pressure and strain independent, while E_N is slightly pressure dependent. In this thesis, we have used the band anticrossing model with an interaction parameter of C_{MN}=2.3 eV for tensiley strained GaInNAs quantum wells on InP substrates [51] and C_{MN}=2.7 eV for compressively strained GaInNAs quantum wells on GaAs subtrates [71]. Using the parameters we calculate these subband energies of E_- and E_+ for versus nitrogen and indium concentration using Eqn.(3.43) for $Ga_{1-x}In_xN_yAs_{1-y}$ as shown in Fig. 4.3. The lower subband energy E_- shifts towards lower energies with both indium and nitrogen concentration. On the other hand, the higher energy E_+ is almost independent of nitrogen concentration and it slightly increases with indium concentration.

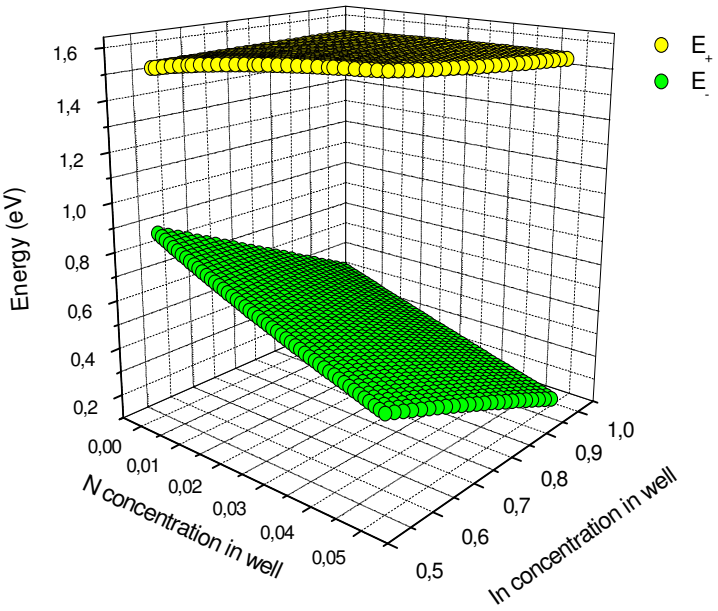

Figure 4.3: Calculated subband energies E_- and E_+ as a function nitrogen and indium concentration for $Ga_{1-x}In_xN_yAs_{1-y}$ on InP substrate , according to BAC model.

As we have mentioned before unlike other conventional alloy semiconductors, the electron effective mass increases when the energy bandgap is reduced by adding nitrogen. We have calculated the change in electron effective mass with increasing nitrogen concentration and increasing indium concentration using Eqn.(3.43) and Eqn.(3.44) for $Ga_{1-x}In_xN_yAs_{1-y}$ on InP substrate system. As can be seen from the Fig.

4.4 the effective mass increases with adding nitrogen concentration but decreased with adding indium concentration to the system.

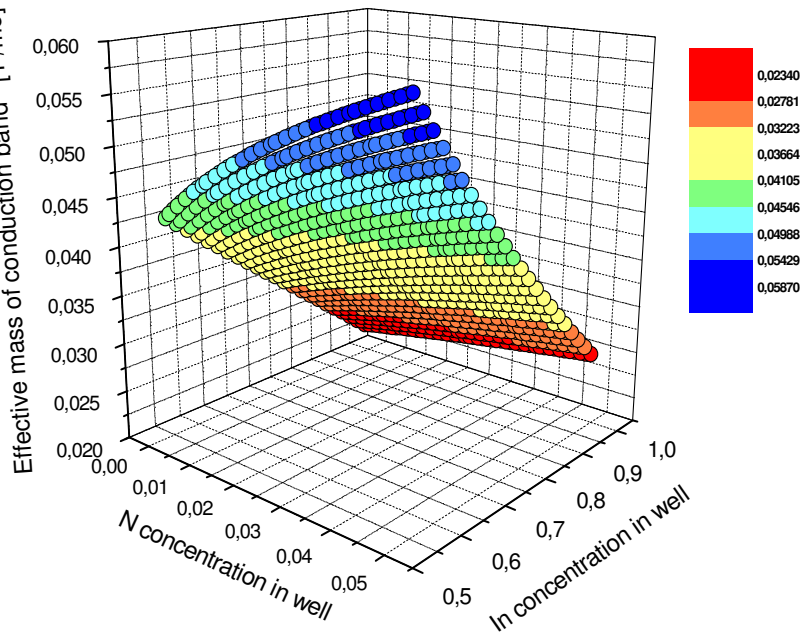

Figure 4.4: The calculated values of electron effective mass with increasing nitrogen and indium concentration for $Ga_{1-x}In_xN_yAs_{1-y}$ on InP substrate, according to BAC model

These calculated results have been shown the unusual and fascinating properties of dilute nitrides. These unusual properties include

i. the giant reduction of band gap energy with decreasing lattice constant,

ii. the appearance of the E_- and E_+ subbands in conduction band, and,

iii. a strong increase of the electron effective mass with decreasing bandgap energy (increasing nitrogen composition).

4.4 Results and Discussions

We first present the band alignment of nitrogen free $Ga_{1-x}In_xAs$ QW on InP substrate in order to provide a comparison of the band alignment of indium rich highly compressively strained $Ga_{1-x}In_xN_yAs_{1-y}$ QWs on InP substrates by means of model solid theory.

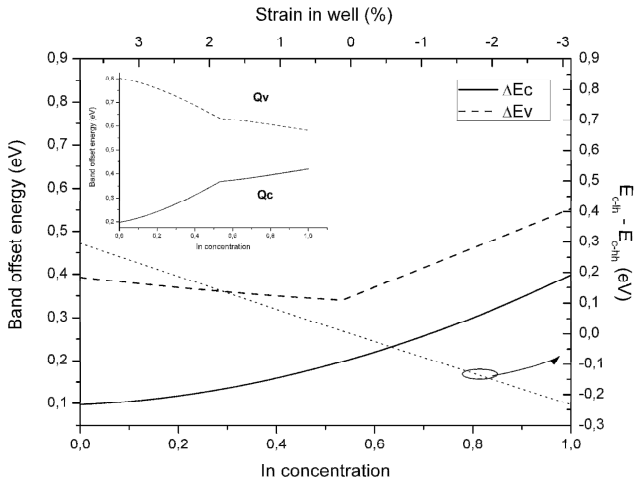

Figure 4.5: The indium concentration dependence of the conduction and valence band offset ratios, Q_c and Q_v, (inset figure) and the corresponding conduction and valence band offsets, ΔE_c and ΔE_v, of the strained $Ga_{1-x}In_xAs$ quantum wells with InP barriers on InP substrates.

Fig. 4.5 presents the band alignment of $Ga_{1-x}In_xAs$ with InP barrier. As can be seen from Fig. 4.5, the valence band offset ratio Q_v is greater than that of the conduction band offset ratio Q_c for the whole range of the indium concentration which is not desirable for high temperature operation. It is seen from Fig. 4.5 that increasing indium concentration of unstrained and strained $Ga_{1-x}In_xAs$ alloy increases the conduction- and decreases the valence-band offset ratio. The $Ga_{1-x}In_xAs$ alloy on InP substrate is compressively strained in the case of $x>0.53$ and tensile strained in the case of $x < 0.53$. The rate of change band offset ratio is different for tension and compression. It is also seen from Fig. 4.5 that the valence band offset ΔE_v is being greater than that of the conduction band offset ΔE_c for the whole range of indium concentrations. Similar calculations have been obtained using lattice-matched GaInAsP and InGaAlAs barriers. It should be noticed from Fig. 4.5 that the wells get deeper in the case of the compressive strain ($x>0.53$) than that of the tensile strain ($x < 0.53$). In addition, although Q_v and Q_c show opposite trend, see Fig. 4.5, with an increase in indium concentration both conduction- and valence-band offsets increase with indium concentration. This strange behaviour of the increase of ΔE_v with decreasing Q_v can be explained as follows; the variation of the valence band offset ΔE_v is a result of the combined effect of the variation of the valence band offset ratio Q_v and the difference of strained band gap of the well and barrier ΔE_g according to $\Delta E_v = Q_v \Delta E_g$. The rapid

increase in $\Delta E_g (= E_{g_{barrier}} - E_{g_{well}})$ with indium concentration eliminates the effect of the decrease in Q_v with increasing indium concentration and results an increase in ΔE_v with increasing indium concentration as an overall. The right-hand-side of the y-axis of Fig.4.5 shows the energy difference between the transition energies of c_1-lh_1 and c_1-hh_1 from the respective band edges. The negative energy difference shows that the polarization transition is transverse magnetic TM since light-hole (lh) band lies above the heavy-hole (hh) band for tensile strain whereas the positive energy difference shows that the polarization transition is transverse electric TE since heavy -hole band lies above the light -hole band for compressive strain.

We want to illustrate at this point how the introduction of N to the well of $Ga_{1-x}In_xAs$ containing more than 53% indium improves significantly the band alignment on InP substrate with InP barriers holding the N concentration being greater than 1.5%. As shown in Fig. 4.6, ΔE_c increases quickly whereas ΔE_v increases slightly with N concentration and ΔE_c becomes greater than ΔE_v when N > 1.5 %. It is also seen from Fig. 4.6 that both wells get deeper with increasing indium concentration. Therefore, in order to achieve long wavelength emission of 2.3μm and more by means of growing GaInNAs on InP with an indium concentration being greater than 0.535, one should keep the N >1.5 % from the band alignment point of view to have high temperature characteristics.

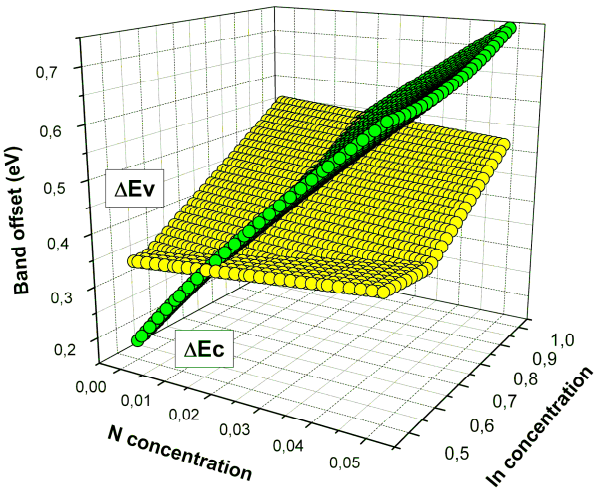

Figure 4.6: The variation of conduction and valence band offsets, ΔE_c and ΔE_v, with nitrogen and indium concentration for compressively strained for $Ga_{1-x}In_xN_yAs_{1-y}$ quantum wells with InP barrier and InP substrate

Köhler *et al* [51] demonstrated the growth of $Ga_{0.22}In_{0.78}N_{0.01}As_{0.99}$ wells with two different lattice–matched barriers of $In_{0.52}Al_{0.48}As$ and $Al_{0.15}Ga_{0.32}In_{0.53}As$ for long wavelength emission up to 2.3 μm. Fig. 4.7 shows our calculated results of the band alignment of $Ga_{0.22}In_{0.78}N_yAs_{1-y}$ well with $In_{0.52}Al_{0.48}As$ barriers. As can be seen from Fig. 4.7, ΔE_c is slightly greater than ΔE_v for the low values of nitrogen. ΔE_c increases rapidly and ΔE_v decreases slowly with an increase of nitrogen and the difference gets bigger for larger nitrogen concentrations.

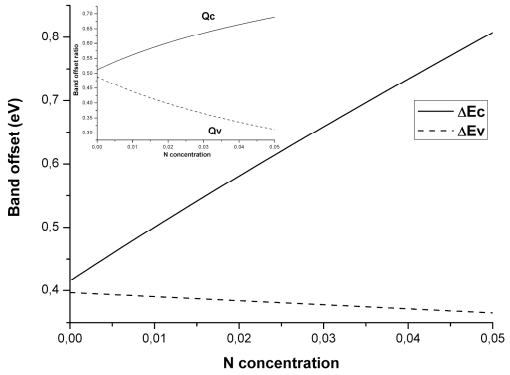

Figure 4.7: The nitrogen concentration dependence of conduction and valence band offset ratios, Q_c and Q_v, (inset figure) and the corresponding conduction and valence band offsets, ΔE_c and ΔE_v, of the compressively strained $Ga_{0.22}In_{0.78}N_yAs_{1-y}$ well with $In_{0.52}Al_{0.48}As$ barriers QW laser system on InP substrates

Fig. 4.8 shows the band alignment of the same QW with a lattice-match quaternary barrier of $Al_{0.15}Ga_{0.32}In_{0.53}As$. It can be seen from Fig. 4.8 that ΔE_c becomes smaller than ΔE_v in the case of the quaternary barrier for low nitrogen concentrations. This brings a disadvantage for the confinement of electrons and results poor temperature characteristics. Therefore, the ternary barrier should be preferred compared to the quaternary barrier. On the other hand, conduction band offset gets deeper with increasing N concentration in both laser structures of ternary and quaternary barriers. We would like to emphasize at this point that, Fig. 4.6 illustrates how the band alignment of the growth of GaInNAs QW containing more than 53% indium with lattice matched $In_{0.52}Al_{0.48}As$ barriers on InP substrates compete with the unique band alignment of GaInNAs quantum wells on GaAs substrates. Therefore, $Ga_{0.22}In_{0.78}N_{0.01}As_{0.99}$ well with $In_{0.52}Al_{0.48}As$ barrier on InP substrates can be offered as a laser system having the ideal band alignment.

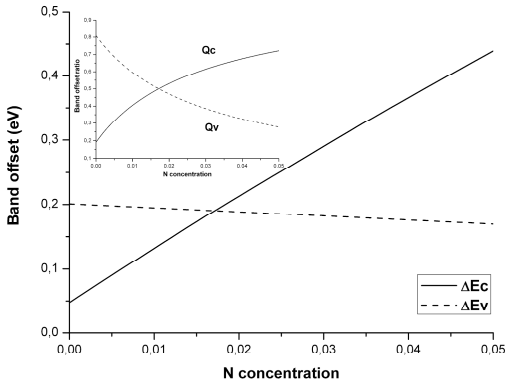

Figure 4.8: The calculated results of the nitrogen concentration dependence of conduction and valence band offset ratios, Q_c and Q_v, (inset figure) and the corresponding conduction and valence band offsets, ΔE_c and ΔE_v, of the compressively strained $Ga_{0.22}In_{0.78}N_yAs_{1-y}$ well with $Al_{0.15}Ga_{0.32}In_{0.53}As$ barriers QW laser system on InP substrates.

We now show how the incorporation of nitrogen into GaInAs with lattice-matched $In_{0.52}Al_{0.48}As$ barrier brings the system having an ideal band alignment although nitrogen free counterpart doesn't have an ideal band alignment. For nitrogen free $Ga_{1-x}In_xAs$ QW with $In_{0.52}Al_{0.48}As$ barrier both conduction- and valence-wells have similar depths as shown in Fig. 4.9. The introduction of nitrogen into $Ga_{1-x}In_xAs$ reduces the energy band gap significantly causing the system having a band alignment of that of the ideal case.

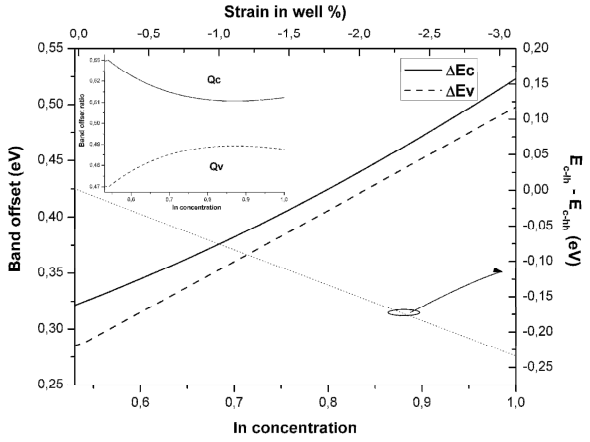

Figure 4.9: The indium concentration dependence of conduction and valence band offset ratios, Q_c and Q_v, (inset figure) and the corresponding conduction and valence band offsets, ΔE_c and ΔE_v, of the nitrogen free compressively strained $Ga_{1-x}In_xAs$ well with $In_{0.52}Al_{0.48}As$ barrier QW laser system on InP substrates.

Fig. 4.10 compares the substrate dependence of strain as a function of nitrogen and indium concentration in $Ga_{1-x}In_xN_yAs_{1-y}$ QW on GaAs and InP substrates. Compressive strain decreases with increasing nitrogen concentration whereas it increases with increasing indium concentration for both substrates of GaAs and InP. This figure reveals the fact that the growth of indium rich $Ga_{1-x}In_xN_yAs_{1-y}$ QW can only be possible on InP substrates since high indium results very high values of the compressive strain in the case of GaAs substrates. This leads to the problem of the critical thickness due to the high compressive strain in the well.

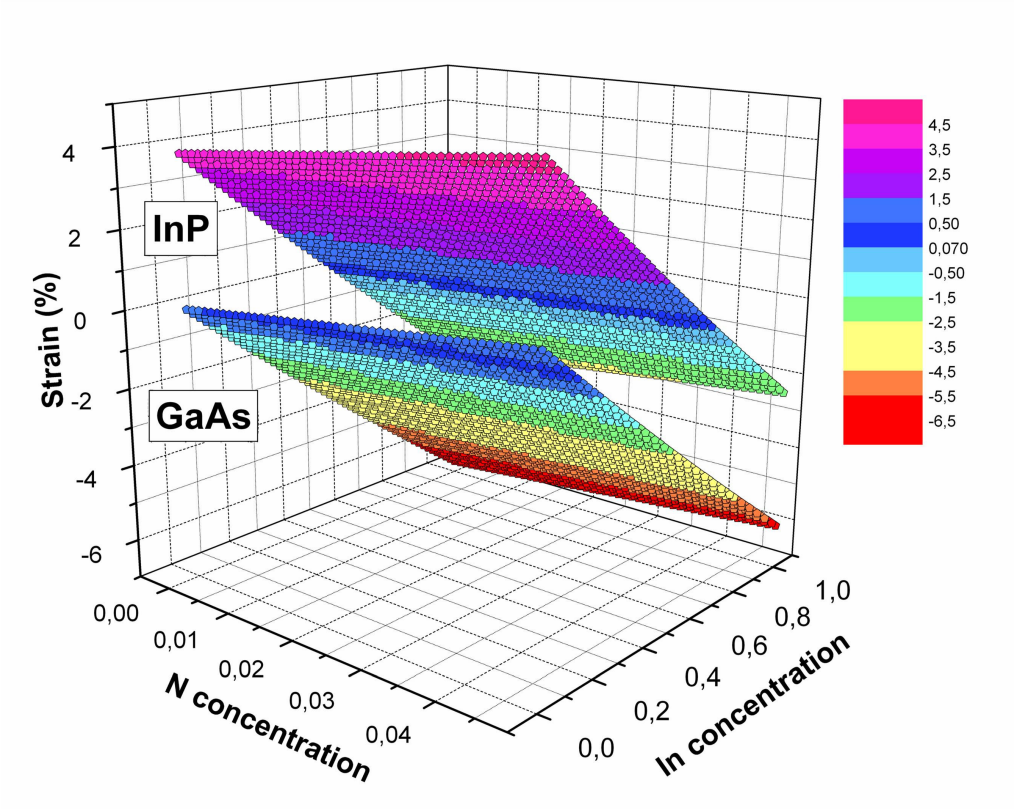

Figure 4.10: The comparison of the substrate dependence of strain as a function of nitrogen and indium concentration in $Ga_{1-x}In_xN_yAs_{1-y}$ QW

It has been stated [50 -54] that long wavelength emission of 2.3 μm can be achieved by means of growing GaInNAs on InP keeping the indium concentration being greater than 0.535 which results compressive strain in conjunction with typical 1-2 % N to compensate the excess strain plus additionally lowering the band gap energy.

4.5 Conclusions

In this work we have examined the band alignment of selected long wavelength laser systems. Our calculations indicate that the band alignment of N-based conventionally strained QW laser systems on InP with high indium concentration (beyond 53%) compete with the ideal band alignment of GaInNAs / GaAs lasers. Therefore, compressively strained $Ga_{1-x}In_xN_yAs_{1-y}$ quantum wells with indium concentrations of $x>0.53$ on InP substrates can be used safely from the band alignment point of view when long wavelength emission of 2.3 μm is required.

CHAPTER 5

THE EFECT of THE INVESTIGATION of THE STRAIN-COMPENSATED BARRIERS ON THE BAND ALIGNMENT of COMPRESSIVELY- and TENSILE-STRAINED GaInNAs QWS on GaAs and InP SUBSTRATES

5.1 Introduction

Recently, there has been much interest in dilute nitride compound semiconductors of GaInNAs. Most attention to date has been focused on GaInNAs/GaAs system, mainly because of its potential for optoelectronic devices covering 1.3-1.5 μm wavelength. Although, the incorporation of nitrogen in GaInNAs allows emission wavelengths as long as 1.55 μm to be reached [49], the optical material quality deteriorate significantly with increasing N mole fractions [72], resulting in a much higher threshold current density of GaInNAs/GaAs lasers compared with that of GaInAs/GaAs lasers. In order to improve the performance of GaInNAs/GaAs quantum well lasers, we must keep nitrogen concentration below the 4 %. In that case if we want to reach longer wavelength we can increase indium concentration in GaInNAs but this leads to an increased strain in the quantum wells. By introducing a strain-compensated barrier to this system it is possible to grow highly strained GaInNAs wells free of misfit dislocations. In strain-compensated QWs opposite strains are introduced in the well and barrier regions. These opposite strains balance each other and the average strain in the structure is reduced. In addition, for some laser configurations, such as short cavity lasers or distributed Bragg reflector lasers, a large number of QWs may be required for optimal performance [73]. As the number of strained QWs is increased, the total strain in the structure accumulates and the total strained layer thickness approaches a critical thickness at which lattice misfit dislocations start to form [74]. In strain-compensated QWs, the well width and the total number of wells can thus be increased, leading to an enhanced optical confinement. By means of introducing strains of opposite signs in the well and barrier layers to simultaneously vary the offsets of the heavy- and light-hole states, it is also possible to reduce the mixing between heavy- and light-hole states by

means of spatially separating them to different layers [75]. Experimental results [76,77] showed that the strain-compensated QW lasers are desirable for optical applications with low threshold current and high efficiency. In addition, strain compensation gives access to a wider range of material composition, and thus improved possibilities to select band-edge offsets tailored to specific needs [78]. Therefore, there has been an interest in strain-compensated quantum well structures. This chapter investigates how the unique features of GaInNAs/GaAs and GaInNAs/InP quantum wells offer the best band alignment. We also investigate the relative band alignment of the band edges of GaInNAs/ InP between the quantum well and the barrier which is very important for modelling semiconductor quantum well structures. The effect of the strain compensation on the band alignments for the GAInNAs on GaAs and InP substrates is examined as well. As far as we know, this is the first theoretical work on the strain compensated GaInNAs on InP substrates .

We used the model solid theory to calculate the band alignment of GaInNAs alloys both InP and GaAs substrates because the systems results were in agreement with experimental data [79]. For the band structures of laser systems, the material parameters except for the band gap energies are linearly interpolated from constituent binary materials, parameters are listed in Table 4.1. The composition dependence of band gap energy of GaInNAs determined by means of band anticrossing model. Band anti-crossing model (BAC) details are given in chapter 3. This model is based on the interaction of the lowest conduction band with the highly localized N-induced energy level E_N, located 1.64 eV above the valence band edge of GaAs for GaInNAs system. We have used the band anticrossing model with an interaction parameter of C_{MN}= 2.3 eV for tensile strained GaInNAs QWs on InP substrates [51] and C_{MN}=2.7 eV for compressively strained GaInNAs QWs on GaAs substrates [41].

5.2 Comparison of Band Alignment of InGaAs and GaInNAs on GaAs Substrate

As can be seen from Fig.5.1 (a) the material band offset energies of ΔE_c and ΔE_v of InGaAs well on GaAs barrier increases with indium concentration. However, the valance band offset ΔE_v energy is greater than conduction band offset energy ΔE_c which is not desired in quantum well lasers. The addition of N to GaInAs causes substantial changes in the band alignments; adding N to GaInAs increases the conduction band offset ratio Q_c and decreases the valence band offset ratio Q_v , see Fig.5.1 (b). At first a rapid and then a gradual change in band offset ratios have been calculated. The corresponding band offsets are also shown in Fig.5.1 (b) which illustrates the fact that the addition of nitrogen into GaInAs leads the N-containing system having a band alignment of that of the ideal case (deep conduction- and shallow valence-wells) certainly.

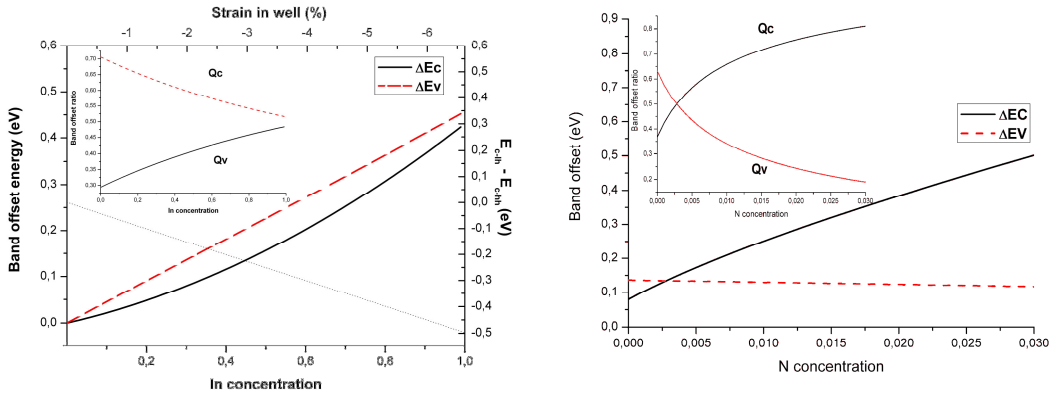

(a) (b)

Figure 5.1: (a) Indium concentration dependence of conduction and valence band offset ratios, Q_c and Q_v, (inset figure) and the corresponding conduction and valence band offsets ΔE_c and ΔE_v of InGaAs well material with GaAs barrier which is grown on GaAs substrate. (b) The nitrogen N concentration (in well) dependence of the conduction and valence band offset ratios, Q_c and Q_v, (inset figure) and the corresponding conduction and valence band offsets ΔE_c and ΔE_v, of the uncompensated compressively strained $Ga_{0.70}In_{0.30}N_yAs_{1-y}$ quantum wells with GaAs barriers on GaAs substrates.

5.2.1 Band alignment of strain compensated GaInNAs/ GaAsP /GaAs system

Figure 5.2 illustrates the effect of compensation of the compressive strain in the well by means of applying tensile strain in the barrier. The well is $Ga_{0.70}In_{0.30}N_yAs_{1-y}$ and the barrier is $Ga_{1-x}AsP_x$. The compressive strain in the well and tensile strain in the barrier is varied by means of increasing nitrogen N concentration in well and phosphorus P concentration in barrier, correspondingly, see figure 5.2. The uncompensated system corresponds to zero P concentration in the barrier. Upper curve represent the variation of the conduction band offset ΔE_c and lower curve represent the valence band offset ΔE_v with nitrogen concentration in well and phosphorus concentration in barrier, correspondingly, for $Ga_{0.70}In_{0.30}N_yAs_{1-y}$ quantum well. First, it should be noticed from the variations of figure 5.2 that ΔE_v (lower curve) decreases and ΔE_c (upper curve) increases with increasing N concentration. It should also to be noted from figure 5.2 that strain compensation by means of using GaAsP barriers instead of GaAs barriers improves the band alignment since ΔE_c further increases with an increase of P concentration in barrier. As an overall, by means of strain compensation, i.e. the increase of P concentration in barrier, it is possible to get deeper wells, leading to much better confinement both in conduction and valence band. Therefore, strain compensation improves the band alignment and brings great advantageous to this laser system of $Ga_{1-x}In_xN_yAs_{1-y}$ with GaAs barrier on GaAs substrate.

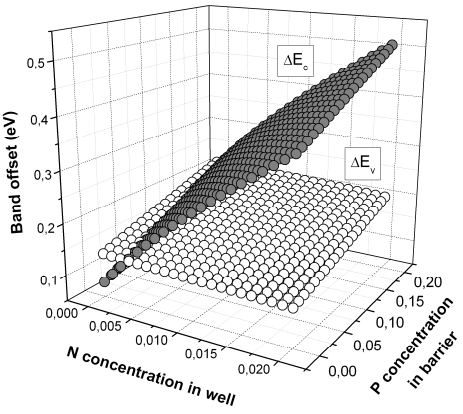

Figure 5.2: The variation of conduction (upper curve) and valance (lower curve) band offsets, ΔE_c and ΔE_v , with nitrogen concentration. The strain is compressive in the well whereas it is tension in the barrier of $Ga_{0.70}In_{0.30}N_yAs_{1-y}/Ga_{1-x}AsP_x$ /GaAs QW system.

5.2.2 Comparison of band alignment of InGaAs and GaInNAs on InP Substrate

It is well known that the $Ga_{1-x}In_xAs$ can be grown lattice matched to InP for x = 0.535. Lowering the indium content or introducing N into the $Ga_{1-x}In_xAs$ induces a tensile strain. A sufficiently high tensile strain will lead the light-hole, lh, band being above that of the heavy-hole, hh, band. So fundamental transition will be due to c_1-lh_1 giving rise a TM-mode polarization emission. There are some reports [80-83] which emphasize the potential advantages of tensile strained QW lasers in terms of threshold current density, radiative characteristics, gain and loss mechanisms. Therefore, it is interesting to investigate the band alignment of $Ga_{1-x}In_xN_yAs_{1-y}$ quantum wells under tensile strain grown on an InP substrate for 1.5-1.6 μm emission wavelength.

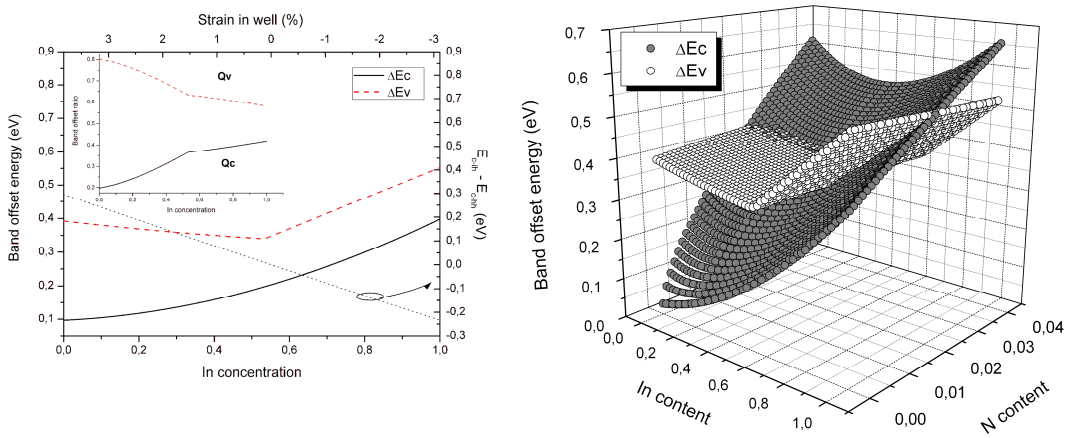

(a) (b)

Figure 5.3 (a) The indium concentration dependence of the conduction and valence band offset ratios, Q_c and Q_v, (inset figure) and the corresponding conduction and valence band offsets, ΔE_c and ΔE_v, of the strained $Ga_{1-x}In_xAs$ quantum wells with InP barriers on InP substrates. (b) The variation of conduction and valence band offsets, ΔE_c and ΔE_v, with nitrogen and indium concentration for compressively strained for $Ga_{1-x}In_xN_yAs_{1-y}$ quantum wells with InP barrier and InP substrate.

In Fig.5.3, we present the band alignment of (a) $Ga_{1-x}In_xAs$ well and (b) $Ga_{1-x}In_xN_yAs_{1-y}$ well with increasing indium concentration with unstrained InP barriers according to the model solid theory. As can be seen from figure we have two region depending indium content, x, below and above 0.535 value. In Fig.5.3 (a) through the all indium region, the valence band offset ratio Q_v is greater than that of the conduction

band offset ratio Q_c which is not desirable for high temperature operation. It is also seen from Fig.5.3 (a) that lowering In concentration of tensiley strained $Ga_{1-x}In_xAs$ alloy decreases both conduction and valence band offset at the expense of increasing the tensile strain in the well. In addition, the valence band offset ΔE_v is greater than the conduction band offset ΔE_c. The right-hand-side of the y-axis of Fig.5.3 (a) shows the energy difference between the transition energies of c_1-lh_1 and c_1-hh_1 from the respective band edges. The negative energy difference shows that the polarization transition is TM since light-hole band lies above the heavy-hole band. We want to illustrate at this point that the introduction of N to the well of $Ga_{1-x}In_xAs$ improves the band alignment on InP substrate significantly; ΔE_c becomes greater than ΔE_v as shown in Fig.5.3 (b). It is clear from Fig.5.3 (b) that ΔE_c increases rapidly and ΔE_v decreases slightly in low indium region of $x \leq 0.535$. Both ΔE_c and ΔE_v increase with increasing In concentration in high indium region of $x > 0.535$. As we have mentioned above when GaInNAs based quantum well laser grown on InP substrate, the behaviour of the band alignment is different in low- and high-indium regions of below 53,5% indium and above 53,5 % indium. Therefore, we now want to examine these regions separately.

5.2.2.1. Low indium (In<0.535%) tensile strained GaInNAs QW

In low indium region ($x < 0.535$), we consider a strain compensated laser device of GaInNAs/InAsP/InP; the well composition is held fixed with a 10% In and 3% N. The arsenide concentration of the barrier of InAsP is varied. This results a compressive strain in the barrier to compensate the tensile strain in the well. Figure 5.4 illustrates the effect of the strain compensation on the band alignment for this laser system; the valence band offset ratio Q_c is being greater than that of the conduction band offset ratio Q_v for the stated range of As concentration and both ΔE_c and ΔE_v increases with increasing As concentration. It is seen from figure 5.4 that compensation decreases the Q_c and increases the Q_v value. Therefore, the compensation can be thought as to bring disadvantageous to this laser system. Fortunately, this is not the case. Although Q_c and Q_v shows opposite trend with compensation, both conduction- and valence-band offsets increases with compensation, as shown in Fig.5.4. This behavior of the increase of Q_v

with decreasing Q_c can be explained as follows; the variation of the conduction band offset is a result of the combined effect of the variation of Q_c and ΔE_g since $\Delta E_c = Q_c \Delta E_g$ and ΔE_g is the difference of the strained bandgap of the barrier and well. The rapid increase in $\Delta E_g (= E_{g_{barrier}} - E_{g_{well}})$ with As concentration eliminates the effect of the decrease in Q_c with increasing As concentration and as an overall results an increase in ΔE_c with increasing As concentration. So compensation again can be considered a solution to balance the tensile strain in the well of GaInNAs alloy on InP substrates as in the case GaAs substrates.

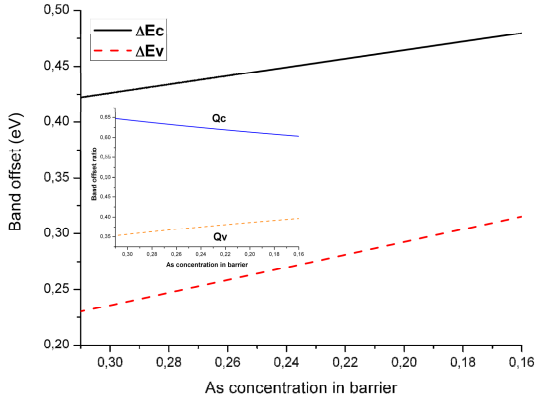

Figure 5.4: The calculated variation of the conduction and valance band offsets, ΔE_c and ΔE_v, with arsenide concentration for compensated $Ga_{0.90}In_{0.10}N_{0.03}As_{0.97}$ / $InAs_xP_{1-x}$ / InP laser system.

5.2.2.2 High indium (In>0.535%) compressively strained GaInNAs QW

We would like to examine at this point how the incorporation of nitrogen into GaInAs with lattice-matched $In_{0,52}Al_{0,48}As$ barrier brings the system having an ideal band alignment although nitrogen free counterparts doesn't have an ideal band alignment. Calculated results of the band alignment shows that ΔE_c is slightly greater then ΔE_v for low values of nitrogen. ΔE_c increases rapidly and ΔE_v decreases slowly with an increase of nitrogen and the difference gets bigger for longer nitrogen concentration.

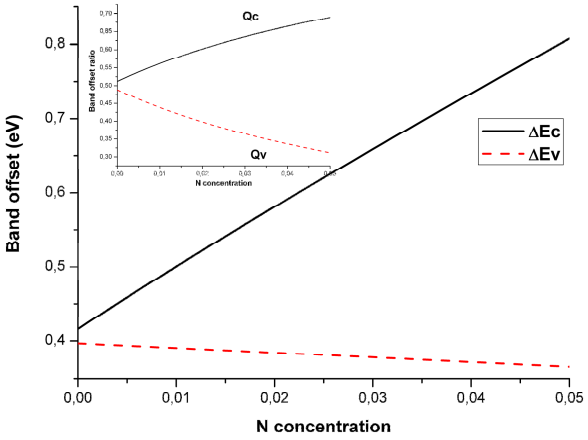

Figure 5.5: The nitrogen concentration dependence of conduction and valence band offset ratios, Q_c and Q_v, (inset figure) and the corresponding the conduction and valence band offsets, ΔE_c and ΔE_v, of the compressively strained $Ga_{0.22}In_{0.78}N_yAs_{1-y}$ well with $In_{0.52}Al_{0.48}As$ barriers QW laser system on InP substrates.

5.3 Conclusions

The design of GaInNAs based devices requires a deep knowledge of the alloy's electronic properties and a development of accurate models. Band alignment of the QWs is one of the important properties while modelling the QW structures since this property determines the high temperature performance of the laser structures. The band alignment of the $Ga_{1-x}In_xN_yAs_{1-y}$ active layers on GaAs and InP substrates in the case of conventionally strained and strained-compensated quantum wells is presented. Our calculated results present that the band alignment of the tensile strained $Ga_{1-x}In_xN_yAs_{1-y}$ quantum wells on InP substrates is better than than that of the compressively strained $Ga_{1-x}In_xN_yAs_{1-y}$ quantum wells on GaAs substrates and both substrates provide deeper conduction wells. Therefore, tensiley strained $Ga_{1-x}In_xN_yAs_{1-y}$ quantum wells with In concentrations of $x \leq 0.53$ on InP substrates can be used safely from the band alignment point of view when TM polarizations is required. Our calculated results also confirm that strain compensation can be used to balance the strain in the well material and it improves especially the band alignment of dilute nitride $Ga_{1-x}In_xN_yAs_{1-y}$ active layers on GaAs substrates.

We also concentrate on the band alignment of indium rich (>53%) highly strained $Ga_{0.22}In_{0.78}N_{0.01}As_{0.99}$ well lattice-matched to $In_{0.52}Al_{0.48}As$ barriers which allows an emission wavelength of the order of 2.3 μm . We have shown that the band alignment of $Ga_{0.22}In_{0.78}N_{0.01}As_{0.99}$ / $In_{0.52}Al_{0.48}As$ quantum wells on InP substrates improves significantly with incorporation of nitrogen concentration and compete with the unique band alignment of GaInNAs/GaAs quantum wells on GaAs substrates.

Our calculations enlighten the intrinsic superiority of N-based lasers and offer the conventionally strained and strain-compensated $Ga_{1-x}In_xN_yAs_{1-y}$ laser system on GaAs and InP substrates as ideal candidates for high temperature operation. If we compare the InP- and GaAs- based GaInNAs at high In concentrations, GaAs substrate have some advantageous with increasing N and In concentrations; band offset energies gets better, E_g decreases quickly, and lasing wavelength gets longer . However, InP based GaInNAs has very low strain compared to GaAs as can be seen from figure 4.10. That's why we can say "In rich GaInNAs QW can only be possible on InP substrate".

CHAPTER 6

THE ROLE of ANTIMONY on THE BAND OFFSETS of GaIn(N)As(Sb) QWs on GaAs and InP SUBSTRATES

6.1. Introduction

The rapid growth of optical communication networks in the last decade has created a significant demand for low-cost, high-performance semiconductor laser sources for the 1.3 and 1.55μm wavelength regimes. Semiconductor lasers operating at 1.3 and 1.55 μm wavelengths are very important light sources for fiber telecommunication. For these wavelengths there are windows of zero dispersion and minimized damping in the currently installed fibres. Up to now lasers at these wavelengths have been almost exclusively fabricated from GaInAsP or AlGaInAs heterostructures on InP. Currently, only the 1.3 μm InGaAsP/InP vertical-cavity surface-emitting diode lasers (VCSELs) seem to close to a commercial availability [84,85] for the wavelength (1.3 and 1.5 μm) optical fibre communication. However, the manufacturing of InGaAsP/InP VCSELs is too expensive and troublesome to become lasing carrier sources in the mass optical-fibre communication. On the other hand, GaAs-based devices are regarded as extremely reliable; their technology is well known and relatively simple. GaAs substrates are much cheaper than InP substrates making the economies of scale favorable towards GaAs-based devices. InGaAsP lasers must use a complex system of InP and InGaAsP (of a different composition) for the distributed Bragg reflectors. The refractive index contrast is low and thus requires a large (~60) number of mirror pairs to obtain a high reflectivity coefficient. For GaInNAs, the mature and well-developed AlAs/GaAs system is used. Refractive index contrast is high and fewer mirror pairs (~30) are required, enhancing heat removal from the active regions of the lasers. The InGaAsP/InP system also suffers from a disadvantageous band lineup. 40% of the band ofsets is found in the condcuction band while 60% of the offsets is in the valence band. For the InGaNAs/GaAs system, 80% of the ofset is found in the

conduction band. This provides better electron confinement and characteristic temperature. Taking advantage of all these remarkable properties GaInNAs/GaAs is considered as a substitutinal material system for InGaAsP/InP. Therefore, much research has been devoted to creating long-wavelength VCSELs on GaAs substrates to leverage the mature AlAs oxidation techniques [86] as well as the large refractive index contrast of GaAs/AlGaAs distributed Bragg reflectors. The GaInNAs material system has generated the most interest as an active material for long-wavelength VCSELs on GaAs substrates primarily because of the large band gap bowing which results from adding relatively small amounts, 1% of nitrogen N [87]. Many researchers have demonstrated 1.3μm VCSELs using GaInNAs as the active material [88-90]. However, there are still essential problems to reach 1.55 μm emissions with these devices. To achieve such a long wavelength emission with GaInNAs/GaAs QWs, the indium concentration should exceed 38% with the high N concentration of about 5%. Because of different crystal structures of GaInN and InGaAs, small sizes of N atoms compared with arsenide As ones and the high electronegativity [91], such a high N concentration leads to creation of many nonradiative centres in the active layer which essentially makes reaching lasing threshold difficult. On the other hand, to reach the 1.55 μm emission GaInNAs/GaAs QWs of lower N concentration and higher In concentration is necessary. Unfortunately, some In segregation, disordering a layer growth and optical degradation of a semiconductor crystal, would follow it. This problem can be overcome in new quinary QW system of GaInNAsSb/GaNAs [91]. It has been recently shown by several groups that the addition of antimonite Sb to the GaInNAs system extends the QW emission wavelength up to 1.55 μm. The photoluminescence properties of 1.5 μm range GaInNAsSb/GaNAs QWs are quite comparable to the 1.3 μm QWs, revealing the positive effect of Sb on improving the optical quality of the QWs. Incorporating Sb to form a quinary GaInNAsSb alloy enables an essential improvement in the quality of semiconductor layers for over 1.5μm emission because Sb (i) acts as a surfactant, improving the surface kinetics thus maintaining two-dimensional growth under high surface stress, (ii) incorporates into the lattice of GaInNAs, shrinking the band gap, and (iii) enhances the differential gain of a laser. All these effects indicate that a quinary QW

might be suitable for 1.4 -1.5 μm lasers. In addition, it has been shown that the surfactant effect of Sb in the GaInNAs system [92,93] enables the growth of GaInNAs quantum wells QWs beyond the calculated critical thickness [94]. The surfactant properties of Sb have also enabled the growth of coherently strained QWs with higher In compositions, 40 % which are necessary for reaching the 1.55 μm wavelength range [95,96].

InGaAs(P) quantum wells grown under tensile strain on InP substrates have been extensively studied for their potential applications in transverse magnetic TM mode polarized lasers and optical amplifiers at 1.55 μm [97]. More recently, they have been used for the fabrication of optical waveguide isolators at 1.3 μm in order to be monolithically integrated with InP-based laser sources [98,99] and wavelength extension up to 1.55 μm has also been investigated [99]. In all these devices the fundamental optical transition induced by tensile strain is the transition between the first electron energy level and the first light hole energy level, giving rise to TM mode light polarization. However, their potential may be limited first because the heterostructures used for device fabrication present a rather poor electron confinement and second because the splitting between the light and heavy hole energ levels has to be larger than the thermal energy, which may be difficult to obtain for QWs emitting around 1.55 μm. Meanwhile, dilute quaternary group-III arsenide nitride compounds InGaNAs grown on GaAs have been studied due to their interest in both their fundamental properties and their potential for laser applications for 1.3 and 1.55 μm. The large conduction band ofset induced by the introduction of nitrogen into InGaAs matrix leads to efficient electron confinement in quantum well. Most attention to date has been focused on $Ga_{1-x}In_xN_yAs_{1-y}$ quantum wells (QWs) on GaAs substrates. Recently, some reports [53,100,101] demonstrated that strained and lattice-matched $Ga_{1-x}In_xN_yAs_{1-y}$ alloys on InP can also extend the wavelength of photonic device operation beyond that accessible to the $Ga_{1-x}In_xN_yAs_{1-y}$/GaAs and InGaAsP/InP system [53]. Increasing In concentration in $In_xGa_{1-x}As$ on InP beyond 53% results in a decrease of the band gap energy which, however, is partially offset by increasing compressive strain. Adding N to $In_xGa_{1-x}As$ reduces the band gap energy even further. Moreover, the incorporation of N compensates for compressive strain in the case of $x>0.53$ and introduces tensile strain in the case of $x \leq 0.53$, resulting an additional reduction of band gap energy for both cases.

It has been stated that tensiley strained $Ga_{1-x}In_xN_yAs_{1-y}$ quantum wells with In concentrations of $x \leq 0.53$ provides the possibility of reaching TM mode emission at 1.55 μm and above in telecommunication band which is difficult to reach with standart InGaAsP strained QW structures [117] . GaInNAs/InP system combined with confinement layers, such as InAsP, could lead to the fabrication of tensile strained QW lasers as well as the development of optical isolators requiring TM polarisation [115, 116]. In addition, GaInNAs on InP have been proposed as an optical source for spectroscopy instead of the InGaAsP material system [54].

Although lots of efforts have been concentrated on the effects of N on the electronic properties of GaInNAs, there has not been any detailed study of the effects of Sb on the band properties of GaInNAsSb. Little work has been done on the effects of N-induced band alignment and no work on the effects of Sb-induced band alignment up to our knowledge. Since the dilute-nitride-antimonides are relatively new, a greater understanding of the heterojunction band offsets is necessary for better design of lasers and understanding of the physical processes in these semiconductor active regions. By means of this theoretical study we try to make clear what effect the addition of antimony would have on the GaAs and InGaNAs band offsets both on GaAs and InP substrates.

6.2. Theoretical Models

6.2.1 Interpolation method

To calculate the lattice constant, elastic stiffness constants and the related parameters we use the linear interpolation of the experimentally determined values of the binary alloy which is tabulated in table 6.1.

Table 6.1: Binary alloy parameters

Material	InN	InAs	InSb	GaN	GaAs	GaSb
Energy gap Eg (eV) at 0K	0.78	0.417	0.235	3.299	1.519	0.812
α (meV/K)	0.245	0.276	0.32	0.593	0.5405	0.417
β (K)	624	93	170	600	204	140
Lattice Constant a_0 (A) at 300K	4.98	6.0583	6.4794	4.50	5.65325	6.0959
Spin-orbit Splitting Δ_0 (eV)	0.005	0.39	0.81	0.017	0.341	0.76
Hydrostatic deformation potential for CB ac (eV)	-2.65	-5.08	-6.94	-6.71	-7.17	-7.5
Hydrostatic deformation potential for VB av (eV)	-0.7	-1.00	-0.36	-0.69	-1.16	-0.8
Elastic Stiffness Constant C_{11} (GPa)	187	832.9	684.7	293	1221	884.2
Elastic Stiffness Constant C_{12} (GPa)	125	452.6	373.5	159	566	402.6
Deformation Potential b (eV)	-1.2	-1.8	-2.0	-2.0	-2.0	-2.0
Ev,av	-	-6.67	-6.09	-	-6.92*	-6.25*

Parameters are taken from [59,60] , $E_{v,av}$ values are taken from ref [103]

A bowing parameter C is usually included in the interpolation of the band parameter P for ternary alloys to account for the deviation from the linear interpolation between two binary alloys A and B (used nonzero bowing parameters are given in table 6.2)

$$P\left(A_{1-x}B_x\right) = (1-x)P(A) + xP(B) - x(1-x)C \tag{3.4}$$

Table 6.2 : Non-zero bowing parameters for ternary alloys formed from Ga, In, N, As and Sb.

Parameter	InAsSb	GaAsSb	InGaSb	InGaAs	InGaN
Eg (eV)	0.67	1.43	0.415	0.477	1.40
Spin-orbit Splitting Δ_0 (eV)	1.2	0.6	0.1	0.15	
Hydrostatic deformation potential for CB ac (eV)				2.61	

The data for the binary alloys and ternary bowing parameters, taken from [12,59,60], are listed in Table 6.1 and 6.2.

Adding bowing parameter in quinary material one must care the interpolation;

EXAMPLE: $In_xAs_{1-y-z}Sb_z$;

$$E_{InAsSb} = \frac{x(1-y-z)E_{InAs} + zxE_{InSb}}{x(1-y-z) + zx} \tag{6.1}$$

Finally with bowing parameter energygap of the InAsSb ternary become;

$$E_{b_{InAsSb}} = E_{InAsSb} - 0.67\left(xz\left(1-y-z\right)\right) \tag{6.2}$$

Other bowing parameters are added in required calculations (Δ, a_c) which are given in Table 6.2. For quaternary alloys $Ga_{1-x}In_xN_yAs_{1-y}$ interpolated using Eqn.(6.3) Where P denotes parameter, i.e lattice constant, spin orbit splitting etc.. Provided that either x or y is strictly between zero and one, i.e. a true quaternary and not a ternary.

$$P_{Ga_{1-x}In_xN_yAs_{1-y}} = (1-x)yP_{GaN} + (1-x)(1-y)P_{GaAs} + xyP_{InN} + x(1-y)P_{InAs} \tag{6.3}$$

For the quinary $Ga_{1-x}In_xN_yAs_{1-y-z}Sb_z$ the average can be expressed in terms of the nine ternary alloys (GaInN, GaInAs, InNAs, GaNAS, GaNSb, InNSb, GaAsSb, GaInSb and InAsSb). If we expand the eqn. 3.9 for $Ga_{1-x}In_xN_yAs_{1-y-z}Sb_z$;

$$P_{GaInNAsSb} = \frac{\sum c_{ijk}P_{ijk}}{\sum c_{ijk}} = \frac{P_t}{P_c} \tag{6.4}$$

where,

$$P_t = (1-x)xyP_{GaInN} + (1-x)x(1-y-z)P_{GaInAs} + (1-x)xzP_{GaInSb} + (1-x)y(1-y-z)PGaNAs + (1-x)yzP_{GaNSb} + (1-x)z(1-y-z)P_{GaAsSb} + (1-y-z)xyP_{InNAs} + xyzP_{InNSb} + (1-y-z)xzP_{InAsSb}$$

$$P_c = (1-x)xy + (1-x)x(1-y-z) + (1-x)xz + (1-x)y(1-y-z) + (1-x)yz + (1-x)z(1-y-z) + (1-y-z)xy + xyz + (1-y-z)xz$$

where,

$$P_{GaInN} = xP_{InN} + (1-x)P_{GaN}$$
$$P_{GaInAs} = (1-x)P_{GaAs} + xP_{InAs}$$
$$P_{InNAs} = (yP_{InN} + (1-y-z)P_{InAs})/(1-z)$$
$$P_{GaNAs} = (yP_{GaN} + (1-y-z)P_{GaAs})/(1-z)$$

$$P_{GaNSb} = (zP_{GaSb} + yP_{GaN})/(z+y)$$
$$P_{InNSb} = (yP_{InN} + zP_{InSb})/(z+y)$$
$$P_{GaAsSb} = (zP_{GaSb} + (1-y-z)P_{GaAs})/(1-y)$$
$$P_{GaInSb} = (1-x)P_{GaSb} + xP_{InSb}$$
$$P_{InAsSb} = ((1-y-z)P_{InAs} + zP_{InSb})/(1-y)$$

Again, it is necessary that at least one of x, y or z is strictly between zero and one so that the denominator is nonzero. One must avoid over generalizing the averaging techniques, as averaging over three quaternary alloys to make up the quinary would give incorrect result. Eqn.(3.9) will only be used sparingly for III-N-V semiconductors since the addition of nitrogen strongly affects many parameters.

The temperature dependence of most parameters is ignored except for bandgap, which is modelled by Varshni eqn. which is already explained in chaper 3. We added temperature effect for all ternary semicondcutor alloys and then obtain the quinary energygap.

6.2.2 The band anti-crossing parameters

As we have mentioned before the band anticrossing model (BAC) explains the conduction band modification due to the presence of nitrogen in GaInNAs and GaInNAsSb alloys. The model has been successfully used to quantitatively describe the dependencies of the upper and lower subband energies on N concentration and on hydrostatic pressure of group III-N-V alloys [65, 104-106]. As given in chapter-3, the low energy edges of the subbands,

$$E_{\pm} = (E_N + E_M \pm [(E_N - E_M)^2 + 4V^2{}_{MNN}]^{1/2})/2 \qquad (6.5)$$

where E_M and E_N are the energies of the extended state and of the N level relative to the top of the valence band, respectively, and V_{MN} ($V_{MN}=C_{MN}\sqrt{y}$ eV, [41] where y is the N concentration) is the matrix element of the term describing the interaction between localised N states and the extended states. C_{MN} is 2.7 eV for GaAs and 2.3 eV for InP substrate. For GaInNAs alloy, the nitrogen level dependence on the nitrogen

concentration is E_N=1.52-3.9 y [44]. The conduction band energy E_M of the matrix semiconductor is taken to vary in the presence of nitrogen as $E_M=E_0$-1.55 y where E_0 is the energy in the absence of nitrogen [44]. E_- transitions shifts towards lower energies with increasing N concentration, on the contrary, E_+ transition shifts towards higher energies with increasing nitrogen concentration, and its intensity increases relative to the E_- intensity [40, 65,107].

The effect of adding antimony to GaInNAs to obtain $Ga_{1-x}In_xN_yAs_{1-y-z}Sb_z$ alloy has not been well parameterized. Combining literature results [12] and used models in this thesis we choose the values for E_N and V_{MN} of GaInnAsSb material system as

$$E_N = 1.65 - 0.2z \quad (eV) \tag{6.6}$$

$$V_{MN} = 2.7 - 0.7x + z \quad (eV) \tag{6.7}$$

E_M of the matrix semiconductor is taken as $E_M=E_0$ where E_0 is the energy in the absence of nitrogen (GaInAsSb).

Fig.6.1 shows the variation of the strained bandgap energy versus lattice constant without the quantum well confinement energy. The three long adjacent curves that extend from the top left to the bottom right of the figure are $In_xGa_{1-x}As$, $In_xGa_{1-x}As_{0.95}Sb_{0.05}$, and $In_xGa_{1-x}As_{0.9}Sb_{0.1}$, as you go to the next curve on the right.

i) From these curves, there are eleven groups of the three curves that extend to the bottom left of the figure due to the increase of nitrogen from zero to three percent. The eleven groups represent zero to one hundred percent indium in steps of ten percent while the three curves per group represent zero to ten percent antimony in steps of five percent.

The decrease in bandgap due to the increased nitrogen concentration gets smaller with increased indium because the nitrogen and the InGaAsSb bands are more separated and the anti-crossing is weaker.

ii) There are three families of curves corresponding to fixed Sb concentrations of 0%, 2%, and 4%. The family also consists of a series of six shorter thin lines (sloping downward for decreasing lattice constant) that describes the bandgap of $In_xGa_{1-x}N_yAs_{1-y-z}Sb_z$ for fixed In concentrations ranging from 0 to 50% in 10% steps as the N concentration is increased continuously from 0 to 4%.

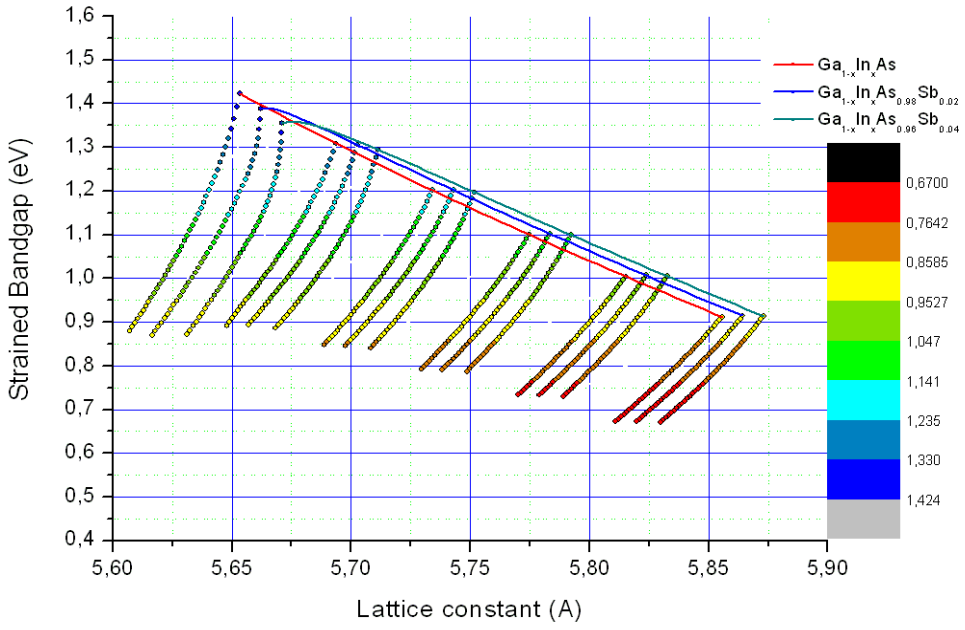

Figure 6.1: The calculated variation of strained bandgap map of InGaNAsSb alloys on a GaAs substrate versus lattice constant without the quantum well confinement energy. There are three families of curves corresponding to fixed Sb concentration s of 0%, 2%, and 4%. Each family consists of a long thick line that describes the bandgap for compositions of $In_xGa_{1-x}As_{1-z}Sb_z$ (nitride free) and six shorter thin lines that describe the bandgap of $In_xGa_{1-x}N_yAs_{1-y-z}Sb_z$ for fixed In concentrations ranging from 0 to 50% in 10% steps as the N concentration is increased continuously from 0 to 4%.

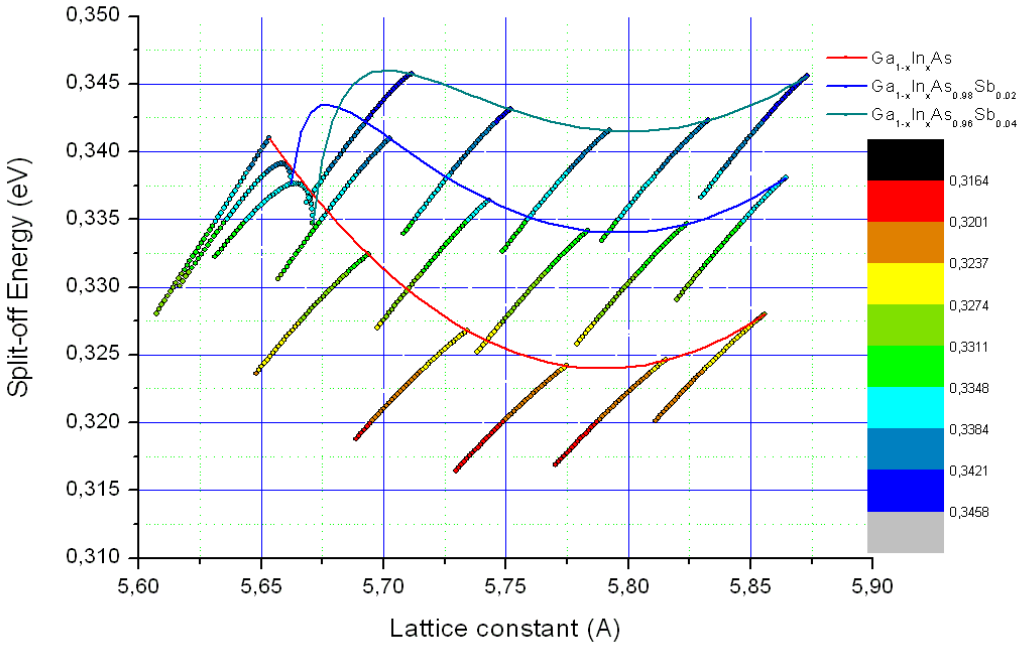

Figure 6.2: The variation of split-off energy, Δ, using the same legend of curve families.

6.3 Calculations and Discussions

In this section, we provide a systematical investigation of the band alignment of quinary GaIn(N)As(Sb) starting from the simplest ternary InGaAs QW system emitting around 1.1 μm and extend the material system to new quinary QW system emitting beyond 1.55 μm.

6.3.1 InGaAs QW on GaAs and InP substrates

The emission wavelength of InGaAs/GaAs QW lasers was limited to 1.1 μm for a long time. Due to the constraints of high strain and limited critical thickness, the optical quality of InGaAs/GaAs QWs degrades rapidly when the indium concentration is higher than 0.35. To get high quality and un-relaxed InGaAs/GaAs QWs with high indium concentration, great care must be taken with respect to the control of the growth condition. Jiang *et al* [108] has shown that by optimizing the growth conditions, especially by using Sb as a surfactant at low temperature it has been successful to grow

highly strained InGaAs/GaAs QWs and extend the emission wavelength to nearly 1.25 μm with a high luminescence efficiency at room temperature. The highly strained InGaAs/GaAs QW laser whose operating wavelength reaches a little beyond 1.2 μm is still a promising candidate for laser applications due to the relatively simple and mature techniques [12,108,109]. Moreover, the proper growth control of highly strained InGaAs QW growth is also an important step for the optimization of GaInNAs QW lasers.

It is well known that $In_xGa_{1-x}As$ can be grown to lattice-matched to InP for x=0.535. Lowering the In concentration of the alloy induces a tensile strain. A sufficiently high tensile strain will lead to a e_1-lh_1 fundamental transition, giving rise to TM-mode polarisation emission. The potential advantages of tensile-strained QW lasers (in terms of threshold current density and loss mechanisms) were predicted more than ten years ago [80-82]. Therefore, in this section we present the substrate dependence of the band alignment of $In_xGa_{1-x}As$ QW by means of Van de Walle's model solid theory.

Fig.6.3 (a) presents the valence band offset ratio Q_v and conduction band offset ratio Q_c of $In_xGa_{1-x}As$ QW on GaAs substrate. We have calculated that Q_v decreases with increasing indium concentration whereas Q_c increases with increasing indium concentration and Q_v / Q_c is in the order of 60/40 for a 30% indium concentration. Fig.6.3 (b) presents the corresponding conduction band offset ΔE_c and valence band offset ΔE_v of $In_xGa_{1-x}As$/GaAs QWs. It is calculated that both ΔE_c and ΔE_v of $In_xGa_{1-x}As$/GaAs QWs increases with increasing indium concentration which cause an increase in compressive strain in turn (see top x-axis of Fig.6.3 (b)). Although Q_v and Q_c show opposite trend with an increase in indium concentration both conduction- and valence-band offsets increase with indium concentration. This behaviour of the increase of ΔE_v with decreasing Q_v can be explained as follows; the variation of the valence band offset ΔE_v is a result of the combined effect of the variation of the valence band offset ratio Q_v and the difference of strained band gap of the well and barrier ΔE_g according to $\Delta E_v = Q_v \Delta E_g$. The rapid increase in $\Delta E_g (= E_{g_{barrier}} - E_{g_{well}})$ with indium concentration eliminates the effect of the decrease in Q_v with increasing indium concentration and results an increase in ΔE_v with increasing indium concentration as an overall. We illustrate the

band alignment configuration of $In_{0.53}Ga_{0.47}As/GaAs$ in Fig.6.3 (c). The valence band offset ΔE_v is greater than the conduction band offset ΔE_c as has been predicted by Fig.6.3 (b).

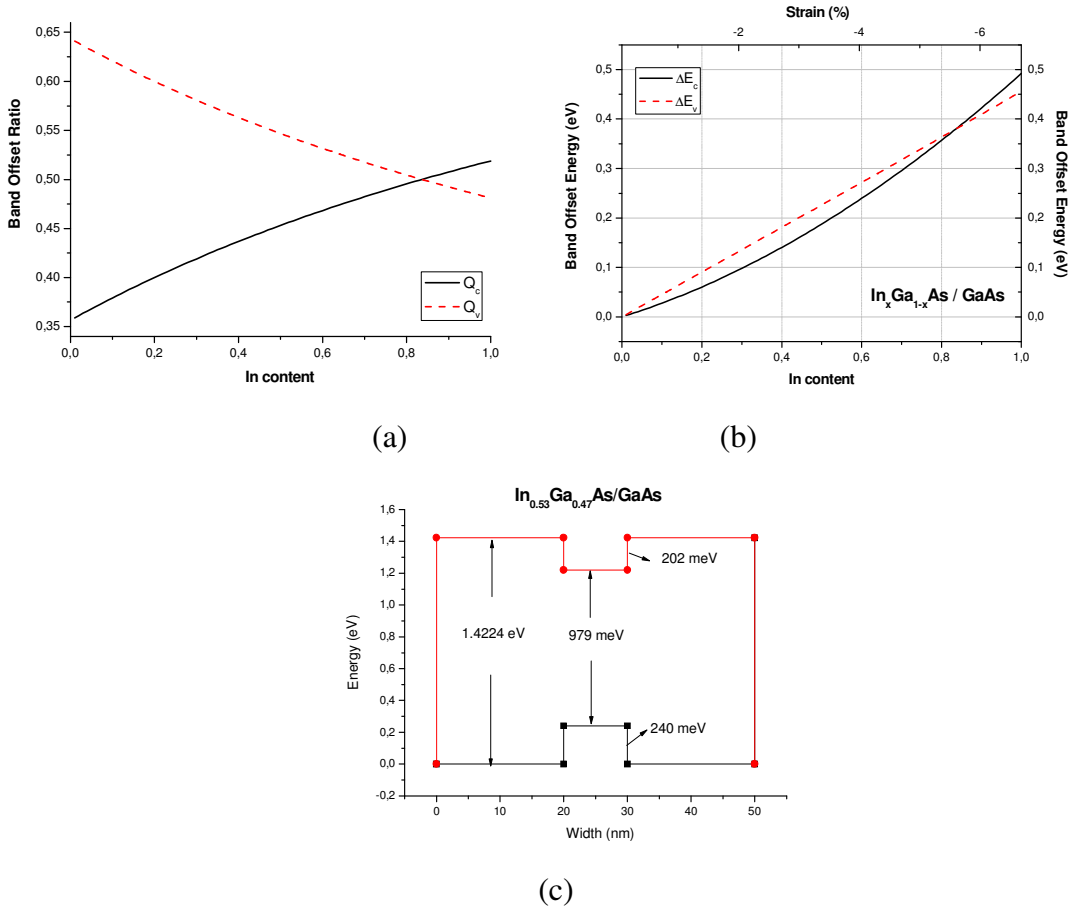

(a) (b)

(c)

Figure 6.3: The calculated variation of (a) valence band offset ratio Q_v and conduction band offset ratio Q_c , and (b) conduction band offset ΔE_c and valence band offset ΔE_v of $In_xGa_{1-x}As/GaAs$ QWs on GaAs substrates as a function of indium concentration, (c) The band alignment configuration of $In_{0.53}Ga_{0.47}As/GaAs$ quantum wells on GaAs substrates.

$Ga_{1-x}In_xAs$ can be grown InP substrate; $Ga_{1-x}In_xAs$ is lattice-matched to InP for an indium concentration of 53%. $Ga_{1-x}In_xAs$ on InP introduces compressive strain in the case of x>0.53 and tensile strain in the case of $x \leq 0.53$. Fig.6.4 provides the similar diagrams in the case of InP substrate and reveals the substrate dependence of $In_xGa_{1-x}As$ QW. As can be seen from Fig.6.4 (a), valence band offset ratio Q_v is much greater than the conduction band offset ratio Q_c for the whole range of indium concentration where Q_v/Q_c is in the order of 80/20 for a 30% indium concentration.

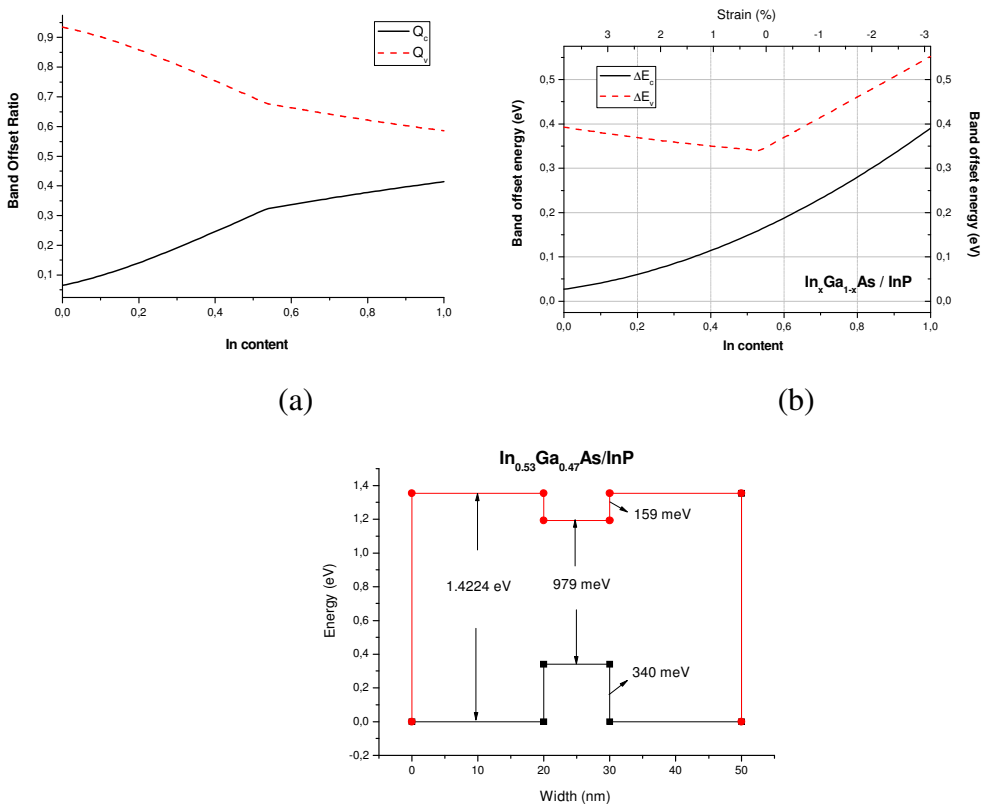

Figure 6.4: The calculated variation of (a) valence band offset ratio Q_v and conduction band offset ratio Q_c, and (b) conduction band offset ΔE_c and valence band offset ΔE_v of $In_xGa_{1-x}As/InP$ QWs on InP substrates as a function of indium concentration, (c) The band alignment configuration of $In_{0.53}Ga_{0.47}As/InP$ quantum wells on InP substrates.

This is a disadvantage since deeper conduction wells are required to eliminate the electron leakage to the barriers. Fig.6.4 (b) illustrates the calculated variation of valence band offset ΔE_v and conduction band offset ΔE_c. The conduction band offset ΔE_c increases rapidly with compressive strain however it decreases with increasing tensile strain. On the other hand, valence band offset ΔE_v increases with both tensile and compressive strain. The band alignment configuration of $In_{0.53}Ga_{0.47}As$ on InP substrates is given in Fig.6.4 (c). As in the case of GaAs substrates, the valence band offset ΔE_v is greater than that of the conduction band offset ΔE_v. However the difference between the two offsets are greater on InP substrate compared to that of the GaAs substrates. Fig.6.4 reveals the negative effect of the InP substrate which cause an increase in ΔE_v and a decrease in ΔE_c when $In_xGa_{1-x}As$ QW is grown on InP substrate.

6.3.2 GaAsSb QW on GaAs and InP substrates

The prospect of realizing active layers for 1.3 μm lasers on GaAs substrate are of special technical interest for making vertical cavity surface-emitting laser (VCSEL) devices [81]. For this purpose, the strained GaAsSb is a potential candidate as demonstrated by Anan *et al* [110] GaAsSb QWs grown on GaAs substrates, with an antimonite fraction of approximately 30% emit at wavelengths near 1.3 μm. However, the critical layer thickness of GaAsSb is limited [80] due to its large lattice mismatch with GaAs substrates and the higher concentration of Sb in GaAsSb/GaAs QW is normally hard to be available for high quality device structures.

We provide in this section the comparison of the band alignment with the incorporation of antimonite Sb in GaAs on GaAs and InP substrates. Fig.6.5 (a) shows the valence band offset ratio Q_v and conduction band offset ratio Q_c of $GaAs_xSb_{1-x}$ as a function of Sb concentration on GaAs substrate. The valence band offset ratio Q_v first decreases for low Sb concentration and then it starts to increase accordingly with increasing Sb concentration on GaAs substrate. The opposite behaviour has been calculated for conduction band offset ratio Q_c, i.e. Q_c first increases with increasing Sb concentration and then it starts to decrease with increasing Sb concentration. The corresponding conduction band offset ΔE_c and valence band offset ΔE_v of $GaAs_xSb_{1-x}$ /GaAs QWs is provided in Fig.6.5 (b). The introduction of Sb into GaAs cause compressive strain throughout whole Sb concentration as shown on top x-axis of Fig.6.5 (b). ΔE_v of $GaAs_xSb_{1-x}$ /GaAs increases with increasing compressive strain. However, ΔE_c of $GaAs_xSb_{1-x}$ /GaAs decreases with increasing compressive strain in general. In addition, it should be noted from Fig.6.5 (b) that the band alignment of $GaAs_xSb_{1-x}$ /GaAs goes from type I to type II beyond 40% Sb concentration. The band alignment configuration of $GaAs_{0.7}Sb_{0.3}$ /GaAs is illustrated in Fig.6.5 (c). As can be seen from Fig.6.5 (c) there is a deep valence well and a very shallow conduction well.

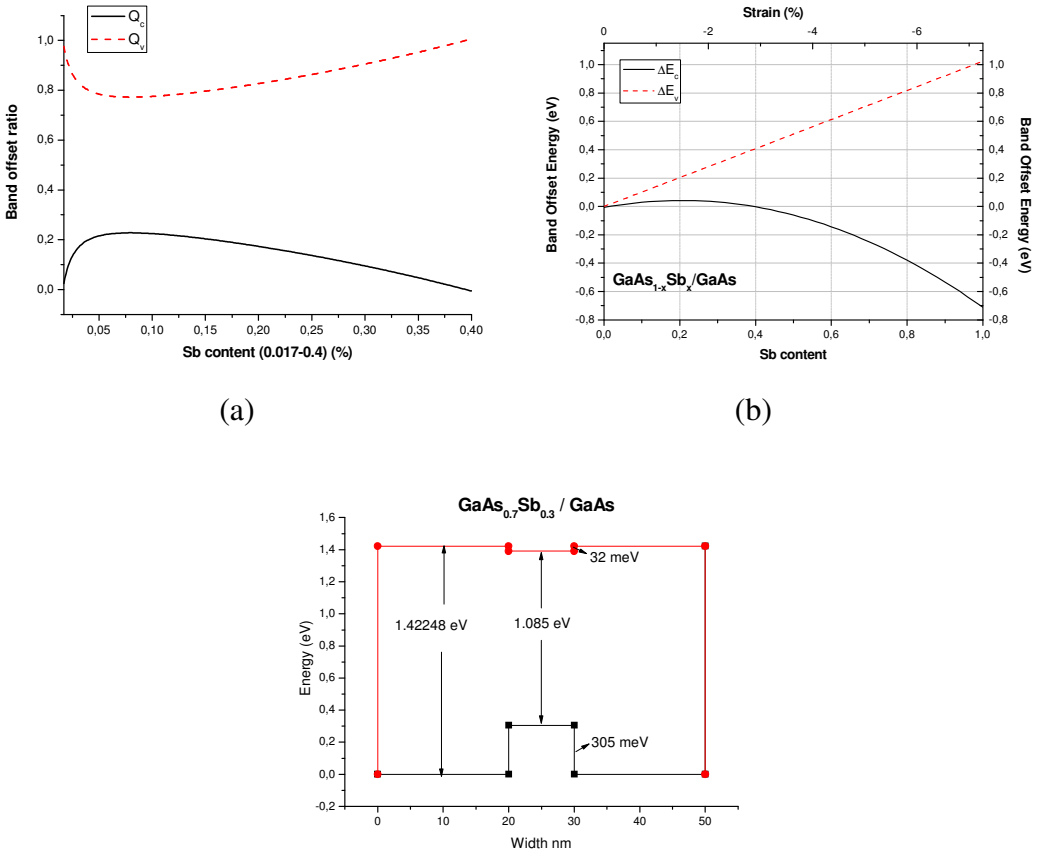

Figure 6.5: The antimony Sb dependence of (a) valence band offset ratio Q_v and conduction band offset ratio Q_c, and (b) conduction band offset ΔE_c and valence band offset ΔE_v of $GaAs_{1-x}Sb_x/GaAs$ QWs on GaAs substrates, (c) The band alignment configuration of $GaAs_{0.7}Sb_{0.3}/GaAs$ quantum wells on GaAs substrates.

We now want to investigate the band alignment of $GaAs_xSb_{1-x}$ on InP substrates and and reveal the substrate dependence of $GaAs_xSb_{1-x}$ QW. As shown in Fig.6.6, the band alignment configuration $GaAs_xSb_{1-x}$ on InP substrate is different than that of the GaAs substrate. The $GaAs_xSb_{1-x}$ well is compressively strained when Sb>50% and tensiley strained when Sb<50%. The band alignment is type I for tension and type II for compression. Although the band alignment is type I for Sb concentrations greater than 50%, $GaAs_xSb_{1-x}$ on InP substrate doesn't have a desirable band configuration. It has a very deep valence well and a shallow conduction well of which it is impossible to confine the electrons in conduction wells.

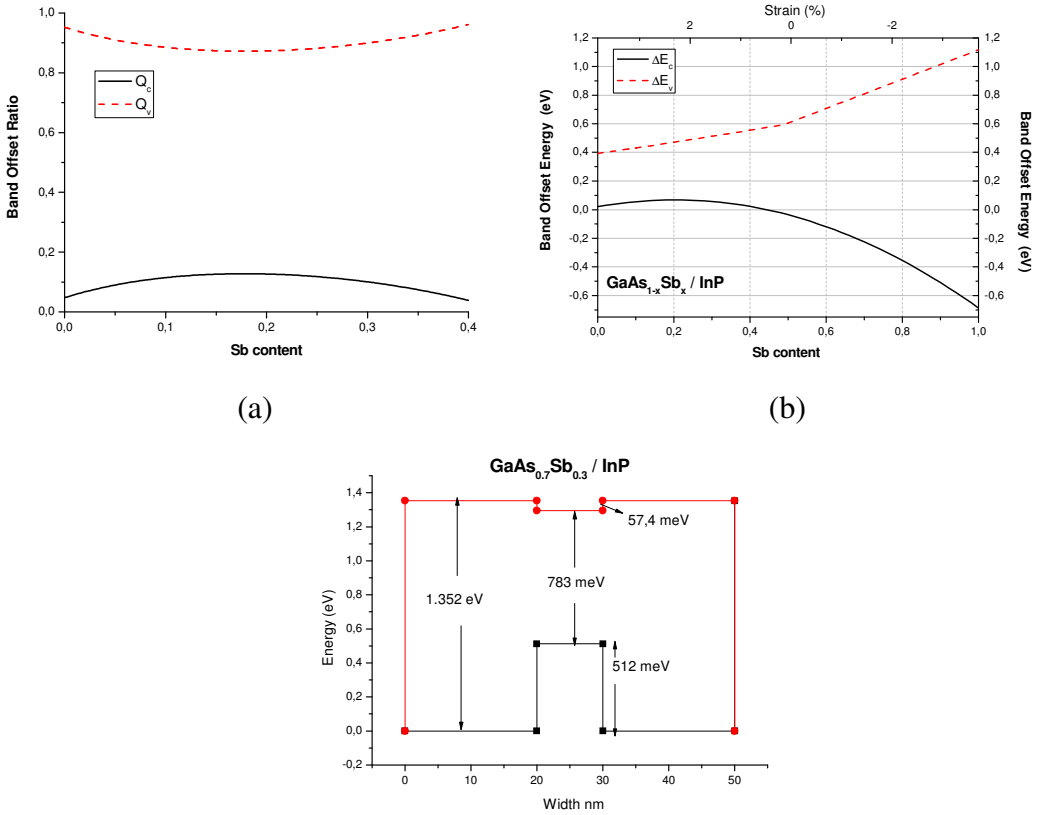

Figure 6.6: The antimony Sb dependence of (a) valence band offset ratio Q_v and conduction band offset ratio Q_c , and (b) conduction band offset ΔE_c and valence band offset ΔE_v of $GaAs_{1-x}Sb_x$/InP QWs on InP substrates, (c) The band alignment configuration of $GaAs_{0.7}Sb_{0.3}$/InP quantum wells on InP substrates.

The comparison of Fig.6.3 and Fig.6.4 with that of the Fig.6.5 and Fig.6.6 reveals that although the magnitudes of strains in both ternaries of $In_xGa_{1-x}As$ QW and $GaAs_xSb_{1-x}$ QW are almost equivalent for layers grown on GaAs and InP substrates, the band alignment gets worse in the case of $GaAs_xSb_{1-x}$. This is due to the fact that the ternary $GaAs_xSb_{1-x}$ has a higher bowing coefficient than $In_xGa_{1-x}As$. As a consequence, for $0<x<0.5$, $GaAs_xSb_{1-x}$ has a lower bandgap than $In_xGa_{1-x}As$ [80].

6.3.3 GaInNAs QW on GaAs and InP substrates

In this section we will provide the band alignment of $Ga_{1-x}In_xN_yAs_{1-y}$ on GaAs and InP substrates. We first present in Fig.6.7 (a) the calculated three dimensional variation of strain in GaInNAs QW grown on GaAs substrate as a function of indium and nitrogen concentration. The compressive strain increases rapidly with In concentration resulting very high values of strain for high In concentration. Fortunately, the magnitude of this high strain can be partially compensated with the introduction of nitrogen into InGaAs. This variation is also illustrated in two dimensional diagram (Fig.6.7 (b)) of strain which shows the indium and nitrogen dependence at the same time. As can easily be seen from this diagram, the addition of small amounts of nitrogen decreases the magnitude of compressive strain in the well of $Ga_{1-x}In_xN_yAs_{1-y}$ on GaAs substrates.

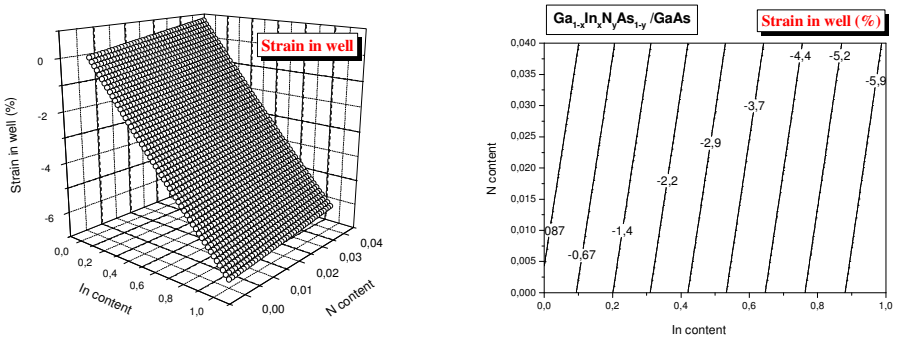

(a) (b)

Figure 6.7: (a) The three dimensional representation of change of variation of strain with indium and nitrogen concentration for $Ga_{1-x}In_xN_yAs_{1-y}$ layers on GaAs substrate, (b) the two dimensional representation of obtion (a).

Fig.6.8 shows the the indium and nitrogen dependence of band offset ratios of $Ga_{1-x}In_xN_yAs_{1-y}$ on GaAs substrates. When the nitrogen concentration is zero, Fig.6.8(a) reduces to Fig.6.3 (a). It is easily seen from Fig.6.8 (a) that the introduction of nitrogen into InGaAs brings significant improvements in the band alignment of $Ga_{1-x}In_xN_yAs_{1-y}$ on GaAs substrates. In order to clarify the improvements we present these variations in two dimensional diagrams of Fig.6.8.(b) and (c) for valence band offset ratio Q_v and conduction band offset ratio Q_c, respectively. The conduction band offset ratio Q_c is

now greater than valence band offset ratio Q_v. This is the desired band alignment which allows good electron confinement. Therefore, the goal of the better electron confinement can be achieved by means of $Ga_{1-x}In_xN_yAs_{1-y}$ /GaAs wells.

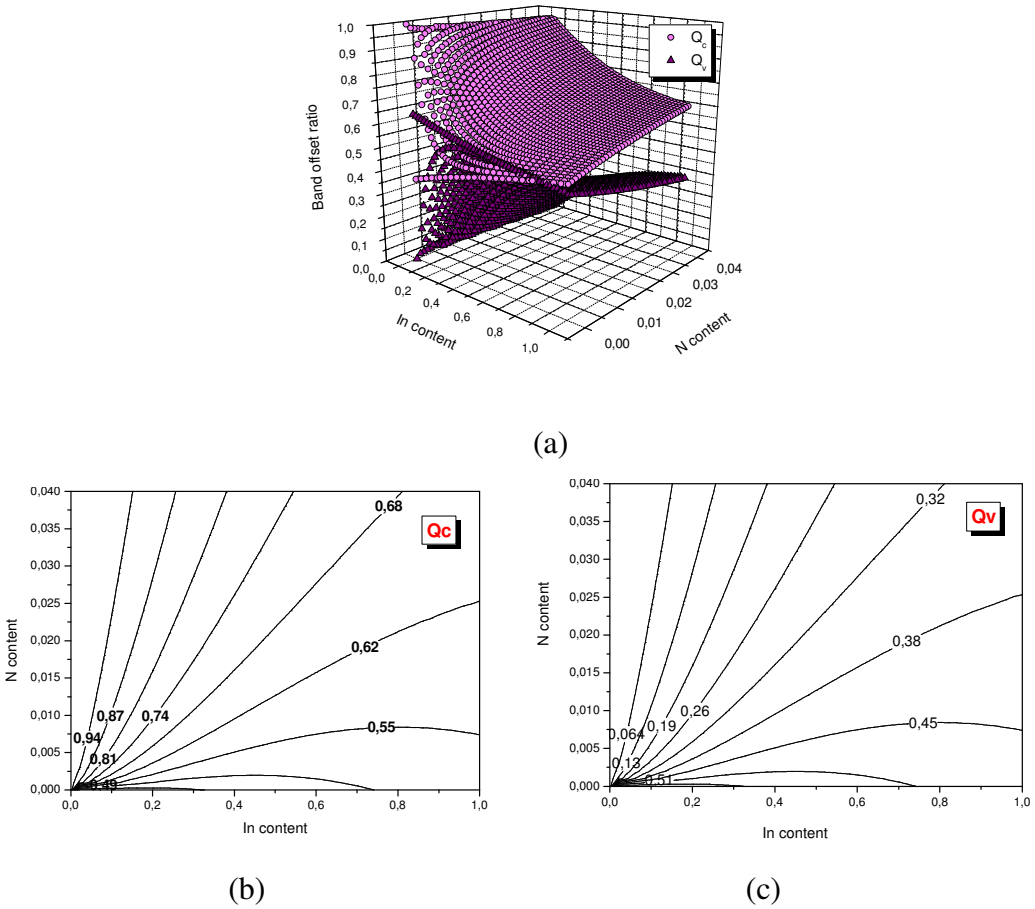

(a)

(b) (c)

Figure 6.8: (a) The illustrated variation of valence band offset ratio Q_v and conduction band offset ratio Q_c with indium and nitrogen concentration for $Ga_{1-x}In_xN_yAs_{1-y}$ layers on GaAs substrates, (b) the two dimensional representation of variation of valence band offset ratio Q_v versus indium and nitrogen concentration, (c) variation of conduction band offset ratio Q_c versus indium and nitrogen concentration.

Fig.6.9 (a) and (b) shows the corresponding valence band offset ΔE_v and conduction band offset ΔE_c, respectively. The introduction of nitrogen into InGaAs firstly cause the conduction band offset ΔE_c is being greater than valence band offset ΔE_v. Secondly, the difference between and ΔE_v gets bigger rapidly with a small increase in nitrogen concentration. Therefore, these figures clearly illustrate how the ideal band alignment can be obtained by means of $Ga_{1-x}In_xN_yAs_{1-y}$ /GaAs wells. This is the

configuraton of the band alignment when the $Ga_{1-x}In_xN_yAs_{1-y}$ dilute nitride quantum wells grown GaAs substrates.

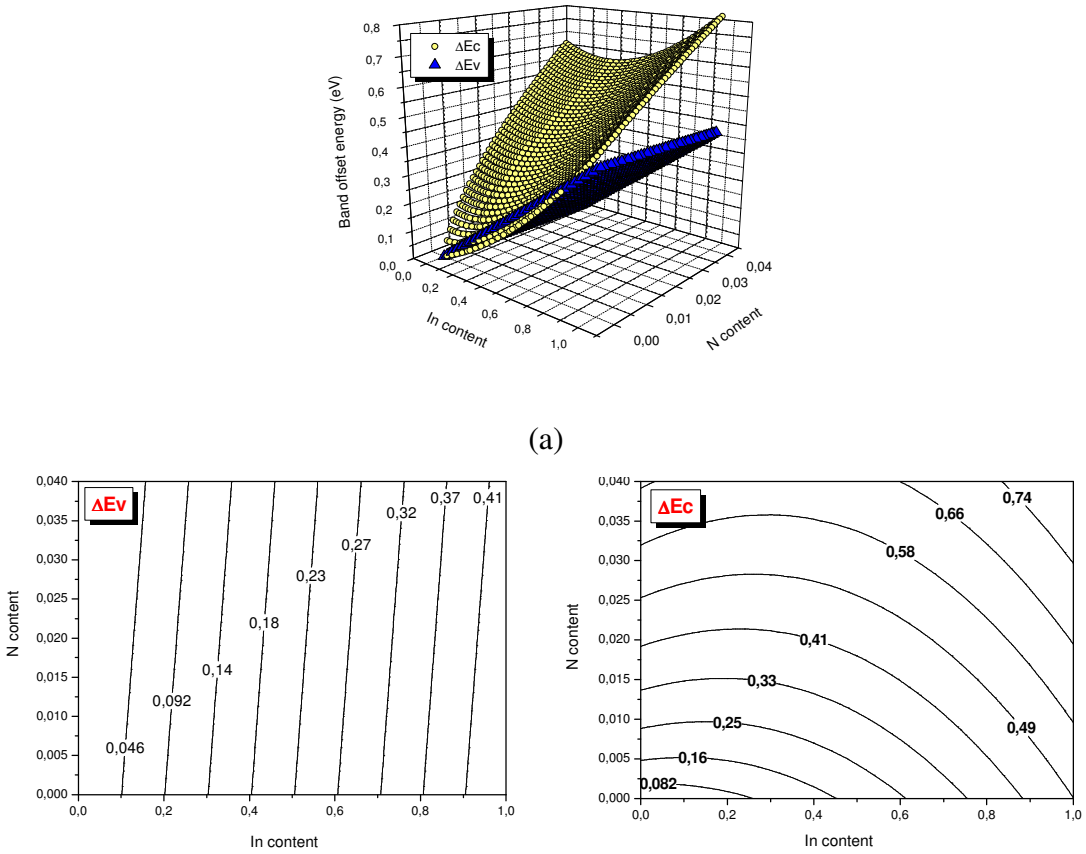

Figure 6.9: (a) The three dimensional representation of change of variation of ΔE_c and ΔE_v with indium and nitrogen concentration. The rate of change of (b) valence band offset ΔE_v (eV) and (c) conduction band offset ΔE_c (eV) as a function of indium and nitrogen concentration for $Ga_{1-x}In_xN_yAs_{1-y}$ /GaAs QWs on GaAs substrates.

We now want to illustrate at this point how the band alignment of InGaAs QWs on InP substrate changes with the introduction of dilute nitrides. The growth of $Ga_{1-x}In_xN_yAs_{1-y}$ on InP substrates results tensile strain for low indium and compressive strain for high indium concentration as shown in Fig.6.10 (a).

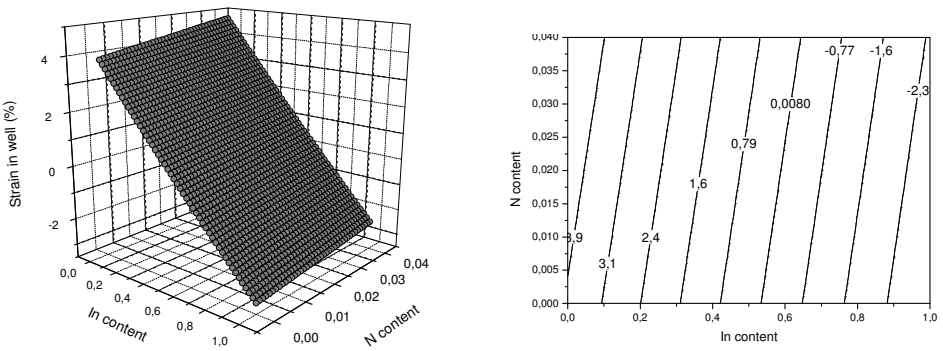

(a) (b)

Figure 6.10: (a) The three dimensional representation of change of variation of strain with indium and nitrogen concentration for $Ga_{1-x}In_xN_yAs_{1-y}$ layers on InP substrate, (b) the two dimensional representation of obtion (a).

The comparison of Fig.6.10 (a) with Fig.6.9 (a) shows that high indium can be safely incorporated on InP substrates due to the decrease in compressive strain. This leads to get longer wavelenghts by means of using dilute nitride quantum wells $Ga_{1-x}In_xN_yAs_{1-y}$ grown on InP substrate. The two dimensional indium and nitrogen dependence of strain of $Ga_{1-x}In_xN_yAs_{1-y}$ QW grown on InP substrates is shown in Fig.6.10 (b). It is seen that although the incorporation of nitrogen decreases the compressive strain, the incorporation of nitrogen cause an increase in tensile strain. We calculate valence band offset ratio Q_v (see Fig.6.11 (a)) and conduction band offset ratio Q_c (see Fig.6.11 (b)) as a function of indium and nitrogen concentration. The three dimensional representation of Q_v and Q_c is provided in Fig.6.11 (c). Although the indium and nitrogen dependence of Q_v and Q_c is quite complicated, we can get the following conclusions from Fig.6.11;

(i) Q_v is greater than Q_c for the entire composition range of indium,

(ii) The introduction of nitrogen decreases Qv and increases Q_c very rapidly.

(iii) For high nitrogen concentraion of Q_c becomes greater than Q_v.

The corresponding variations of conduction band offset ΔE_c and valence band offset ΔE_v is presented in Fig.6.12 (a)-(c). Similar conclusions can be get from Fig.6.12 as we have got from Fig.6.11.

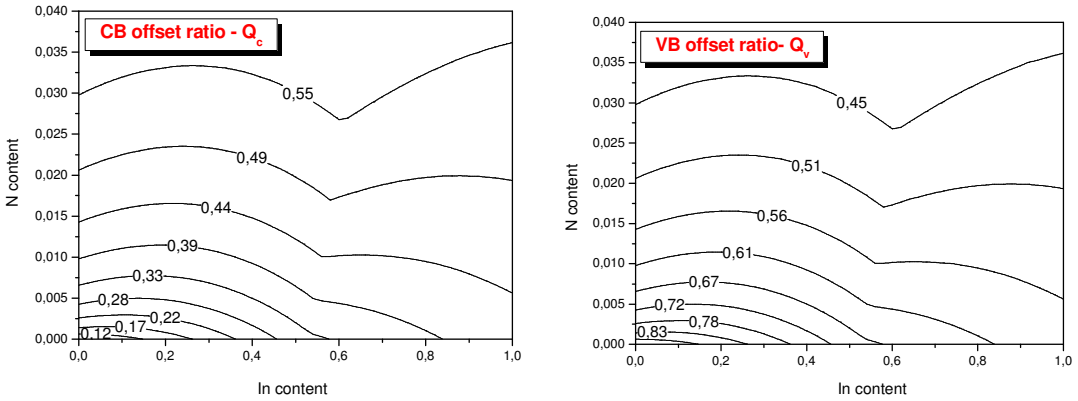

(a) (b)

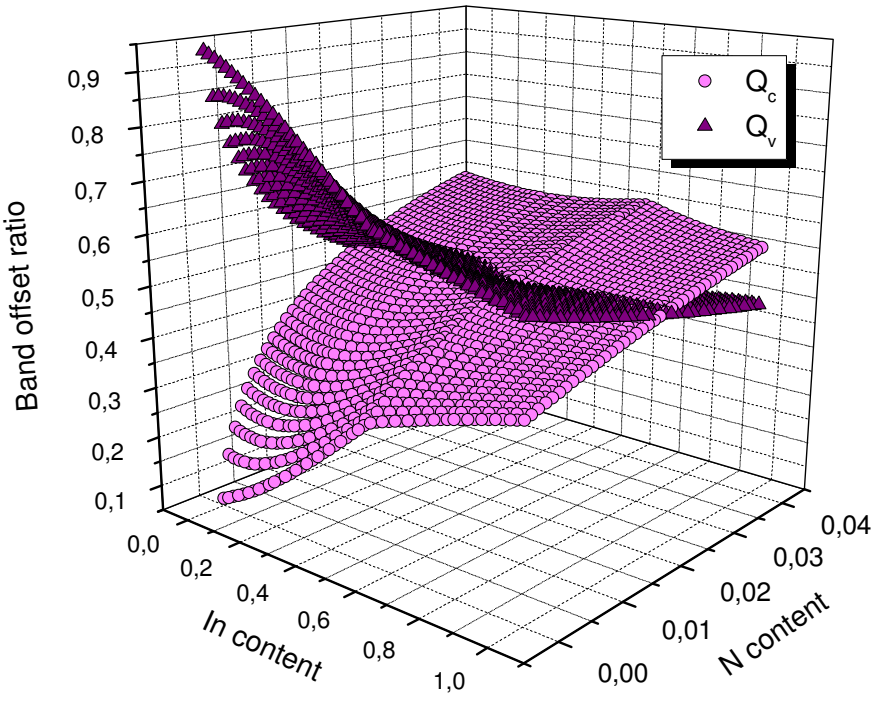

(c)

Figure 6.11: (a) The illustrated two dimensional representation of the variation of valence band offset ratio Q_v versus indium and nitrogen concentration for $Ga_{1-x}In_xN_yAs_{1-y}$ layers on InP substrate, (b) two dimensional representation of variation of conduction band offset ratio Q_c versus indium and nitrogen concentration. (c) The three dimensional representation of of the variation of valence band offset ratio Q_v and conduction band offset ratio Q_c with indium and nitrogen concentration for $Ga_{1-x}In_xN_yAs_{1-y}$ layers on InP substrate.

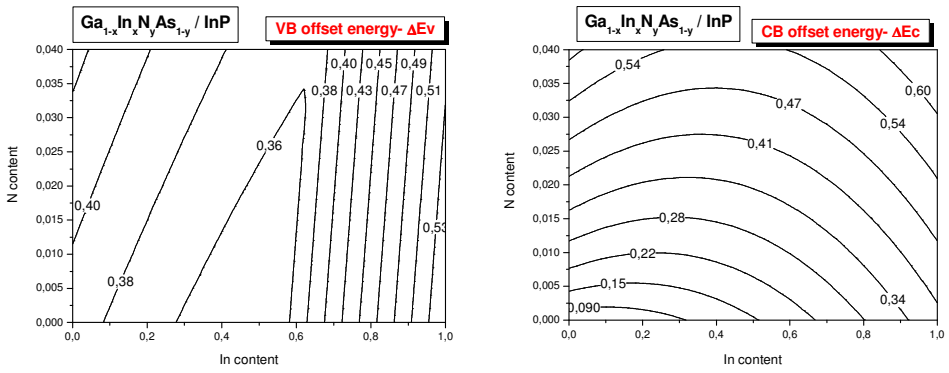

(a) (b)

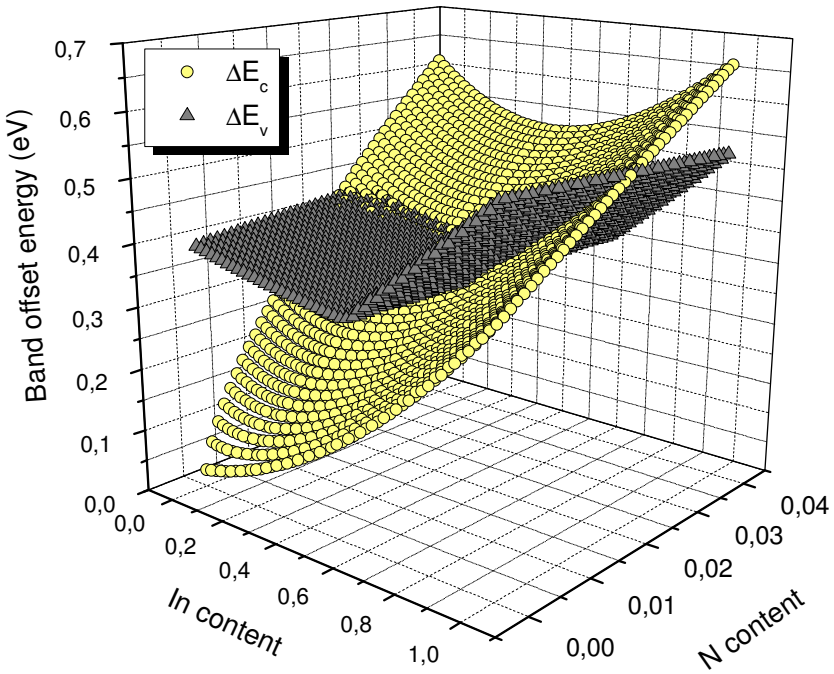

(c)

Figure 6.12: (a) The two dimensional rate of change of valence band offset ΔE_v versus indium and nitrogen concentration for $Ga_{1-x}In_xN_yAs_{1-y}$ layers on InP substrate, (b) two dimensional representation of variation of conduction band offset ΔE_c versus indium and nitrogen concentration. (c) The three dimensional representation of the variation conduction band offset ΔE_c and valence band offset ΔE_v with indium and nitrogen concentration for $Ga_{1-x}In_xN_yAs_{1-y}$ layers on InP substrate.

6.3.4 Effect of antimonite on band alignment

The growth of high quality dilute nitrides is quite difficult; the incorporation of nitrogen can degrade the optical properties due to the nonradiative traps [53, 54], ion damage [111, 112] and/or phase segration [113]. These problems become increasingly apparent when the indium and nitrogen concentrations in GaInNAs are increased to extend the emission wavelength beyond 1.55 μm. The addition of antimonite as a surfactant and constituent dramatically improves the material and optical qualities in dilute nitrides, reduces band gap, and enables the lowest threshold GaAs-based edge emitting lasers at 1.55 μm. It is expected that antimonite also influences the band alignment configuration of QWs. In this section, we investigate the effects and behaviour of antimonite on GaInNAs alloys with widely varying compositions of antimonite, indium and nitrogen**.** A detailed study of the interactions between these atoms is useful to help to understand the role of antimonite on the band alignment of the dilute nitride materials and how to use it properly from the band alignment point of view.

6.3.5 $Ga_{1-x}In_xN_y\ As_{1-y-z}Sb_z$ QW on GaAs and InP substrates

We have mentioned previously that $Ga_{1-x}In_xN_y\ As_{1-y-z}Sb_z$ has been considered as a potential material for improving the threshold current of existing GaInNAs-based lasers. In this section we would like to investigate whether the incorporation of Sb into GaInNAs brings improvements to band alignment. We first present the results on GaAs substrates; these will be followed by on InP substrates. Fig.6.13 shows the variation of lattice mismatch with nitrogen concentration for various antimonide values. It can be seen from the diagram that the mismatch between the lattice constant of $Ga_{1-x}In_xN_yAs_{1-y-z}Sb_z$ with GaAs increases with increasing indium concentration. Fortunately, the mismatch decreases with increasing antimonide concentration which will lead to smaller compressive strain.

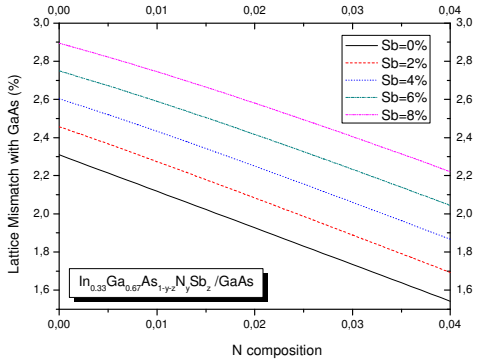

Figure 6.13: The calculated variation of lattice mismatch of quinary $Ga_{1-x}In_xN_y As_{1-y-z}Sb_z$ layer on GaAs.

The nitrogen and antimonide dependence of conduction band offset ΔE_c and valence band offset ΔE_v is shown in Fig.6.14. As we have calculated previously, Fig.6.9 shows the decrease of valence band offset ΔE_v and increase of conduction band offset ΔE_c with increasing nitrogen concentration. It is also seen from Fig.6.4 that both band offsets increases with increasing antimonide concentration. Since both antimonide and indium have similar effects, the increase in indium concentration increases both band offsets of ΔE_v and ΔE_c as can be seen from Fig.6.15.

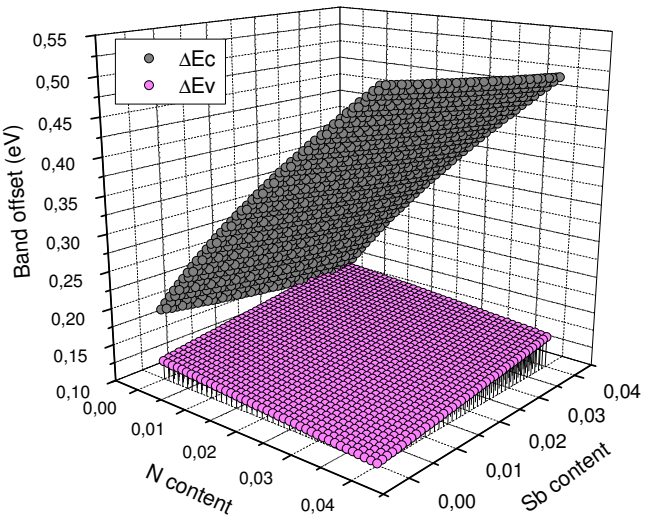

Figure 6.14: The nitrogen and antimonide dependence of valence band offset ΔE_v and conduction band offset ΔE_c of the new quinary $Ga_{1-x}In_xN_y As_{1-y-z}Sb_z$ /GaAs QW on GaAs substrate.

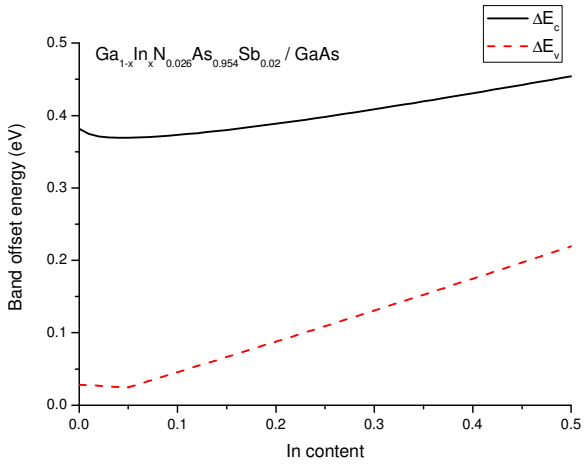

Figure 6.15: The indium dependence of valence band offset ΔE_v and conduction band offset ΔE_c of $Ga_{1-x}In_xN_y\ As_{1-y-z}Sb_z$ on GaAs substrate.

We now investigate the variation of strain of $Ga_{0.62}In_{0.38}N_y\ As_{1-y-z}Sb_z$ wells on InP substrate as a function of nitrogen and antimonide concentration for an indium concentration of 38%, see Fig.6.16. The strain decreases with antimonide and increases with nitrogen concentration.

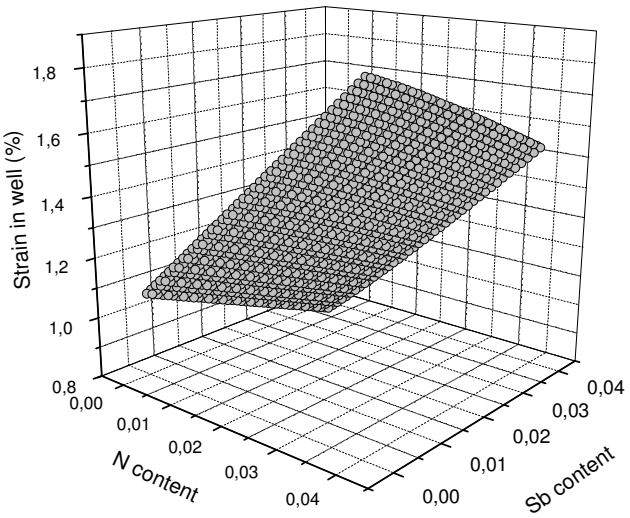

Figure 6.16: The calculated variation of lattice mismatch of $Ga_{0.62}In_{0.38}N_y\ As_{1-y-z}Sb_z$ layer with InP as a function of nitrogen and antimonide concentration.

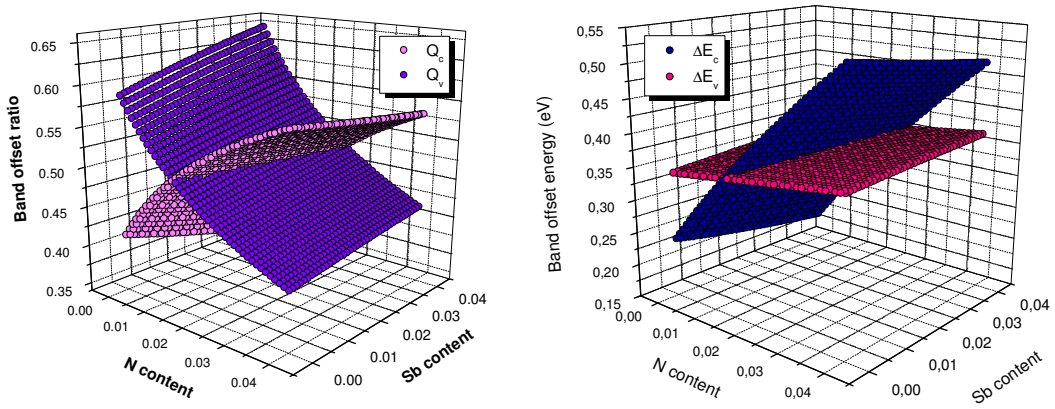

(a) (b)

Figure 6.17: The change of the variation of (a) valence band offset ratio Q_v and conduction band offset ratio Q_c and, (b) conduction band offset ΔE_c and valence band offset ΔE_v of $Ga_{0.62}In_{0.38}N_y\ As_{1-y-z}Sb_z$ wells on InP substrates versus nitrogen and antimonide concentration.

Fig.6.17 shows the corresponding conduction band offset ΔE_c and valence band offset ΔE_v of $Ga_{0.62}In_{0.38}N_y\ As_{1-y-z}Sb_z$ wells on InP substrate. Valence band offset ΔE_v is almost independent from both nitrogen and antimonide concentration. Although conduction band offset ΔE_c strongly dependent on nitrogen concentration, it is almost independent from antimonide concentration.

In summary, the close investigation of Fig.6.14 and Fig.6.17 reveals that the addition of antimony cause almost no change on the conduction band offset ΔE_c and increases the valence band offset ΔE_v. These conclusions were drawn experimentally by Yuen MRS *et al* confirming the validity of theoretical calculations.

6.4. Conclusions

In this work, we have investigated the role of N and Sb on the band alignment of strained GaInNAsSb QWs on GaAs and InP substrates. There have been many theoretical studies on band offsets of commonly accepted III-V semiconductors, however there have been none for InGaNAsSb. By means of this study we have tried to make clear what effect the addition of antimony would have on the GaNAs and

InGaNAs band offsets. We have calculated that role of nitrogen atoms in GaInNAsSb compounds is the assurance of the deep confinement potential for electrons whereas the role of antimony atoms in GaInNAsSb compounds is the avalibility to incorporate more indium to reach longer wavelengths and wider wavelength range. We have calculated that the only effect the antimony had on the band lineup was the increase in valence band offset while not affecting the conduction band any significant degree on both GaAs and InP substrates. Although forming a five element quinary system adding antimony to GaInNAs has made an already complex alloy even more complicated, the new quinary GaInNAsSb QW can be shown as an ideal candidate for long wavelength lasers to eliminate the growth limitations of high quality dilute nitrides, the degradation of the optical properties due to the nonradiative traps, ion damage and/or phase segration and allow wide wavelength range coverage.

CHAPTER 7

THESIS SUMMARY

Long wavelength semiconductor lasers in the range of 1.3-1.55 μm are very important sources for optical fiber communication. The incorporation of nitrogen atoms into Ga(In)As host material led to the surprising revelation that both the band gap and lattice parameter could be simultaneously reduced, contrary to the behaviour of most III-V semiconductors. A noticeable band gap reduction of 100-150 meV percent of N in GaInNAs makes the alloy particularly interesting. The reduction of the band gap with nitrogen atoms opens the possibility of these devices to emit light beyond 1.5 μm. Due to the highly nonlinear effects of N on the InGaAs band gap grown on GaAs substrate, N is incorporated in InGaAs to decrease the band gap and make GaInNAs material a suitable material for long wavelength semiconductor laser diodes at 1.3-1.55 μm. Successful realizations of GaInNAs-based laser diodes operating at the telecommunication wavelengths of 1.3 and 1.55 μm were demonstrated [114-117]. Before the development of GaInNAs, it was impossible to obtain these wavelenghts from a coherently grown material on GaAs due to the very high strain in the active region. Therefore, these desired wavelengths can only be obtained from a coherently grown GaInNAs on GaAs with the expense of high strain in the well material. Although the strain in well material is high, it can be compensated by means of using appropriate barriers with opposite strain. Therefore, by means of the flexibility of the band gap of the coherently grown GaInNAs alloys on GaAs, the wavelength of photonic device operation can be extended beyond 1.5 μm which is impossible to obtain with InGaAsP/InP and AlGaAsP/InP. The conduction-band offset of GaInNAs/GaAs is larger than the GaInAsP/InP system. A larger band offset will lead to stronger electron confinement and therefore better characteristic temperature. Enormous progress has been achieved in GaInNAs semiconductor alloy on GaAs substrate for both its fundamental properties and its potential applications for 1.3 and 1.55 μm lasers [118,119]. In contrast to this large amount of work reported on dilute $Ga_{1-x}In_xN_yAs_{1-y}$ on

GaAs, only a few studies have been published so far on the growth of strained $Ga_{1-x}In_xN_yAs_{1-y}$ on InP substrates [49-52,100-102,120,121] and there is a few theoretical work about the comparison of the band alignment of the $Ga_{1-x}In_xN_yAs_{1-y}$ alloys on GaAs and InP substrates up to our knowledge [58,,122].

The work carried out in this thesis considered the strain, substrate and alloying dependence of the band alignment of dilute-nitride-antimonide QW laser structures operating at long wavelengths. In each of the results chapters appropriate conclusions have already been presented. However, it is going to be useful in this chapter to briefly summarize and gather together the major conclusions from the work described in this thesis.

The investigation of the effect of adding nitrogen into InGaAs on the band offsets of QWs on InP substrate revealed the fact that the long wavelength emission of 2.3 μm can only be obtained when GaInNAs QWs grown on InP substrates. We have calculated that the band alignment configuration of GaInNAs QWs on InP substrates can compete with the ideal band alignment of GaInNAs QWs on GaAs substrates.

The effect of the compensation of high strain of the well by means of using strained barriers is studied in chapter 5. It was found that by means of compensating the strain of the well material, one can improve the band alignment of GaInNAs QW on both GaAs and InP substrates. We have shown that GaInNAs QWs on InP substrates with an indium concentration of the smaller than 0.53 provide deep conduction- and shallow valance-wells. Therefore, these tensile-strained lasers can be used safely when TM polarisation is required. Our calculated results also shows that the band alignment of indium rich highly strained GaInNAs/ InAlAs/ GaAs is improved with the incorporation of N into well allowing an emission wavelength of the order of 2.3 μm. It is also seen from our results that indium rich GaInNAs QW can only be possible on InP substrate.

In order to obtain an emission wavelength of 1.55 μm by means of using GaInNAs/ GaAs QW, one must keep the N concentration as low as possible. This will lead the indium concentration being high. This will in turn cause the optical degradation of semiconductor crystal. Fortunately, it has been shown by several groups that the addition of antimony to GaInNAs system allows to reach the emission wavelength of 1.5 μm with good PL characteristics. We have examined the effect of Sb on the band alignment of the new quinary system of GaInNAsSb and shown that the antimony increases only the valance band. It hasn't got any significant effect on the conduction band. Therefore, it has been concluded that the presence of antimony allows incorporating more indium to reach longer wavelengths.

REFERENCES

[1] M. I. Nathan, W. P. Dumke, G. Burns, F. H. Dill, Jr., and G. Lasher. (1962). *Appl. Phys. Lett.*, vol. **1**, no. **3**, pp. 62–64

[2] J. Böhrer, A. Krost, and D. B. Bimberg, (1993). *Applied Physics Letters*, Vol. **63**, No.**14**, p1918-1920

[3] Haris Jr., J.S. (2002). *Semicond.Sci.Technol*. **17,** 880-891

[4] Irina A.Buyanova and Weimin M.Chen. (2004). *Physics and Applications of dilute nitrides* New York London, Taylor & Francis p 397-399

[5] M. Kondow, K. Uomi, A. Niwa, S. Watahiki, and Y. Yazawa, Japan. J. (1996). *Appl.Phys.,* **35**, 1273

[6] Irina A.Buyanova and Weimin M.Chen. (2004). *Physics and Applications of dilute nitrides* New York London, Taylor & Francis p 309-320

[7] P. Krispin, S. G. Spruytte, J. S. Harris, and K. H. Ploog. (2002). *Applied Physics Letters*, vol**. 80**, no. **12**, pp. 2120

[8] Y. Zhang, B. Fluegel, M. C. Hanna, J. F. Geisz, L. W. Wang, and A. Mascarenhas. (2003). *Physica Status Solidi B*, vol. **240**, no**. 2**, pp. 396 – 403

[9] S. B. Zhang and S. H. Wei. (2001). *Phys Rev Lett*, vol.**86**, no.**9**, pp. 1789 – 92

[10] URL http://www.cisco.com/ univercd/ cc/ td/ doc/ product/ mels/ cm1500/dwdm /dwdm_ovr.htm#wp1037303

[11] URL http://www.fiber-optics.info/fiber-history.htm#top%20of%20page

[12] Lynford Goddard. (2005). Ph.D. thesis, Stanford Univ.

[13] URL http://www.internetworldstats.com/emarketing.htm

[14] HBYuen. (2006). Ph.D. thesis, Stanford Univ.

[15] Marvin J. Weber Ph.D. (1999). *Handbook of Laser Wavelengths* Lawence Berkeley National Laboratory University of California Berkeley, California p 15-20

[16] URL http://en.wikipedia.org/wiki/List_of_laser_types#Semiconductor_lasers

[17] E.F.Shubert. (2005). *Physical Foundations of Solid State Devices,*Rensselaer Polytechnic Institute Troy, New York, p196-212

[18] R. Dingle and C. H. Henry. (1976). *Quantum Effects in Heterostructure Lasers*, U.S. Patent 3 982 207

[19] Chuang S L. (1995). *Physics of Optoelectronic devices,* Godman J W New York, Wiley Series in Pure and Applied Optics p 421

[20] A. F. Phillips, S. J. Sweeney, A. R. Adams, and P. J. A. Thijs. (1999). *IEEE J. Sel.Top. Quantum Electron.* **5**, 301

[21] M. Yano, H. Imai, and M. Takusagawa. (1981). *J. Appl. Phys.* **52**, 3172

[22] N. K. Dutta and R. J. Nelson. (1981). *Appl. Phys. Lett* **38**, 407

[23] Vegard L (1921). *Z. Phys.* **5** 17

[24] Y. P. Varshni. (1967). Physica, vol. **34**, pp. 149-154

[25] Chih-Sheng Chang and Shun Lien Chuang. (1995). *Senior Member Ieee,* Ieee Journal Of Selected Topics In Quantum Electronics, Vol. **I**. No. 2

[26] Keith Barnham, Dimitri D Vvedensky. (2001). *Low-Dimensional Semiconductor Structures: Fundamentals and Device Applications*

[27] Joachim Piprek. (2003). Semiconductor *Optoelectronic Devices: Introduction to Physics and Simulation, Technology&Industrial Arts,* Elsevier

[28] Seoung-Hwan Park, Weon-Guk Jeong and Byung-Doo Choe. (1995). *Appl.Phys.Lett*.**66** (2)

[29] G.Zhang, A.Ovtchninnikov. (1993). *Appl.Phys.Lett.*, **62**, 1644

[30] C.Silfvenius, B. Stalnacke, G. Landgren. (1997). *Journal of Crystal Growth*, **170**, 122

[31] C. G. van de Walle. (1989). *Phys. Rev*. B **39**, 1871

[32] C. G. van de Walle and R. M. Martin. (1986). *Phys. Rev.* B **34,** 5621

[33] C. G. van de Walle and R. M. Martin. (1987). *Phys. Rev*. B **35**, 8154

[34] T. Y. Wang and G. B. Stringfellow. (1990). *J. Appl. Phys***. 67**, 344

[35] M. P. C. M. Krijn. (1991). *Semicond. Sci. Technol.* **6**, 27

[36] S. Satpathy, R. M. Martin, and C. G. van de Walle. (1988). *Phys. Rev*. B **38**, 13237

[37] Chuang S L (1995). *Physics of Optoelectronic devices,* Godman J W New York Wiley Series in Pure and Applied Optics p 661

[38] S.Chuang. (1991). *Phys.Rev*.B **43,** 9649-9661

[39] Chuang S L (1995). *Physics of Optoelectronic devices,* Godman J W New York Wiley Series in Pure and Applied Optics p 442

[40] Shan W, Walukiewicz W ,Ager III J W, Haller E E, Geisz J F, Friedman D J, Olson J M and Kurtz S R.(1999). *Phys. Rev. Lett.* **82** 1221

[41] Suemune I, Uesugi K and Walukiewicz W. (2000) *Appl. Phys. Lett*. **77** 3021

[42] W.Walukiewicz, W. Shan, J. Wu, and K.M. Yu *Band Anticrossing in III-N-V Alloys: Theory and Experiments* Materials Sciences Division, Lawrence Berkeley National Laboratory, Berkeley, California

[43] P. Perlin, P. Wisniewski, C. Skierbiszewski, T. Suski, E. Kaminska, S. G. Subramanya, E. R. Weber, D. E. Mars, and W. Walukiewicz. (2000). *Appl. Phys. Lett.* **76**, 1279 46.

[44] J. Hader, S. W. Koch, J. V. Moloney, and E. P. Oreilly. (2000). *Appl. Phys. Lett.* **76**, 3685

[45] M.Oduncuoğlu. (2004). Ph. D Thesis University of Gaziantep,

[46] C. Skierbiszewski et al. (1999). *Physica Status Solidi* B **216**, 135

[47] Perlin P, Subramanya S G, Mars D E , Kruger J, Shapiro N, Siegle H and Weber E R. (1998). *Appl. Phys. Lett.* **73** 3703

[48] Kondow M, Uomi K, Niva A, Kitatani T, Watahiki S, and Yazawa Y. (1998) *Jpn. J. Appl. Phys. Lett*. **73** 3703

[49] Elmers C, Hohnsdorf F, Koch J, Agert C, Leu S, Karaiskaj D and Hofmann M. (1999). *Appl. Phys. Lett.* **74** 2271

[50] Serries D, Geppert T, Ganser P, Maier M, Köhler K, Herres N and Wagner J. (2002). *Appl. Phys. Lett.* **80** 24488

[51] Köhler K, Wagner J, Ganser P, Serrier D, Geppert T, Maier M and Kirste L (2004). *J. Phys. Condens. Matter.* **16** S2995

[52] Gokhale M R, Wei J, Wang H and Forrest S R. (1999). *Appl. Phys. Lett.* **74** 1287

[53] Bellaiche L. (1999). *Appl.Phys.Lett.* **75** 1287

[54] Ubukata A, Dong J, atsumoto K and Ishihara Y. (2000). *Japan.J.Appl.Phys.* 1 **39** 5962

[55] Buyanowa I A, Chen W M and Monemar B. (2001). *MRS Internet J. Nitride Semicond. Res.* **6** 2

[56] Gönül B, Koçak F, Toktamış H and Oduncuoğlu M. (2004). *Chinese J. Appl. Phys.* **42** 3312

[57] Lin G and Lee C P. (2002) *Optical and Quantum Electronics* **34** 1191

[58] Gönül B, Köksal K and Bakır E. (2006) *Physica E* **31** 148

[59] Vurgaftman I, Meyer J R and Ram. Mohan L R. (2001). *J. Appl. Phys*. **89** 5815

[60] Vurgaftman, I. and Meyer, J.R. (2003). *J. Appl. Phys*., Vol. **94**, No. 6, 15,3681.

[61] Chuang S L (1995). *Physics of Optoelectronic devices* Godman J W New York Wiley Series in Pure and Applied Optics p709

[62] Minch J, Park S H, Keating T and Chuang S L. (1999) *IEEE J. Quantum. Electronics,* **35** 771

[63] M.Kondow, K.Uomi, A.Niwa, T.Kitatani, S.Watahiki and Y.Yazawa. (1994). *Jpn.J.Appl.Phys,* **33**, L1058

[64] M.Kondow, K.Uomi, A.Niwa, T.Kitatani, S.Watahiki and Y.Yazawa. (1996). *Jpn.J.Appl.Phys,* **35**, 1273-1275

[65] W.Shan, W.Walukiewicz, J.Ager, E.Haller, J.Geisz, D.Friedman, J.Olson, and S.Kurtz. (1999). *J.Appl.Phys*. **86**, 2349-2351

[66] L. Pauling. (1932). *J.Am.Chem.Soc*. **54**, 3570

[67] A.Alred. (1961). *J.Inory.Nucl.Chem.* **17**, 215-221

[68] A.Alred and A.Hensley. (1961). *J.Inory.Nucl.Chem*. **17**,43-54

[69] Y. Saito, et. al. (2001). *Jpn. J. Appl. Phys.* **40**, L90

[70] W. Walukiewicz, W. Shan, Y. M. Yu, J. W. Ager III, E. E. Haller, I. Miotkowski, M. J. Seong, H. Alawadiii, and A. K Ramdes. (2000). *Phys. Rev. Lett*. **5**, 1552

[71] I. Suemune, K. Uesugi and W. Walukiewicz. (2000). *Appl. Phys. Lett.* **77** 2271

[72] H. P. Xin, C. W. Tu. (1998). *Appl. Phys. Lett.* **72** 2442.

[73] T. L. Koch, U. Koren, R. P. Gnall, C. A. Burrus and B. I. Miller.(1988). *Electron. Lett.* **26** 1431.

[74] J. W. Matthews and A. E. Blakeslee. (1974) *J. Cryst. Growth* **24** 188.

[75] A. Ghiti and U. Ekenberg. (1994). *Semicond. Sci. Technol.* **9** 1575.

[76] B. I. Miller, U. Koren, M. G. Young and M. D. Chieh. (1991). *Appl. Phys. Lett.* **58** 1952.

[77] G. Zhang and A. Ovtchinnikov. (1993). *Appl. Phys. Lett.* **62** 1644.

[78] C. Silfvenius, B. Stalnacke, G. Landgren. (1997). *J. Cryst. Growth* **170** 122.

[79] M.Hetterich, M.D.Dawson, A.Yu.Egorov, D.Bernklau, H.Riechert. (2000). *Appl. Phys. Lett.* **76** 2271

[80] E. P O'Reilly, G. Jones,A. Ghiti and A. R. Adams. (1991). *Electron. Lett*. **27** 1417.

[81] P. J. A. Thijs, L. F.Tiemeijer, K. I. Kuindersma, J. J. M. Binsma and T. Van Dongem. (1991). *IEEE J. Quantum Electron.* **27** 1426.

[82] P. J. A. Thijs, L. F.Tiemeijer, J. J. M. Binsma and T. Van Dongem. (1994). *IEEE J. Quantum Electron.* **30** 477.

[83] B. Gönül. (1999). Physica E **5** 50.

[84] Sarzala R P and Nakwaski W. (2006) *Optical and Quantum Electronics* **38** 293

[85] Dudley J J, Ishikawa M, Babic D I, Miller B I, Mirin R, Jiang W B, Bowers J E, Hu E L. (1992). *Appl. Phys. Lett* **61** 3095

[86] Choquette K D, Geib K M, Ashby C H, Twesten R D, Blum O, Hou H Q, Follstaedt D M, Hammons B E, Mathes D and Hull R. (1997) *IEEE J. Sel. Top. Quantum Electron.* **3** 916

[87] Kondow M and Kitatani T. (2002). *Semicond. Sci. Technol.* **17** 746

[88] Jackson A W, Naone R L, Dalberth M J, Smith J M, Malone K J, Kisker D W, Klem J F, Choquette K D, Serkland D K and Geib K M. (2001). *Electron. Lett.* **37** 355

[89] Steinle G, Riechert H and Egorov A Yu. (2001). *Electron. Lett.* **37** 93

[90] Sato S, Nishiyama N, Miyamoto T, Takahashi T, Jikutani N, Arai M, Matsutani A, Kogayama F and Iga K. (2000). *Electron. Lett.* **36** 2018

[91] Purvis G. (2004). *III-Vs Review* **17**: 43

[92] Yang X, Jurkovic M J, Heroux J B and Wang W I. (1999). *Appl. Phys. Lett.* **75** 178

[93] X. Yang, J. B. Heroux, M. J. Jurkovic, and W. I. Wang. (2000). *J. Vac. Sci. Technol. B* **18** 1484

[94] Shimizu H, Kumada K, Uchiyama S and Kasukawa A. (2001). *IEEE J. Sel. Top. Quantum Electron.* **7** 355

[95] Gambin V, Ha W, Wistey M, Yuen H, Bank S R, Kim S M and Harris J S Jr. (2002). *IEEE J. Sel. Top. Quantum Electron.* **8** 795

[96] Bank S, Ha W, Gambin V, Wistey M, Yuen H, Goddard L, Kim S and Harris J S Jr. (2003). *J. Cryst. Growth* **251** 367

[97] Shan, W., Walukiewicz, W., Ager, J.W., Haller, E.E., Geisz, J.F,Friedman, D.J., Olson, M., and Kurtz, S.R. (1999). *Phys. Rev. Lett.,* **82**, (6), 1221-1224

[98] Kim. K., and zunger, A. (2001). *Phys.Rev. Lett*., **86**, (12), 2609-2612

[99] Kondow, M., Uomi, K., Niwa, A., Kitatani, T., Wakahiki, S. and Yazawa, Y. (1996). *Jpn. J. Appl. Phys.*, **35**, (B), 1273-1275

[100] Zaets W and Ando K. (1999). *IEEE Photonics Technol. Lett.* **11** 1012

[101] Takenaka. (1999). *Proc. 11th Int. Conf. on Indium Phosphide and Related Matrials*, Davos, Switzerland, 289

[102] Carrere H, Marie X, Barrau J, Amand T, Bouzid S B, Sallet V and Harmand J C. (2004). *IEE Proc.-Optoelectron* **151** 402.

[103] A.Oteish and R.J.Needs., (1992)., *Physical Review B*, **45**, 3

[104] Yu K M, Walukiewicz W, Shan W, Ager J W III, Wu J and Haller E E, Xin H P and Tu C W. (2000). *Phys. Rev. B.,* **61** R13337

[105] Shan W, Walukiewicz W, Yu K M, Ager J W III, Haller E E, Xin H P and Tu C W. (2000). *Appl. Phys.Lett*., **76** 3251

[106] Yu K M, Walukiewicz W, Shan W, Wu J, Beeman J W, Ager J W III, Haller E E, Xin H P and Tu C W. (2001). *Appl. Phys Lett.* **78** 1017

[107] Perkins J D, Mascarenhas A, Zhang Y, Geisz J F, Friedman D J, Olson J M and Kurtz S R. (1999). Phys. Rev. Lett. **82** 3312

[108] Jiang D S, Qu Y H, Ni H Q, Wu D H, Xu Y Q, Niu Z C. (2006). *Journal of crystal growth,* **288** 12

[109] Oka T, Mishima T, Kudo M. (2001) *Appl. Phys. Lett.* **78** 483

[110] Anan T, Nishi K, Sugou S, Yamada M, Tokutome K and Gomyo A. (1998). *Electron. Lett.* **34** 2127

[111] Tu C W (2001). *J. Phys. Condens. Matter* **13** 7169

[112] Ptak A J, Johnston S W, Kurtz S, Friedman D J and Metzger W K (2003). *J. C ryst. Growth* **251** 392

[113] Kurtz S R, Allerman A A, Seager C H, Sieg R M and Jones E D (2000). *Appl. Phys. Lett.* **77** 400

[114] K. Kurihara, M. Takashima, K. Sakata, R. U. M. Takahara, H. Ikeda, H. Namita, T. Nakamura, and K. Shimoyama, (2004). *J. Cryst. Growth* **271**, 341

[115] A. J. SpringThorpe, M. Extavour, D. Goodchild, E. M. Griswold, G. Smith, J. K. White, K. Hinzer, R. Glew, R. Williams, and F. Robert., (2003).*J. Cryst. Growth* **51**, 760

[116] M. Yamada, T. Anan, K. Tokutome, A. Kamei, K. Nishi, and S. Sugou, (2000). *IEEE Photon. Technol. Lett.* **12**, 774

[117] H. C. Kuo, Y. H. Chang, H. H. Yao, Y. A. Chang, F. I. Lai, M. Y. Tsai, and S. C. Wang, (2005). *IEEE Photon. Technol. Lett.* **17,** 528

[118] Cunniingham J E, Dinu M, Shah J, Quochi F, Kilper D and Jan W Y. (2001). *J. Vac. Sci. Technol. B* **19** 1948

[119] Tian Y and Wang H. (2006). *Microelectronics Journal* **37** 38

[120] Harmand J C, Caliman A, Rao E V K, Lergeau L, Ramos J, Teissier R, Travers L, Ungaro G, Theys B and Dias I F L. (2002). *Semicond. Sci. Technol.* **17** 778

[121] Kondow M, Uomi K, Niva A, Kitatani T, Watahiki S andYazawa Y. (1996). *Japan. J. Appl. Phys.* **35** 1273

[122] Gönül B., Bakır E., and Köksal K., (2006). *Semicond. Science and Technol.* **21** 876

PUBLICATIONS

[1] Gönül B., Bakır E. and Köksal K., "Analysis of the band alignment of highly strained indium rich GaInNAs QWs on InP substrates", *Semicond. Science and Technol.* **21** 876 (2006).

[2] Gönül B., Köksal K. and Bakır E., "Comparison of the band alignment of strained and strain-compensated GaInNAs QWs on GaAs and InP substrates", *Physica E* **31** 148 (2006).

[3] Gönül B., Bakır E. and Köksal K., "An Alternative Treatment of Yukawa-type Potentials", *Physica Scripta*, **73** 279 (2006).

[4] Gönül B., Oduncuoğlu M., Bakır E. and Köksal K., "A theoretical study of the laser characteristics of GaInNAs QW's", *International Conference on Superlattices, Nano-Structures and Nano-Devices*, İstanbul, Türkiye, ICSNN (2006).

[5] Köksal K., Gönül B. and Bakır E., "A theoretical investigation of carrier and optical mode confinement in GaInNAs QW's on GaAs and InP substrates", *International Conference on Superlattices, Nano-Structures and Nano-Devices*, İstanbul, Türkiye, ICSNN (2006).

[6] Köksal K., Bakır E. and Gönül B., "Band Structure Calculations in Dilute GaInNAs-based QWs Under Compressive and Tensile Strain" , *Türk Fizik Dernegi 22. Fizik Kongresi (TFD-22)*, Özetler-s.560, Muğla, (2005).

[7] Bakır E., Köksal K. and Gönül B., "A Theoretical Comparative Study of Dilute GaInNAs on GaAs and InP Substrates", *Türk Fizik Dernegi 22. Fizik Kongresi (TFD-22)*, Özetler-s.519, Muğla, (2005).